Technical University of Crete

Department of Mineral Resources Engineering

TIME LAPSE SEISMIC MONITORING OF STEAM INJECTION FOR EOR PROJECTS

By

Katerina Stathopoulou

Scientific Advisor: Prof. Antonios Vafidis

Master of Science in Petroleum Engineering

Diploma Thesis

Chania, October 2015

TECHNICAL UNIVERSITY OF CRETE

SCHOOL OF MINERAL RESOURCES

Master of Science in Petroleum Engineering

The undersigned certifies that the members of the Examination Committee have read and approve the content of the thesis, entitled "Time Lapse Seismic Monitoring of Steam Injection for EOR Projects" submitted by *Katerina Stathopoulou* in partial fulfilment of the requirements of the degree of Master of Science in Petroleum Engineering.

_____

Prof. Antonios Vafidis
(Scientific Advisor-Applied Geophysics Laboratory)

_____

Prof. Dionissios T. Hristopulos
(Member Committee- Geostatistics Laboratory)

_____

Prof. Nikolaos Varotsis
(Member Committee-PVT and Core Analysis Laboratory)

Date   _____

Abstract

The current thesis is based on a time - lapse synthetic seismic reflection study of a steam injection project in Prinos field, northern Greece. The basic attempt is to investigate whether the synthetic seismic reflection data applied on the surface of the geologic section is capable of detecting changes in the reservoir model, which are provoked by the injected steam within the reservoir formations. Two seismic reflection surveys (2D) are simulated through generation algorithm based on finite differences method. Time-lapse monitoring is comprised of a baseline survey recorded before the onset of the steam injection process, when the reservoir is fully saturated with brine and oil and a monitor survey recorded after a period, when the whole reservoir is steam injected. The final time-lapse seismic section is derived from the subtraction of the two already mentioned seismic surveys. Another way to clarify whether all the reservoir layers are stimulated over their entire length by the injected steam, is to calculate the time lag of the seismic waves caused by the lower seismic velocity of the steam saturated formations. The seismic processing was conducted with the aid of MATLAB^{TM} Software.

Acknowledgements

Contents

List of Tables

List of Figures

Introduction

Reservoir geophysics, in comparison with exploration and development geophysics, is a relatively new field in oil industry. Geophysics is now increasingly being applied for the characterization of the internal geometry and quality of reservoirs themselves and is often used as a tool for monitoring reservoir changes not only during production, but also during Enhanced Oil Recovery methods. Current advances in the reliability of seismic observations and in methods that refer to the interpretation of these observations in terms of reservoir properties have, in pace with economic considerations, provided the driving forces for the development of reservoir geophysics.

This study consists part of reservoir geophysics field for monitoring purposes. Specifically, it refers to a time-lapse survey through synthetic seismic reflection data over a steam injection project in Prinos field. The first part refers to a monitoring seismic survey that was conducted before any production of the specific reservoir, while the second survey refers to a post-injection period.

Analytically, the chapters that are included in the thesis are described below:

- ➢ The necessity of reservoir monitoring in the oil industry, the Enhanced Oil Recovery Methods and mainly that of steam flooding, as well as the connection of reservoir induced changes caused by an EOR process with the seismic parameters that are directly affected, are all described in *Chapter 1.*
- ➢ Case studies referring to time-lapse reservoir monitoring for EOR purposes are presented in *Chapter 2*.
- ➢ *Chapter 3* includes the description of the geological setting of Prinos Field and the geologic section that synthetic seismic data are applied.
- ➢ Detailed description of the generation algorithm based on finite difference method for the creation of synthetic seismic data is presented in *Chapter 4.*
- ➢ In *Chapter 5* the process that was followed for the creation of the synthetic model is described, including the technical parameters concerning the structure of the seismic surveys.
- ➢ The processing of seismic signal is described step by step in *Chapter 6.* In each processing procedure are indicatively presented the results of the pre-injection project.
- ➢ *Chapter 7* includes all the post-injection seismic sections as well as the difference sections that consist the time -lapse resulting seismic sections.
- ➢ Finally, in *Chapter 8* all the final conclusions that result for this current study, as well as recommendations for future activity on this survey are included.
- ➢ The algorithm used for seismic processing of the synthetic seismic reflection data is presented in *Appendix.*

CHAPTER 1

Reservoir Monitoring

1.1.   Introduction

Reservoir monitoring is the application of multiple surveys of reflection seismology integrated with reservoir description and reservoir simulation, solved at each time level in an iterative manner, to track the movement of fluid saturations in a petroleum reservoir. Reservoir monitoring includes both the measurement of past and current location of fluids and the prediction of how the fluids will move in the future. Though predictions have been made for many years using other technologies, the advantage of reservoir monitoring is the increase in accuracy which allows the petroleum professional to modify field operations with certainty and thereby maximize both productivity and recovery. This more accurate monitoring and prediction of the position and movement of fluids in a producing hydrocarbon reservoir can yield major economic benefits.

The reliability of reservoir simulation and production forecasting is often limited by the accuracy of the reservoir description. Many enhanced-oil-recovery project failures can be attributed to poor-quality reservoir modeling leading to overoptimistic forecasts of reservoir performance, usually the result of inadequate reservoir-heterogeneity descriptions. Seismic measurements are the main source of information about the reservoir away from wellbores. Extracting reservoir-related information from seismic data in addition to the usual structural information is a continuing trend. Of particular interest is time-lapse seismic reservoir monitoring *(Smith et al. 1998)*.

The recent increase in oil demand and oil prices make unconventional reservoirs (especially heavy oil reservoirs) more attractive for the industry. Heavy oil reservoirs demand a tremendous effort to develop new solutions, mainly because the recovery factor for these reservoirs is still very low. Steam injection is the only proven thermal technique to be used for this purpose and it can be achieved through continuous or cycle injection.

The capability for monitoring enhanced oil recovery (EOR) processes in situ has become increasingly important. A knowledge of the developing processes in real time allows the possibility of controlling and/or modifying the processes involved. In particular, one would

like to determine the size, position and details on the shape or preferred direction of growth of the steam zone. Information about the distribution of fluids inside the zone is also highly desirable. Diagnosis of the above features could lead to improved heavy oil extraction techniques and more efficient field operations.

In enhanced oil recovery (EOR) a number of processes such as steam stimulation, steam drive, combustion (fire flooding) and CO_2 stimulation can be used to initiate recovery in the case of heavy oil sands, or to increase recovery efficiency. Reservoir characterization is very important before starting an EOR project because of the possibility of failure due to reservoir heterogeneities and anisotropy. Also, reservoir surveillance during an EOR process is critical for the evaluation of EOR efficiency.

In a steam injection project, it is desirable to determine the size and shape of the heated zone around a steam injection well and to determine the distribution of fluids in the subsurface without carrying out expensive exploratory drilling. Drilling, in any case, modifies the properties of the stratigraphic layers so there is uncertainty as to the true subsurface conditions *(Kanasewich et al. 1999)*. Furthermore, the drilling fluids circulating within the observation wells are known to alter the conditions of the medium in the immediate vicinity of the well. The result is that the obtained measurements are believed to give an inaccurate representation of the changes occurring within the reservoir during enhanced oil recovery (EOR) operations *(Kanasewich et al. 1999)*.

1.2.   Enhanced Oil Recovery (EOR)

Enhanced Oil Recovery is generally considered as the third and finally the last phase of useful oil production, usually called tertiary production *(Donaldson et al. 1985)*. The primary phase of oil production begins with the discovery of an oilfield using the natural stored energy to move the oil to the wells by expansion of volatile components and/or pumping of individual wells to assist the natural drive. Natural drive mechanisms during primary production are: solution gas, water influx and gas cap drives, or gravity drainage. When this energy is depleted, production declines and a secondary phase of oil production initiates when supplemental energy is implemented to the reservoir by injection of water. As the water to oil production ratio of the field approaches an economic limit of operation, the tertiary period of production begins, called Enhanced Oil Recovery (EOR) *(Donaldson et al. 1985)*. Tertiary processes are designed to recover oil, commonly described as residual oil left in the reservoir

after both primary and secondary (waterflooding) recovery techniques have been exploited to their respective economic limits.

In addition to economic reasons concerning the existence of residual oil, there are also some technical ones. In the first place, a common waterflood, operated at practical rates with ordinary water or brine, is physically incapable of displacing all the oil from reservoir rock. Capillary forces acting during the waterflood process may cause part of the oil to be retained, in water-wet rock at least, as disconnected structures which do not flow under the pressure gradient that arises from flow of water *(Donaldson et al. 1985)*. The detail of these structures is directly related to the microscopic mechanism of oil entrapment. Thus, even in those regions of the reservoir which are relatively well-swept, a residual oil saturation S_{or} (15 to 40% of pore space) will be retained. The residual oil saturation in these well-swept regions, of proven accessibility with respect to injected fluids, is an important target for tertiary oil recovery *(Donaldson et al. 1985)*.

Secondly, oil is present in large areas of waterflooded reservoirs at saturations over and above those typical of swept regions. These saturations are determined by macroscopic processes such as sweep in the reservoir. This oil, which is present in less accessible parts of the reservoir but at higher saturations, is a second challenging target for tertiary oil recovery *(Donaldson et al. 1985)*.
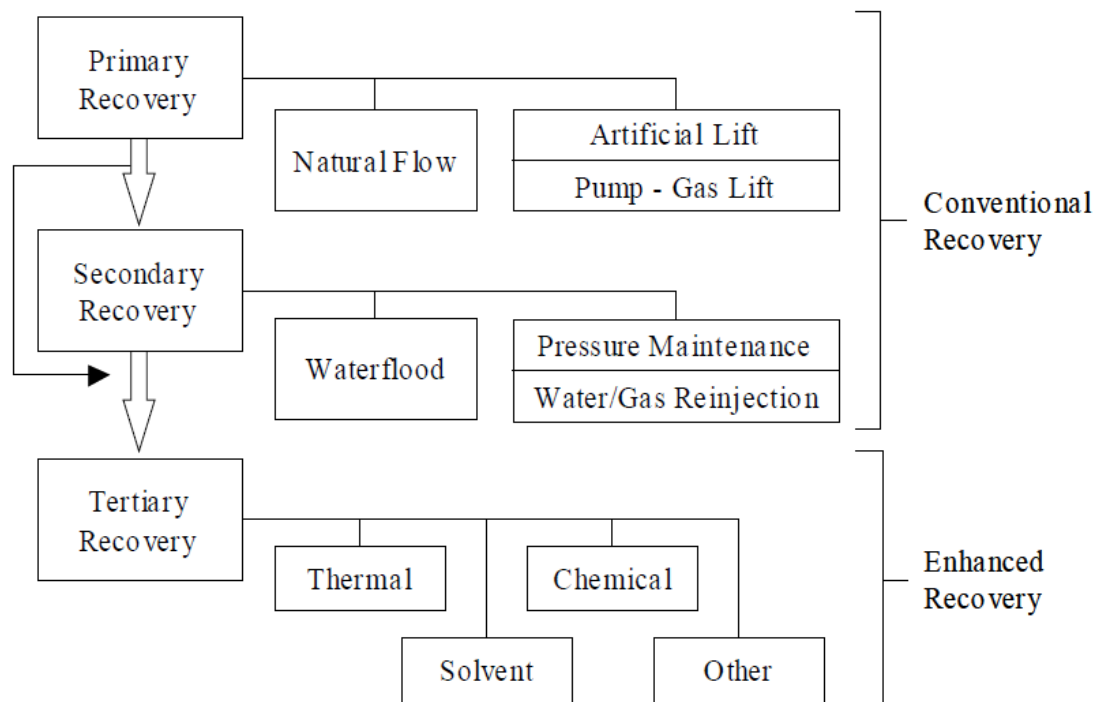
Figure 1.1: Types of oil recovery (Donaldson et al. 1985)

Secondly, oil is present in large areas of waterflooded reservoirs at saturations over and above those typical of swept regions *(Donaldson et al. 1985)*. These saturations are determined by macroscopic processes such as sweep in the reservoir. This oil, which is present in less accessible parts of the reservoir but at higher saturations, is a second challenging target for tertiary oil recovery *(Donaldson et al. 1985)*.

In practice, is difficult to distinguish between these two categories of residual oil. Certainly in either case, for a successful EOR operation, the residual oil will have to be displaced from its present location and moved to the production wells.

1.2.1. Steam flooding

Steam flooding, as illustrated in *Figure 1.2* is a simple process in principle. Steam is generated at the surface and injected into a central well to drive the oil to peripherical production wells through a combination of:

1.   thermal release of the oil from the sand,
2.   reduction of the oil viscosity and
3.   pressure drive of the oil to the production wells.

The mechanism of oil displacement is a combination of interacting physical changes, such as viscosity reduction and steam distillation, which can be visualized as separate advancing fronts *(Donaldson et al. 1985)*.

Steam injection is a method of thermal recovery in which steam produced at surface is injected into the reservoir through spatially distributed injection wells. In steam injection, temperatures are high enough so as to lower viscosities and as a consequence to mobilize oil. Steam quality, or even liquid water content, may vary substantially both in time and among different project regions. Nevertheless, the steam eventually condenses into water, often near the injection wellbore. Pressures are usually low, since this is typically a near surface process. As temperature increase, density and seismic velocities will decrease, primarily due to the temperature effects on the pore fluid. These velocity decreases are followed by a further reduction as the pore fluid changes phase from liquid water to steam *(Figure 1.3)*.

STEAM FLOODING

Heat, from steam injected into a heavy-oil reservoir, thins the oil making it easier
for the steam to push the oil through the formation toward production wells.

Heat reduces viscosity of oil and increases its mobility.
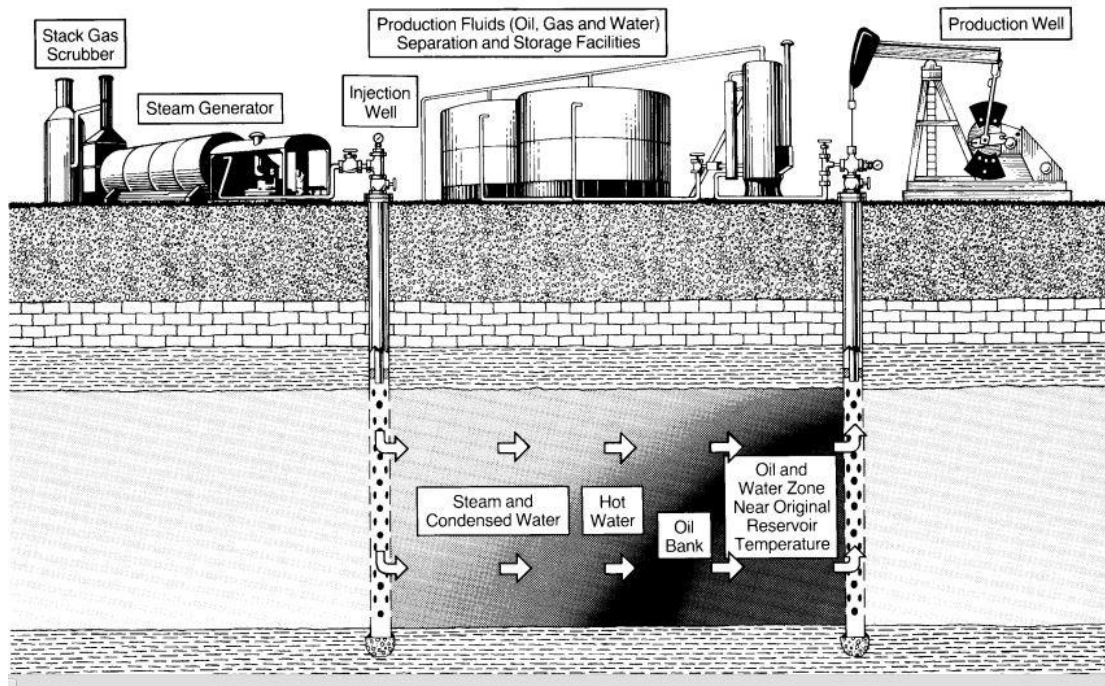
Figure 1.2: Schematic diagram of steam flooding (Donaldson et al. 1985)
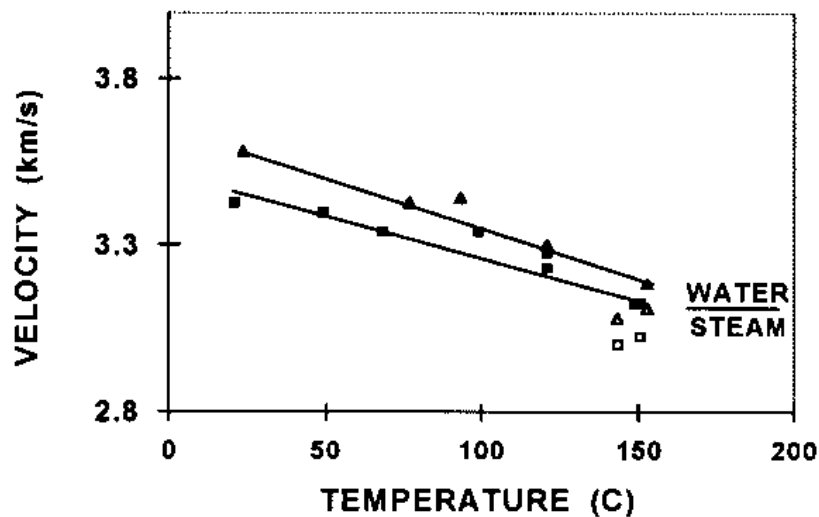
Figure 1.3: Temperature and saturation effects on compressional velocity. (Solid symbols: water saturated, open symbols: steam saturated) (Batzle, Christiansen, and Han 1998)

The steam injected into the reservoir displaces the heavy oil from the pores of the medium and consequently causes an increase in compressibility of the formation; hence the

compressional seismic velocity is decreased. Since only volumetric changes occur, shear seismic wave velocities do not change as much.

Steam injection into heavy oil formations has become an integral part of thermal oil recovery operations. Remarkable recovery problems can be encountered in these accumulations as the oil in place has very high viscosity and is practically immobile within the geologic formations of occurrence. Compositions and phase vary across the reservoir profile. Both the elevated temperature and gas (steam) saturation result in low velocities near the injector. *Figure 1.4* shows the expected pore fluid profile and velocity profile expected across such a steam process. The initial steam, saturated zone may not be extensive. As heat is dispersed into the reservoir formation, hot water condenses and finally a bank of high water saturation is formulated in front of the steam front. A bank of mobilized oil preludes the hot water bank. Just from fluid saturation conditions, there are expected lower velocities in the steam zone but greater velocities in the water and oil zones. Usually, these types of floods are performed in shallow reservoirs with low pore and effective pressures and therefore rocks are sensitive to injection pressures.
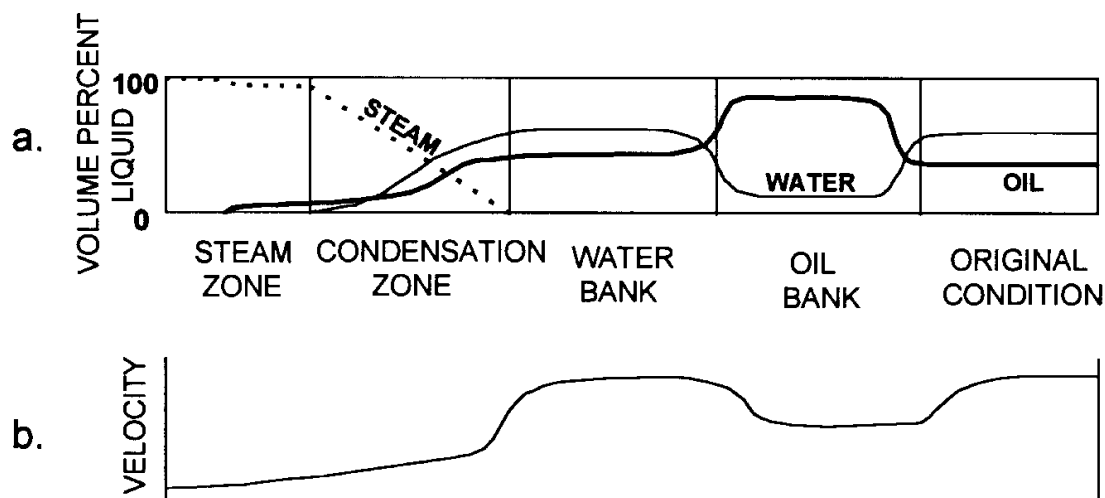
Figure 1.4: (a) Schematic fluid saturation profile during a steam flood (modified from Tadema, 1959). (b) Expected compressional velocity (Batzle, Christiansen, and Han 1998)

Another cooperating factor that enhances oil production during steam injection process is relevant to near wellbore cleanup. In this case, steam reduces the artificial tension that ties paraffins and asphaltenes to the rock surfaces while steam distillation of light ends of crude oil creates a small solvent bank that can miscibly remove trapped oil. Steam injection is also called steamflooding or even steam drive.

Steam EOR processes are concerned with the liquid and gas phases and the changes from one phase to another. The phase change region that water co-exists as liquid and gas is where our interest lies considering steam for use in the oil field.

1.3.   Seismic Reflection and Time – Lapse Reservoir Monitoring

Reflection seismology is a method of geophysical prospecting that uses the principles of elastic wave propagation to quantitatively estimate and image properties of the Earth's subsurface. Seismic exploration is the primary method of exploring for hydrocarbon accumulations, and although the technology of exploration techniques has improved dramatically in the past 50 years, the basic principles for acquiring seismic data have essentially remained the same. In simple terms, the general principle is to send sound energy into the Earth and record the sequence of reflected energy that returns from different layers in the subsurface. Once this energy is recorded, it can be processed to make images and extract quantitative information about the subsurface *(Bianco 2008)*.

Time-lapse seismology is the term used to describe the practice of collecting multiple seismic data sets over a period of time at a place where the subsurface properties are changing. Time-lapse reservoir monitoring enables geoscientists to study the evolutionary behavior of fluid-producing reservoirs. This knowledge is extremely important and increasingly urgent for the energy industry.

Staging seismic surveys over time to monitor producing reservoir can establish fluid positions today vs. yesterday and can be used to predict fluid movement more accurately. The also help identify bypassed oil and hydraulic barriers and can reduce the risk of early breakthrough and lost wells. Thus, filed operations can be modified more efficiently to maximize reservoir productivity and percentage recovery.

The simple physical principles of the time-lapse seismic method are shown in ***Figure 1.5***. If we survey a producing oil or gas reservoir before and during production, there can be estimated changes to the reservoir. As hydrocarbons are replaced by other fluids, and as pressure and temperature change, the seismic velocity and density of the reservoir will change. From time-lapse surveys, we can measure the effects of those changes and identify where the changes are occurring in the reservoir. Time lapse monitoring is valuable anytime fluids are under pressure into the subsurface, whether for CO_2 sequestration or for enhanced oil recovery

(EOR). For safety and also for economic reasons, it is important to track where the injected fluids are going.
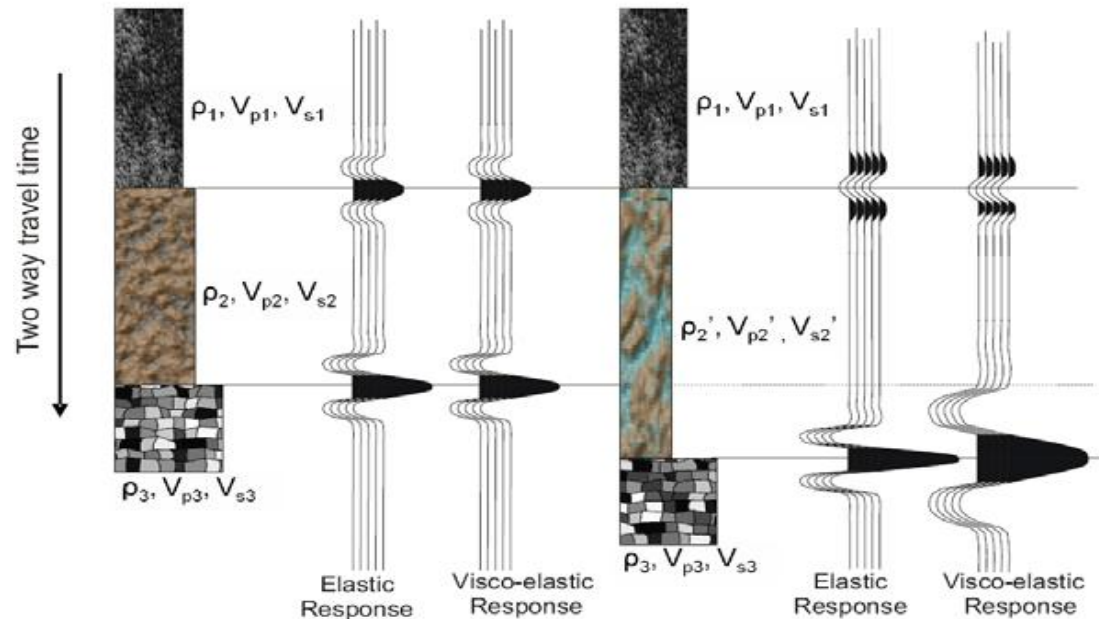
Figure 1.5: *Schematic of geophysical time-lapse monitoring. The width of the hypothetical lithology blocks shown here are proportional to the elastic impedance of each rock type. Density, P-wave velocity and S-wave velocity change as a result of production and recovery processes. The full visco-elastic response will be sensitive to changes in the travel time, the amplitude and the frequency characteristics of each reflection event. Elastic waves do not take into account dispersion and attenuation, so they are an approximation of real earth materials (Thompson 1960)*

Seismic velocity and density changes that are caused to a producing reservoir depend on many factors, such as: the rock type, the fluid properties and finally the depletion mechanism. Time-lapse seismic responses may be caused by numerous factors. External factors such as ambient noise and seasonal variations in the weathering layer can have significant changes over time and may overwhelm any time lapse differences coming from the reservoir (*Figure 1.5*). Geometry and equipment repeatability is a major issue with time-lapse surveys.

Time-lapse analysis is becoming popular as many reservoirs are being depleted and tertiary recovery methods are applied. This is because time-lapse analysis helps detect remaining oil and gas in a reservoir.

It is important to recognize that differences may occur in seismic data even though there are no changes in reservoir properties, due of variations in acquisition or processing of the data sets. The observations made on seismic time – lapse studies usually include changes both in amplitude and in time. Any changes in amplitude can often be used to directly image fluid migration because the reflection character changes as a consequence of replacing oil/water.

Other changes in reservoir properties must always be taken into consideration, such as effective pressure acting on the rock matrix.

The change in seismic velocity between different monitoring surveys will also result in a differentiation of two – way travel time to reflectors that lie below the reservoir. This velocity may be monitored and provides an indication of the spatial location of reservoir changes.

In an effective time lapse study, changes in the reservoir must cause a detectable change in the seismic parameters. A time lapse study is based on two fundamental factors, called repeatability and detectability. Repeatability is the indicator of how identical is the baseline survey in comparison with the monitor surveys concerning acquisition and processing. For efficient time-lapse seismic surveys both acquisition and processing repeatability should be almost identical. In this case, they would have identical traces at respective locations *(Dixit and al., 2012)*.

The term detectability signifies the ability of the reservoir parameters, such as pressure, saturation and temperature to create considerable change in seismic properties. Basic constants that are immediately affected by production are bulk modulus, shear modulus and density, which all subsequently affect P-wave, S-wave and density *(Dixit et al., 2012)*

Changes in the reservoir rocks:

- Confining pressure
- Fracturing / damage / creep
- Pore pressure
- Temperature
- Chemical weakening / strengthening
- Volumetric expansion / contraction

Changes in the reservoir fluids:

- Fluid substitutions
- Saturations
- Pore pressure
- Temperature
- Viscosity

Changes in the overburden:

- Subsidence / expansion
- Fracturing / damage / creep

SIGNAL

What we measure. . .

- Travel time delays
- Amplitude changes
- Frequency changes
- Attenuation / energy losses
- Scattering effects

Things that might get in the way. . .

- Weathering conditions, velocity changes in the near surface (seasonality)
- Source type
- Source coupling (vibrator source ground force)
- Source positioning (geometry repeatability, directivity effects)
- Receiver type
- Receiver coupling
- Receiver positioning (geometry repeatability)
- Cultural noise, electronic noise, ambient noise, and shot generated noise

NOISE

Figure 1.6: Many parameters and properties change both inside and outside of the reservoir when the fluids are produced. Seismic monitoring is faced with the challenge of ensuring useful information (signal) can be distinguishable and extracted in the midst of 'noise (Thompson 1960)

1.4.　　Seismic parameters affected by other factors

The objective of this study is to determine the locations of the injected steam within the reservoir using time-lapse analysis. It is known where the injection well is in the reservoir but through this process we try to identify where the injected steam has moved to within the reservoir.

Seismic wave velocities within a rock are dependent on the elastic constraints of the rock, including porosity, pore fluid, consolidation, temperature and effective pressure. Any deviation in these parameters will result in changes in the seismic wave velocity throughout the rock. Steam injection into a reservoir causes changes to some of the elastic constraints, resulting in reductions in P-wave velocity. Reductions in shear-wave velocities were also noted but to a lesser extent than the decrease in P-wave velocity.

Seismic reflections arise from contrasts in the acoustic impedance (velocity and density) of rock. Laboratory investigations focused on the impact of EOR processes on acoustic impedance in reservoir rocks and fluids imply that changes in reservoir properties may be detected in-situ using seismic methods.

Velocity changes related to recovery processes may be caused by:

1. Changes in the compressibility of the pore fluids and thus in the overall rock. The injected fluids displace hydrocarbons, increasing the overall compressibility of the reservoir rock and lowering the velocity. During steam injection, because of high pore pressure, the free gas present in oil-sand reservoir is forced back into solution. The free gas reduction will cause a decrease in the fluid compressibility and thus a velocity increase and a decrease in the corresponding seismic amplitude *(Kalantzis et al., 1996)*.

2. Gas cap formation and movement. Gas is highly compressible and the compressibilities of both the pore fluid and the overall rock will increase substantially, decreasing the seismic velocity. The density also decreases. This is the basis for conventional direct hydrocarbon indicators such as seismic 'bright spots'.

3. Temperature changes and the presence of gases in thermal EOR processes. Both an increase in temperature and the presence of gas decrease seismic velocities and density.

4. Pore fluid pressure changes because of fluid injection or withdrawal. Fluid injection will increase fluid pressure, decreasing the effective stress and lowering seismic velocities. Pressure decline will result in increasing velocity until the bubble point is reached. At that point, gas release will result in a decrease in seismic velocity.

1.4.1. Pressure

The seismic parameters, and foremost the seismic velocity and the density, are affected by pressure, temperature, fluid type and porosity. Another parameter is:

$$\sigma = S - p$$

where

σ: the net or the effective pressure

S: the overburden pressure

p: the pore pressure.

The effective pressure (σ) that acts on materials is usually taken to be the simple difference between lithostatic pressure and pore pressure. The moduli of rocks can be highly dependent on the effective pressure and consequently changes in the effective pressure will result in variations in the seismic velocities. Low effective stress and high dilation during a steam injection process, results in higher rock frame compressibility. This, as a consequence, results in lower compressional velocity and higher amplitude seismic events *(Kalantzis et al., 1996)*.

Usually, the overburden pressure remains the same in time-lapse seismic but the pore pressure will change during production. A decrease in pore pressure would mean an increase in net pressure. Increasing net pressure in the reservoir would cause the velocity to increase and the density to increase.

Usually, velocities tend to increase with the effective pressure. The explanation for this behavior is that the pores close at higher pressures. This compaction consequently increases the effective stiffness of the rock and results in the better grain-to-grain coupling which directly leads to the velocity increase. This increase, however, is not unlimited. Once all cracks and pores are closed, despite the continuous increase in the effective pressure, the velocity only increases slightly. When the effective pressure remains constant, the velocity is usually considered not to change in clean sandstone rocks.

1.4.2. Temperature

Temperature dependent variations of seismic velocities are mainly due to the rock property variations represented by the two parameters, the bulk modulus and the density. In general, the viscosity of the

bitumen decreases as its temperature increases. Consequently, the bitumen's bulk modulus decreases. When temperature increases, compressional velocity usually decreases significantly and shear velocity increases slightly.

It should be mentioned that time-lapse changes are easier to detect in steam injection recovery processes than in CO_2 and gas injection recovery processes, because an increase in temperature and pressure can significantly affect the physical property of the rock.
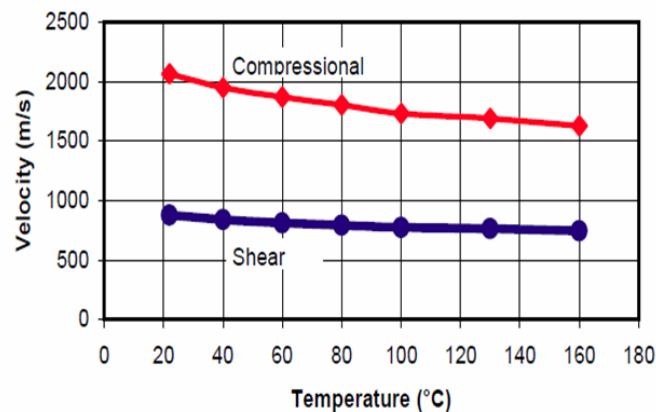
Figure 1.7: Many parameters and properties change both inside and outside of the reservoir when the fluids are produced. Seismic monitoring is faced with the challenge of ensuring useful information (signal) can be distinguishable and extracted in the midst of 'noise (Watson et al., 2002)

The compressional velocity decreases by 10% to 15% in well-consolidated sandstones saturated with heavy oil and by 15% to 40% in unconsolidated heavy oil and tar sands. The temperature dependence of the velocities is interpreted in terms of a phase transition of the heavy hydrocarbons and high pore pressure generated by the thermal expansion of the hydrocarbons *(Kanasewich et al. 1999).*

1.4.3. Effects of pore fluid type and saturation

Fluid saturation increases the P-wave velocity in the rock as predicted by Gassman's relation *(1951)* due to the increase of bulk modulus of the rock-fluid aggregate. The influence of the pore fluid type on the acoustic velocities, separately from its pressure, depends on its compressibility. When pore fluid is relatively incompressible (brine), the effective bulk modulus of the rock is high. In general, pore fluids tend to increase the compressional wave velocity because of their bulk modulus, but decrease the shear wave velocity slightly because of their density. When the pore fluid changes to steam, the compressional velocity drops sharply in comparison with that in the same rock fully saturated with water, however, the shear velocity does not change much *(Kanasewich et al. 1999).*

CHAPTER 2

Time Lapse Analysis Case Studies

Since the mid of 1980, there have been numerous applications of time-lapse seismic monitoring reported in the literature. Most applications to enhanced recovery have been thermal projects although the industry is gaining experience in monitoring CO_2 and other gas injection processes. Repeated seismic data have also been used to monitor gas leaks from casing failures. Seismic reflections arise from contrasts in the acoustic impedance (velocity x density) of rock. Laboratory investigations and theoretical analyses on the effects of enhanced oil recovery processes on acoustic impedance in reservoir rocks and fluids imply that changes in reservoir properties may be detected in-situ using seismic methods. Surprisingly, large changes are observed with temperature and pressure changes and with CO_2, flooding and hydrocarbon solvent flooding. Laboratory studies also show that waterflooding can, under certain conditions, result in detectable acoustic velocity changes.

2.1. 1st Case Study: Seismic monitoring of steam flooding in a depleted mobile heavy oil field: model studies of Steam Drive (SD) and Steam Assisted Gravity Drainage (SAGD)*

Time-lapse seismic monitoring has been one of the most efficient methods for detecting steam chambers. In most cases, the seismic velocities of a steam-saturated reservoir are very low compared to the oil-saturated case. However, in this study, it was found that free gas exists everywhere in the reservoir due to the long period of cold production prior to a steam injection. The velocity change after steam flooding is relatively low, less than 3 %. Thus, seismic monitoring of the steam chamber becomes such a challenging matter in these conditions. The modeling study shows that it requires high signal-to-noise ratios, greater than 10 dB, to estimate an accurate geometry of the steam chamber. In addition, it is observed that the time-lapse seismic images result to insights of the variations in hydrocarbon gas saturation.

Many different kinds of steam flooding methods have been developed such as Cyclic Steam Stimulation (CSS), Steam drive (SD), and Steam Assisted Gravity Drainage (SAGD). During these steam flooding processes, there should be monitored the expansion and migration of the steam chambers. Time-lapse seismic monitoring is one of the effective methods to estimate the volume of the steam

chambers. In this study, oil is mobile and its gravity is 8°. The reservoir is first produced based upon depletion. At some point, pressure becomes less than the bubble-point pressure and gas is released into the reservoir. Before starting steam injection, the seismic velocity of the reservoir is already low due to the presence of the hydrocarbon gas. As a result, the expected impact of steam flooding on seismic velocities is uncertain. Thus, a feasibility study is performed to investigate how steam flooding can be detected by time lapse seismic monitoring.

In this study, steam flooding is simulated with a thermal and compositional flow simulator which provides information concerning pressure, saturation and pressure information at continuous times (every six months). Then, the rock physic properties are computed based on laboratory measurements and well logs. Finally, the time-lapse seismic modeling is performed, based on the results of the flow simulation, for every 6 months.

Figure 2.1 shows the seismic velocity as a function of gas (mixture of hydrocarbon gas and steam) saturation with various temperature and pressure conditions. The main parameters which control seismic velocities are gas saturation and pressure. The temperature effects are rather small. The minimum gas saturation considered on the *x*-axis is 1 % since we assume that free gas exists due to the depletion. Thus, the injection of steam doesn't dramatically lower the seismic velocity.
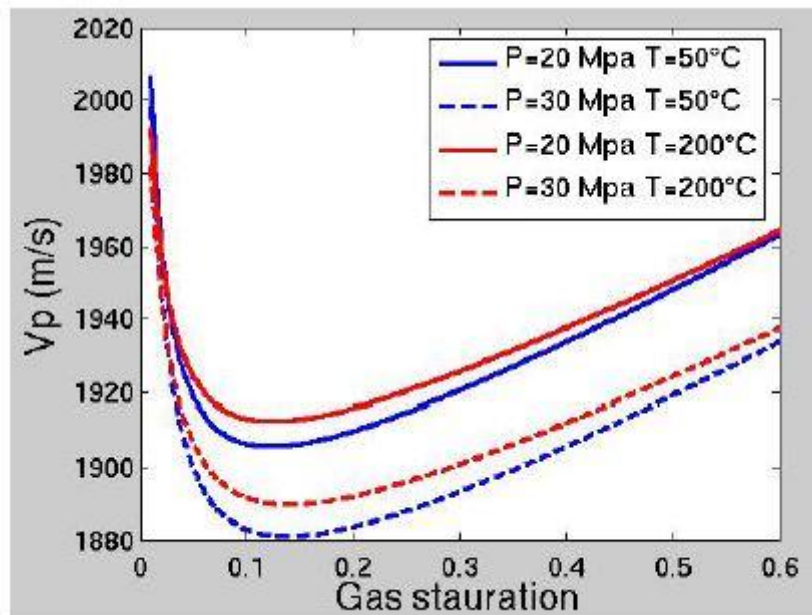
Figure 2.1: *P-wave velocity as a function of gas (mixture of hydrocarbon gas and steam) saturation at different pressure and temperature conditions. The minimum gas saturation on the x-axis is 1 %* (Yuh et al. 2009)*.

The reservoir is located at a depth of 300 m, with a pay zone thickness of 30 m, with no active aquifer. It consists of a homogenous sand with 30 % porosity and 15 mD permeability. The top and bottom of the reservoir consists of shale with a 1 % porosity and 1 mD permeability. The reservoir dimensions

are 550 × 300 × 30 m^3. The initial oil and water saturations in the reservoir are 0.8 and 0.2, respectively. The initial reservoir temperature and pressure are 46 °C and 41 bars. The reservoir simulation history includes a depletion period for 6 years followed by a steam injection phase for 20 years. After depletion, reservoir pressure drops to about 10 and 20 bars for SD and SAGD, respectively. Due to gravity, the released free gas is mainly observed on the top of the horizontal production wells.

A 2D full-wave seismic modeling is computed with 75 shots with 10 m spacing and 41 receivers, with 10 m spacing. These profiles cover the entire well configurations. The input wavelet for seismic modeling is Ricker with 90 Hz dominant frequency. After simple time processing, they applied the Kirchhoff pre-stack depth migration to enhance the images of the steam chambers.

There are simulated 20 years of steam flooding, after the 6 years of depletion period, for both SD and SAGD. The results after 4 years of steam flooding are shown in *Figures 2.2 and 2.3*. For the SD case, hydrocarbon free-gas disappeared after steam injection due to the high pressure injection of steam, (*Figure 2.2a*). The steam chamber is generated at the injection well with the maximum steam saturation of 60 % (*Figure 2.2b*). It has triangular shape. The pore pressure had increased as an amount of 5 bar compared to before steam injection. Pore pressure at production wells is lower than the injection well (*Figure 2.2c*) but there are not observed any bubble shape of pressured zone at the injection well. The temperature at the injection point is about 210 °C (*Figure 2.2d*). The zone of high temperature is much larger than the actual steam chamber. The seismic velocity, *Vp*, is computed based on the flow simulation results *(Figure 2.2e)*. The triangle shape of the red-colored zone represents high velocities. These high velocities are due to high steam saturation (>40 %) at the top of the reservoir and low steam saturation (<5%) at the bottom of the steam chamber. The velocity perturbations due to steam injection vary depending on the steam saturation. Thus, the size of the high velocity zone (red color in *Figure 2.2e*) is larger than that of the actual steam chamber.

The results obtained for the SAGD simulation after 4 years of steam flooding are shown in *Figure 2.3*. In this case the hydrocarbon gas has migrated to the top of the reservoir due to gravity (*Figure 2.3a*). *Figure 2.3b* shows two steam chambers. The pore pressure had increased as an amount of 9 bar compared to before the steam injection. It is lower at the steam chamber due to the same locations of production/injection wells (*Figure 2.3c*). The zone of high temperature is much larger than the actual steam chamber (*Figure 2.3d*). The V_p values are relatively lower than in the SD case, since the pore pressure is higher in SAGD. The top of the reservoir in the middle of the two wells shows a low velocity due to the occurrence of hydrocarbon gas. At the level of the steam chambers, the velocities are relatively low (*Figure 2.3e*).
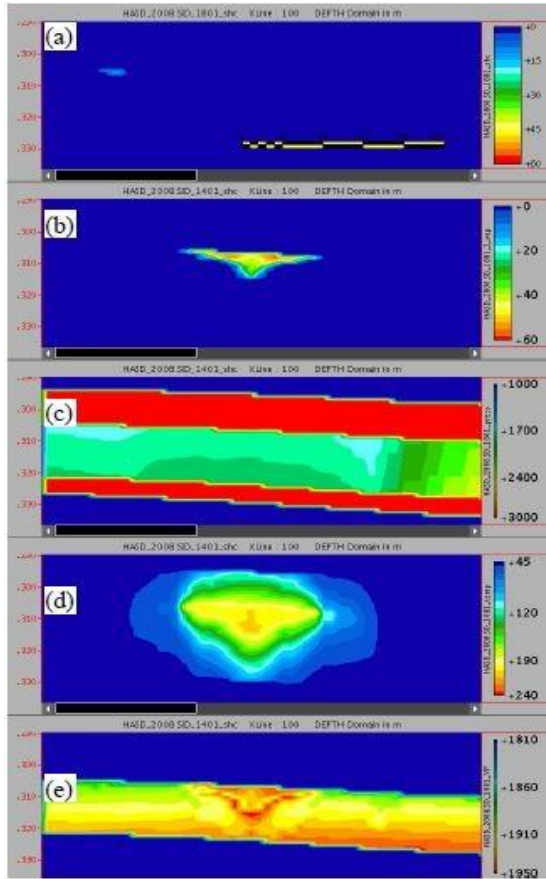
Figure 2.2: Thermal simulation results after 4 year process of Steam Drive (SD). Above figures represent (a) hydrocarbon gas saturation, (b) steam saturation, (c)pore pressure (KPa), (d) temperature (°C), and (e) P-wave velocity (m/s). (Yuh et al. 2009)
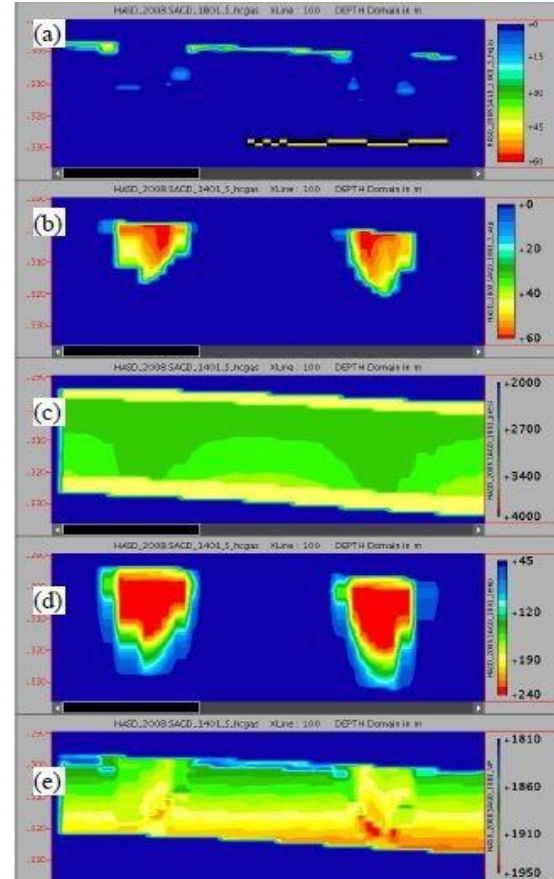
Figure 2.3: Thermal simulation results after 4 year process of Steam Assisted Gravity Drainage (SAGD). Above figures represent (a) hydrocarbon gas saturation, (b) steam saturation, (c) pore pressure (KPa), (d) temperature (°C), and (e) P-wave velocity (m/s). (Yuh et al. 2009)

The baseline survey for time-lapse seismic monitoring is given after six year depletion and just before the steam flooding starts. *Figure 2.4* displays the outcome from modeling of seismic monitoring every 6 months, and *Figure 2.5* one example of monitor surveys after a 4 year period of steam. Since there is a depletion period, there was at least 1 % of hydrocarbon free gas in the entire reservoir, especially at the top of the production wells. This caused the seismic velocity to be lower in the reservoir. Based on the rock physics model, the baseline Vp of the reservoir is lower than the steam flooded reservoir. *Figures 2.4a* and *2.5a* show that Vp increases after the steam injection in both the SD and SAGD cases. The blue colored areas in *Figures 2.4a and 2.5a* represent velocity decreases due to the increase of hydrocarbon gas saturations as an amount of 1 to 40 %. The seismic differences of (monitor line − baseline survey) are shown in *Figures 2.4b and 2.5b*. The steam chambers can be identified in the seismic images. Some polarity reversals of seismic traces are observed between the steam bubble and the hydrocarbon gas area in the SD case (*Figure 2.4b*).

In the SAGD case, two steam chambers apparently look like connected to each other (*Figure 2.5b*). This is not because two steam chambers are connected but because hydrocarbon gases exist between the two wells. The events below the steam chambers are not true 4D seismic anomalies. They are caused by the time-shifts after the steam flooding since they applied the same velocity model for PSDM. To estimate the magnitude of time-lapse seismic anomalies due to steam flooding, they normalize the seismic difference by the baseline seismic data *(Figures 2.4c and 2.5c)*. In the SD case, if we have the S/N ratios greater than 10 dB (blue color), they can accurately estimate the size of steam chamber *(Figure 2.4c)*. In the SAGD case, due to hydrocarbon gas, it is difficult to separate time-lapse anomalies purely caused by the steam chamber; and also, the bottoms of steam chamber are not clear if S/N ratios are less than 10 dB.
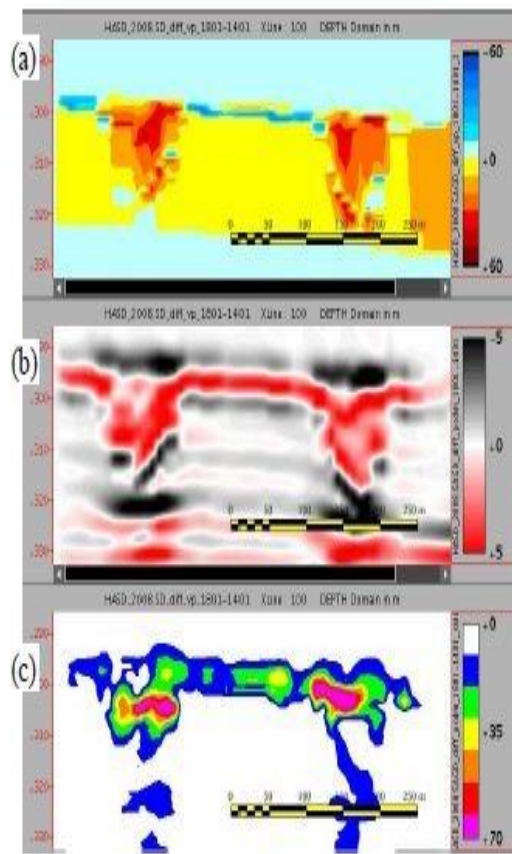
Figure 2.4: Time-lapse images after 4 year SD process. Above figures represent (a) Vp change (m/s), (b) Time-Lapse seismic difference of (monitor – base line), and (c) amplitude ratios of difference-seismic to base-line seismic (Yuh
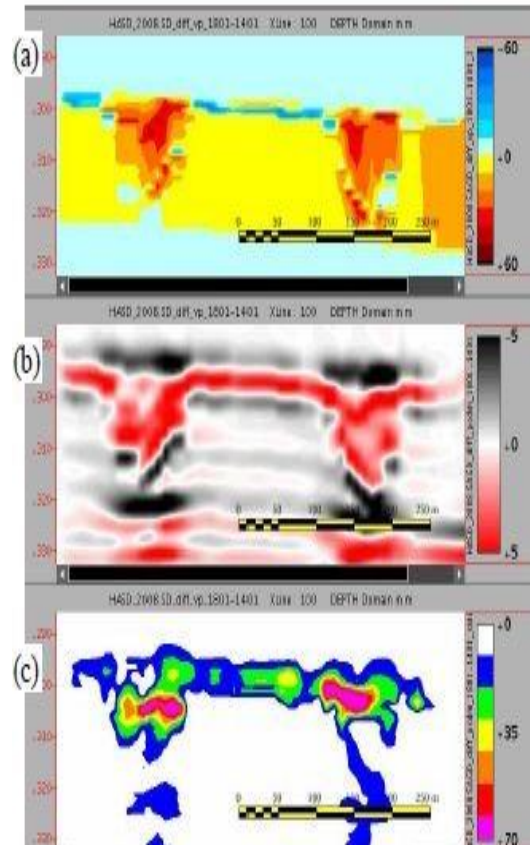
Figure 2.5: Time-lapse images after 4 year SAGD process. Above figures represent (a) Vp change (m/s), (b) Seismic difference of (monitor – base line), and (c) amplitude ratios of difference-seismic to base-line seismic (Yuh et al. 2009).

* *The paper entitled "Seismic monitoring of steam flooding in a depleted mobile heavy oil field: model studies of Steam Drive (SD) and Steam Assisted Gravity Drainage (SAGD)" by Yuh et al. (2009) is used as a reference for the above case study.*

2.2. 2nd Case Study: Seismic reflection modelling and imaging of a thermal enhanced oil recovery project at Cold Lake, Canada*

Enormous reserves of heavy oil appear in complex reservoirs of sands of Lower Cretaceous age in Alberta, Canada. This bitumen is a low gravity high-viscosity oil, which in fact is immobile under reservoir conditions. The movement of fluids away from the heated sources at the perforation level is controlled by permeability heterogeneities or fracturing and the induced anisotropy can play an important role in the efficiency of the EOR process. Therefore, it is useful to image the shape, areal extent of the heated zone and determine the rate of movement of the thermal front.

For the needs of that survey, wave simmulations (2D elastic and also 3D acoustic wave modelling) are carried out in order to model wave propagation through the reservoir prior to any EOR process, and during the steam injection and production cycles of the process. The resultant time-lapse seismic images may map the steam-heated zone, image changes in porosity and permeability, detect fractures and monitor gas caps.

Typical Alberta oil sand porosity is equal to 32% with tar saturation almost 81% and water saturation 19%. The sands are saturated with bitumen of a very high viscosity (about 150000cP). Generally, the Clearwater reservoir has an excellent horizontal continuity. However, the vertical continuity is occassionally interrupted by discontinuous shale barriers , tight cemented siltstones and calcified tight streaks that can affect the vertical conformance of the steam stimulation.

In 1990 there was initiated a 3D high resolution seismic reflection programme in the Cold Lake area. The first survey was carried out in 1990 during the 6th production cycle and the second survey was carried out in 1992 during the 8th steam injection cycle. The field acquisition geometry was identical in both surveys.

Each survey consisted of 296 geophones, buried 10m below the surface in an effort to improve the frequency content of the seismic signal, minimize statistical noise due to the weathering layer and eliminate subsequent survey difference caused by seasonal variations. Also, each survey consisted of 215 shot points buried at 18m depth below the surface. The energy source was dynamite at 125g per shot. The field data sample rate was 1ms. After stacking the data, each survey consisted of 89 inlines and 73 crosslines with bin size of 8x8m. The average fold of the data in the area of study is 20.

Computer simulations of seismic wave propagation were essential for the interpretation of field data. Two-dimensional and 3D finite difference modelling of seismic waves in acoustic and elastic media in the region of steam-heated zone, was performed in order to examine the relationship between rock properties and seismic characteristics, such as velocity and amplitude. A density model was generated

from density logs and a number of velocity models were used that were generated from sonic logs, the cross-well data and the migrated seismic data.

Synthetic zero offsets are shown in ***Figure 2.6***. The positive reflection event at about 0.44s has an increased amplitude (bright spot) during the steam cycle and is associated with the top of the steam zone. On the other hand, the reflection character between 0.45 and 0.5s is different in the two sections. Also, the positive reflection event ftom the top of the Devonian at 0.52s is reduced in amplitude (dim spot) during steam cycle.
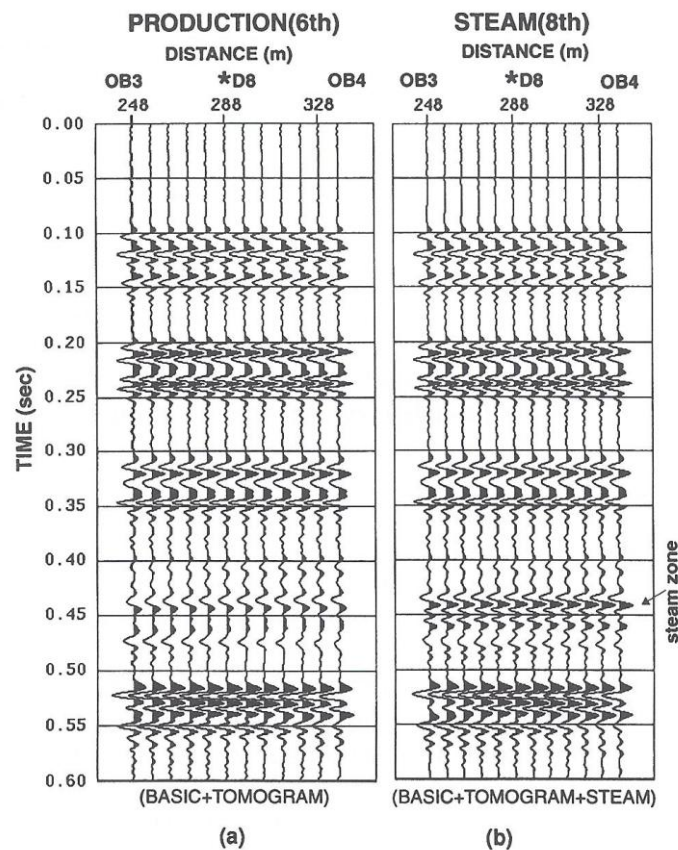
Figure 2.6: *Synthetic zero offset sections (vertical particle velocity component) from 2D elastic wave simulations during the 6th production cycle (a) and the 8th steam cycle (b). The seismic data are zero phase and negative polarity. (Kalantzis et al., 1996)*

Seismic analysis was performed on the migrated data over a 64x64 bin area that extents between inline 15-78 and cross-line 6-69. ***Figure 2.7*** shows inline 42 (depth profile) from both production (1990) and steam (1992) migrated data volumes. The reflectors in the area of the steam-heated reservoir (Clearwater) are highly resolved and significant seismic changes can be observed between the two data sets. Some of the profiles image fracturing that occurs during the steaming process.

Seismic analysis was performed on the migrated data. The generated images showed time delays and depth pushdown anomalies that are associated with the expanding steam-heated zone during the steam injection phase and the gas presence during production.

Based on the described reservoir conditions during the thermal process, the time, depth and amplitude anomalies that result from the differencing of the seismic images between steam and production cycles are the combined result of a decrease in the effective stress, temperature increase and gas reduction during the steam phase with respect to the production phase.
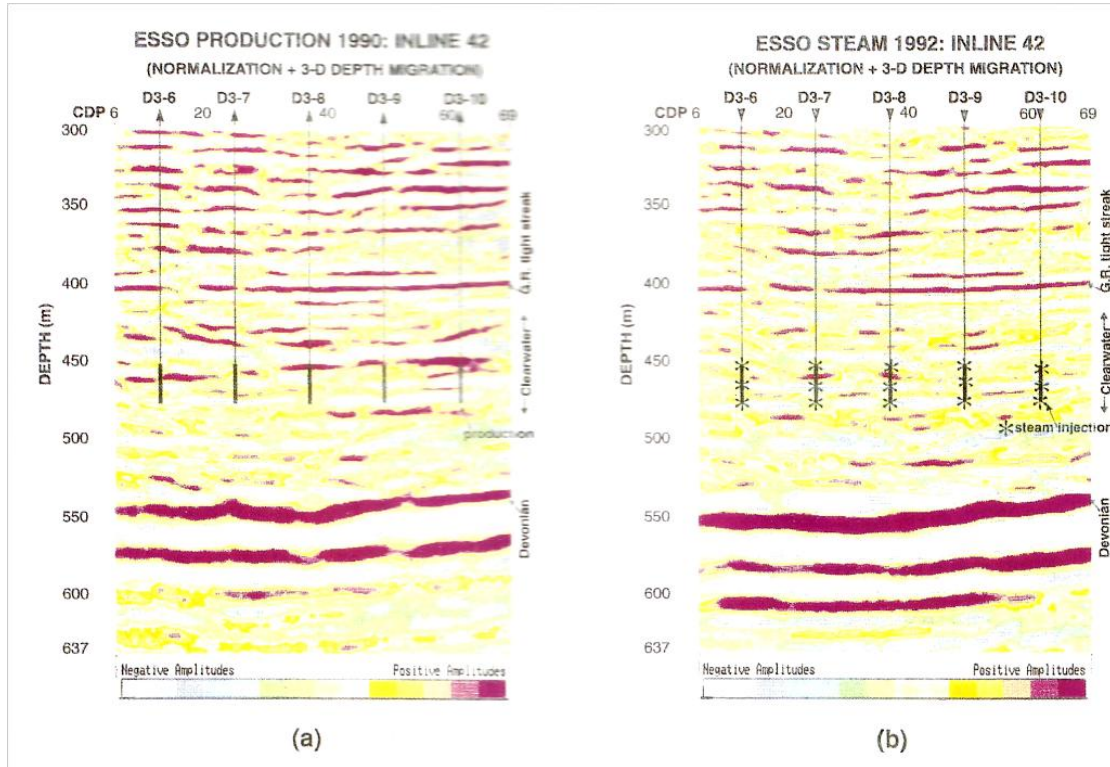
Figure 2.7: *Inline 42 from: (a) the production (1990) and (b) the steam (1992) depth-migrated data volumes. The seismic data are zero phase and negative polarity. (Kalantzis et al., 1996)*

The paper entitled "Seismic reflection modelling and imaging of a thermal enhanced oil recovery project at Cold Lake, Canada" by Kalantzis et al. (1996) is used as a reference for the above case study.

CHAPTER 3

Description and Characterization of Prinos Oil Field

The Prinos Oil Field is the main structure in the Prinos-Kavala basin located offshore the Gulf of Kavala. It covers an area of 4km^2 and is located in the North Aegean Sea, 6km northwest of the Greek island of Thassos, in water depths that do not exceed fifty meters. The only adjacent field is the small gas reservoir of South Kavala, 11km to the south. Both fields are traps in anticlines within the young taphrogenic Prinos basin. An ultimate oil production of 90 million bbl has been estimated.

The Prinos basin is the only geological region in Greece where oil and gas are being produced for more than twenty years. Exploration for hydrocarbons in this exact offshore area has started in the beginning of seventies and the first seismic campaign took place in the sea of Thrace in 1970 and the first oil recovery occurred in 1973. The search for oil in this place is under continuation. The total area covers 800km^2*(Proedrou et al. 2004)*.

3.1.   Tectonics

The Prinos basin is located at the southern edge of the pre-alpidic Rhodope massiv. It remained above the sea level during the Tethys-cycle and only during the middle Miocene started subsiding as a result of the pull-apart postalpidic tectonics that led to the breaking of the Aegean plate. The strike slip faulting of the North Aegean Sea left untouched the Prinos basin and the adjacent Miocene basins. The vertical pull-apart gravity tectonics is the dominant factor in the formation and development of these basins *(Proedrou et al., 2004)*.
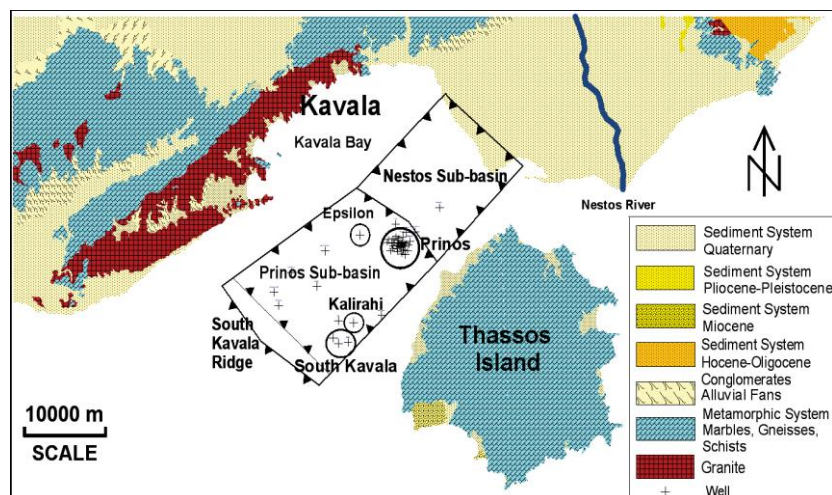
Figure 3.1: Oil and gas fields in Prinos-Kavala Basin (Kiomourtzi, Pasadakis, and Zelilidis 2008).

Marginal, long - extended and of large scale gravity faults of various angles surround the basin in NE-SW and NW-SE direction from the Nestos delta in the north to the South Kavala ridge in the south. These faults led to the taphrogenetic evolution of the Prinos basin. Many of them are active still today. Major internal faults, striking mainly northwest – southeast cross the basin and initiated the trapping mechanism *(Proedrou et al., 2004).*

Rollover type anticlines are formed syngenetically in front of these faults. The anticline formation goes in parallel with the sedimentation and occupies a large lithological section. The taphrogenetic Prinos basin with a length of 38 km and a width of approximately 20km between the islands of Thassos and Thassopoula and the mainland is subdivided into two sub basins separated by a topographic basement high located in the Ammodhis area *(Proedrou 1979).* The northern part forms the Nestos sub-basin and the southern, the most deep, the Prinos sub-basin. Additional sliding movements assisted by the salt deposition complicated further this area. Such a sliding fault underlies the Prinos field along the basal salt and moved the overlying formation to the south forming the broad North Prinos 1 anticline *(Figure 3.2)*. In this densely faulted area the majority of the Prinos traps are bound as rollover anticlines in front of syngenetic faults. Typical example is the Prinos field. The Epsilon and Ammodhis anticlines belong to the same classification. The South Kavala field in the south and the Nestos structure in the north are also dome-like anticlines in front of the marginal faults. The activation of the faults goes hand by hand with the sedimentation and their down thrown movement continues until recently. Their prints in the sea bottom can be traced in the seismic sections. Due to the flank steepness sliding events take place very often. A broad mainly E-W fault with a displacement of few decades to a few hundred meters crosses the basin in the southern part and leads to the formation of the peculiar fault trap of Kallirachi in conjunction with the NE-SW directed marginal fault.

The Prinos basin was open to the south to the open sea at the first stage of sedimentation. Gradually the Kavala ridge, a basement high between the island of Thassos and the opposite mainland, started to arise and led to the isolation from the sea and the transformation of the basin to a lagoon in the Messinian time. Similar the ridge, where the small island Thassopoula is sitting, in the northeast side, more probably was part time closed and participated to the full isolation of the basin. By that time a system of land-locked basins was developed in the North Aegean Sea *(Proedrou, 1979)*. It is very important to mention that all neogene basins adjacent to Prinos have similar geological evolution and consequently are the subject of high exploration interest.
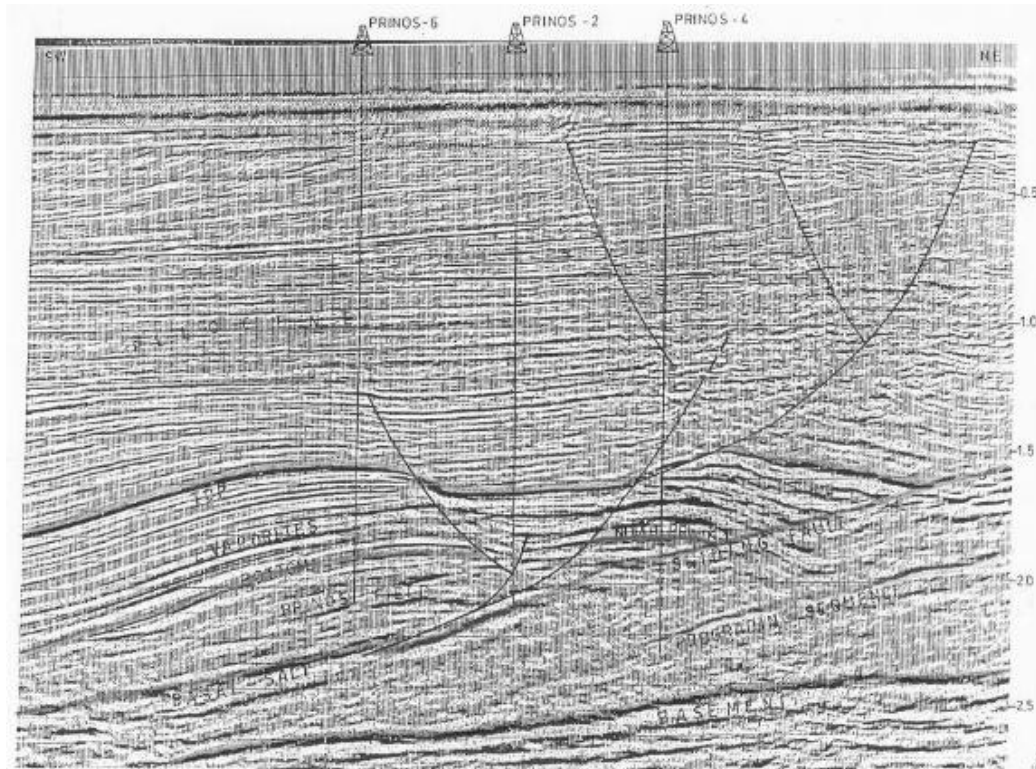
Figure 3.2: Northeast – southwest seismic section across the Prinos and North Prinos1 anticlines. The rollover of the seismic horizons in front of the faults is well illustrated (Proedrou 2004).

3.2.   Stratigraphy

Three main series dominate throughout the basin with distinct boundaries between them. They are the following:

➢ The Pre-Evaporitic Series

➢ The Evaporitic Series

➢ The Post-Evaporitic Series

They represent different sedimentological environments and normally their thickness increases towards the center of the sub basins. The basement consists of metamorphic rocks mainly gneiss, quartzite and dolomitic marble. The pre-evaporitic series starts with the breakup of the basin with the basal sediments and terminates just before the deposition of the main evaporite bodies *(Figure 3.3)*. The first deposits are of continental character, conglomerates with large basement components, sandstones, feldspatic, mainly immature, claystones and thick coal seams. According to the seismic interpretation these continental deposits were transported from northeast and southwest and moved with diminished thickness towards the center of the sub basins. The total section of the clastic deposits of the pre-evaporitic series is becoming very thick towards the basin center. The youngest of them have marine character and are mainly shale with sandstone intercalations getting coarser at the

25

periphery of the basin. They overlay the older ones with an unconformity. The above mentioned units are followed by a zone of limestone, dolomite and anhydrite layers alternated with clastics that cover the southern part of the Prinos - subbasin. Towards the center, to the deepest part of the basin, the anhydrite is replaced by salt layers, usually a few meters thick. At the top of the pre-evaporitic series an extended dark gray claystone deposition, characterized as zone D, dominates all over the southern sub-basin. It is petroliferous and strong carbonaceous. Sandstone intercalations are very often. Turbidite events of huge mass movement took place during that time and interrupted the still deposition mainly in the upper part of this zone. The Prinos turbidite (300m thick) is the most characteristic example. Equivalent to this zone is the prodeltaic zone of varves in the Nestos area.

The overlying evaporitic series is characterized by two facies. In the northern subbasin anhydrite and limestone layers 3 to 5 meters thick alternate with each other and with sandstones, claystones and marls. In the south seven to eight salt layers with increasing thickness towards the base of the section alternating with clastics comprise this series with total thickness up to 800 meters *(Figure 3.3)* The salt is white, gray, crystalline and often intergrown with anhydrite. Anhydrite and dolomite layers are often intercalated in this series. Postdiagenetic anhydrite nodules appear very often in the claystones.

The thoroughly clastic post-evaporitic series is characterized by the abundance of foraminiferes, nannoplactons and rests of algae that postulate a marine origin of Pliocene age. Towards the top coarse clastic sediments with abundant rests of molluscs point out to a deltaic, according the seismic, progressive sequence. Marine clastic sediments transgrate again over these deposits.
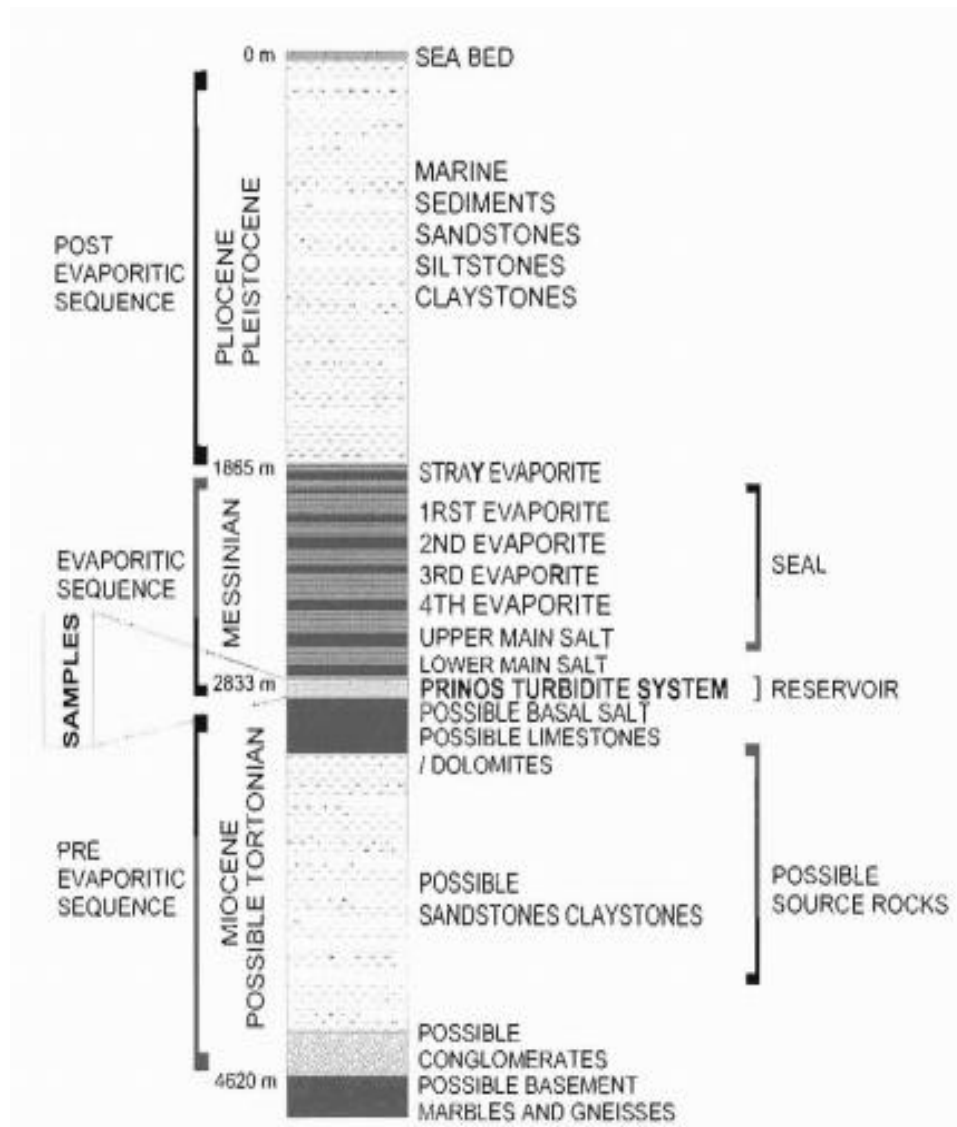
Figure 3.3: Chronostratigraphic column of the Prinos Basin (Kiomourtzi et al., 2007).

Sandstones and in minor degree siltstones compose the reservoirs. The depositional environment is deltaic, marine and turbiditic. But in the stratigraphic intervals where the oil has been trapped just below the evaporites or between them the depositional model is of turbiditic nature. The fast subsidence of the basin created a steep relief that led to the sediment movement from the flanks to the basin center or along its axis from areas topographically higher to the lower ones. The turbiditic nature is a very common type of sedimentation.

The evaporite horizons cover the whole basin and hold the upwards hydrocarbon movement below them. The A4/B2, C, D and E facies were recognized according to the turbidite facies classification. The A4/B2 facies provides the best reservoir quality representing channel deposits with high porosities and permeabilities. The C face still provides good permeable reservoirs as front channel

deposits. In opposite, E and D facies represent interchannel and distal deposits and consist mainly of claystones with thin sandstone intercalations forming reservoirs of low to very low quality.

Porosities and permeabilities are generally decreasing with increasing depth due to compaction, clay content and dolomitisation. There is a rapid decrease in the porosity and permeability parameters below the oil - water contact due to the dolomitisation that took place after the oil migration and was influenced by the formation water.

3.3.   Depositional Model

Miocene sedimentation began with continental deposits and was followed by deposits of marine shales with interbedded sandstones. Restricted environments, during which salt and anhydrite beds were formed, occurred at least three times during the Miocene. The first interval, 40 – 50 m thick, is found very close to basement. The second, a few tens of meters thick, accumulated just before deposition of the Prinos fan (main reservoir sandstones) and includes some dolomite. The third episode of restricted environment came at the end of the Miocene (Messinian) and resulted in the main evaporitic sequence within the Prinos Basin; it consists of several thick salt layers interbedded with sandstone and shale and has a maximum thickness of 800m. Deposition of marine clastics resumed in the Pliocene and has continued to the present.

3.4.   Exploration Concept

A small basin of such a young age can generate enormous quantities of hydrocarbons. This is the main conclusion that can be drawn from the long time exploration and production activity in the Prinos basin. This of neogene age taphrogenetic basin combines all the prepositions for oil generation, migration and accumulation in the trapping mechanisms.

The fast subsidence of this taphrogenetic basin created the frame for the accumulation of such a thick section of neogene and quaternary deposits and led to the extend deposition of turbiditic sediments and the good preservation of the organic matter as source for the oil generation. The existence of a good and thick salt cap rock holds the whole oil migration below it and prescribes the stratigraphic modeling of the prospects. The oil migration in the southern part of the basin reached up to the margins.

The growth fault tectonism led to the formation of the rollover anticlines, as trapping mechanism, all of them around the central deepest part of the basin where the main oil generation took place. The migration paths are consequently few kilometers long. The 3-D seismic helps to map the most complicated structures but it helps little locating the reservoirs. It is the task of the geological science to create the sedimentological models and locate the reservoir targets. The tracing of the turbidities for the location of reservoirs is the most difficult task in this basin.

Searching further for hydrocarbons the exploration is directed to any type of trapping located at the base of the evaporitic zone. Well sealed traps containing a sufficient permeable reservoir section are promising for more discoveries in an oil mature basin. Prinos basin established model should be considered as a guide in the exploration of the neogene basins in the Northern Aegean Sea with similar geological and geochemical evolution to that of Prinos.

3.5. Properties of Prinos Field

The main Prinos oil reservoirs are Miocene anticlines discovered in 1974, rich in H_2S with 60%.in the associated gas and the aquifer saturated in H_2S. The main Prinos oil field consists of three pressure independent stacked reservoirs having thickness 223, 109 and 48 meters separated by impermeable shales. The reservoirs are characterized by high permeability channels of 2000 mD with low permeability regions around 100 mD and even lower at the oil-water contact. Prinos oil gravity is 29° API, its Sulphur content is 3% and the Gas-Oil-Ratio is 820 SCF/BBL. Prinos associated gas contains 60% and 4% CO_2.

Prinos oil production started in 1981 and maximum production rate reached 27,250 B/D in 1984. The current volumetric estimate of 270 MM Bbls OOIP is considered low taking into account the inefficient Prinos oil displacement by the injected water. Initial pressures in the Prinos reservoir were between 5,850 to 6,100 psia. The current pressure is approximately at the range of 2000psia.
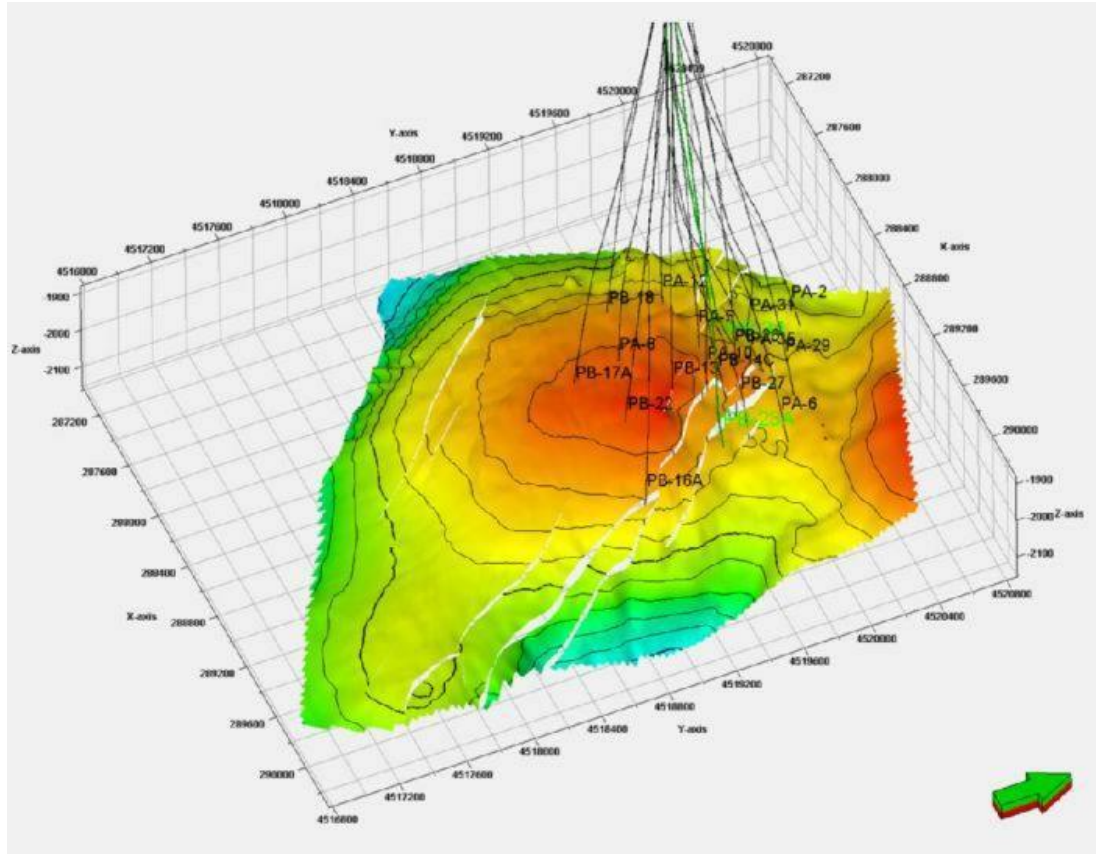
Figure 3.4: Prinos field 3D model visualization

Figures 3.5 and 3.6 show the exact section in Prinos field, where the seismic simulation is conducted. The direction of the seismic section is NW-SE and is mentioned with the colored diagonal line in the plan view of Prinos field.
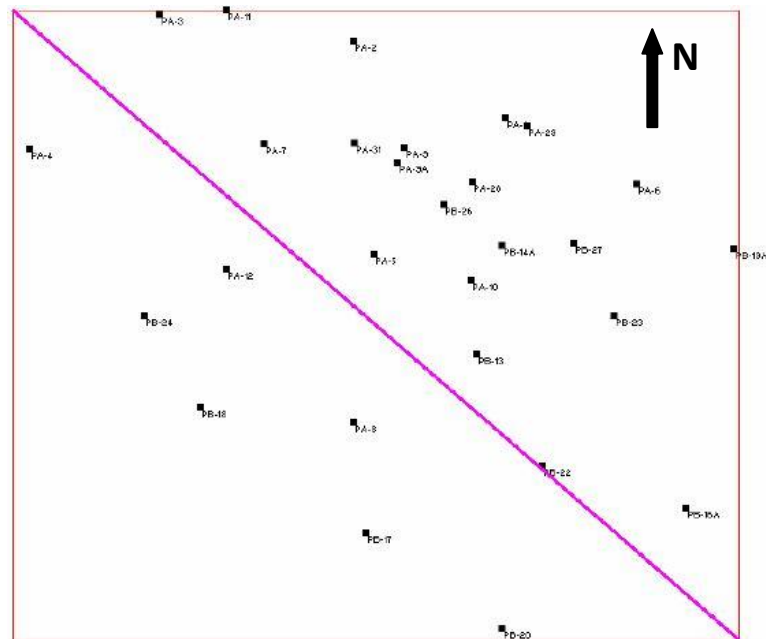
Figure 3.5: Plan view of Prinos Field and the diagonal (NW - SE) section where the synthetic reflection survey was implemented. (Michelakis, 2010).

The reservoir model is comprised of four sandstone layers (A1, A2, B, C). The seal of the reservoir (cap-rock) as well as the bedrock are geologically characterized as layered evaporites with alternations of clastics, according to the geologic data that are available. *Figure 3.6* was used in a digitization process with the aim to obtain all the coordinates of the section.
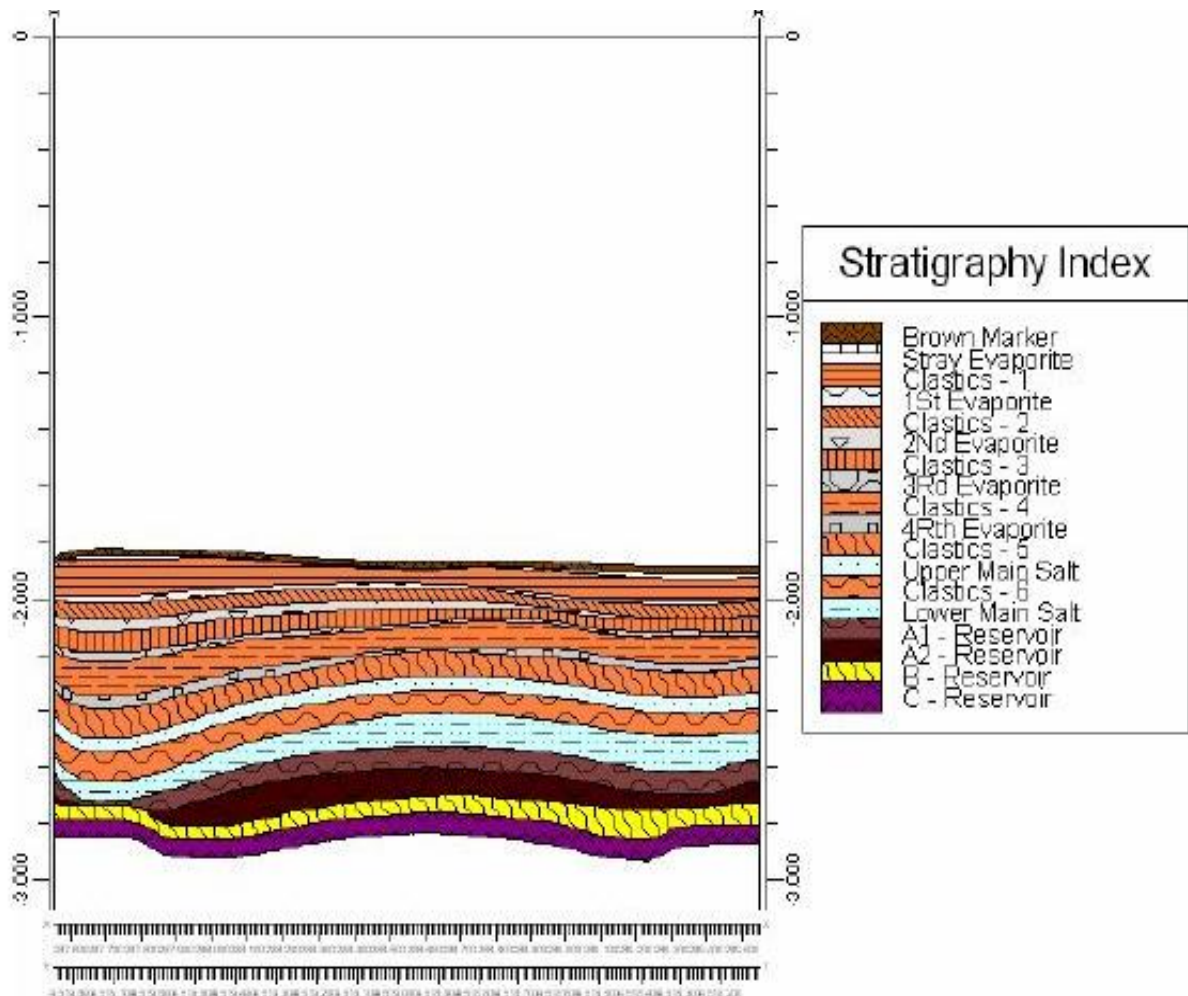
Figure 3.6: *Geologic section of NW-SE direction in Prinos field (Michelakis, 2010*

)

CHAPTER 4

Generation algorithm of synthetic seismic data

Synthetic seismogram is the result of one of many forms of forward modeling to predict the seismic response of the Earth. The synthetic seismogram is generated by the convolution of the reflectivity derived from digitized acoustic and density logs with the wavelet derived from seismic data. Synthetic seismograms, generated by solving numerically the elastic wave equations, represent a basic tool in seismology. As the acoustic wave equation does not provide for converted phases, a more realistic simulation is performed, using the heterogeneous elastic wave equation, allowing coupling between P and SV waves.

Finite-difference solutions to elastic wave problems can be obtained by either the homogenous formulation *(Alterman and Karal, 1968)* or the heterogeneous formulation *(Boore, 1972)*. Finite differences can be applied directly either to the second-order momentum equations (*Kelly et al., 1976)* or to the equivalent first-order *(Virieux, 1984, 1986; Bayliss et al., 1986)*. On conventional computers, finite-difference methods are time consuming and require large memory space for realistic models. The vectorization procedure of finite-difference schemes is based on the algorithm for matrix multiplications by diagonals which takes advantage of the vector operations.

A first-order system in two dimensions can be expressed as:

$$\partial_t U(x,z,t) = A\partial_x U(x,z,t) + B\partial_z U(x,z,t) \qquad (1)$$

, where U is a vector function of x, z and t. In problems of seismic wave propagation, U includes any relevant components of displacement and stress. A, B are matrices, containing the properties of the medium as functions of x and z with $0 < x < H_x$, $0 < z < H_z$. The symbol ∂_s denotes partial derivative with respect to a spatial or temporal coordinate s.

To set up the finite-difference method, there are selected two integers J > 0, M > 0 and the time step κ > 0. If H_x and H_z are the endpoints of the grid and h = H_x / J = H_Z / M, the mesh points (x_j, z_m, t_n) are defined by:

$$x_j = jh \text{ for each j=0, 1, . . . J}$$

$$z_m = mh \text{ for each m= 0, 1, . . . M}$$

$$t_n = n\kappa \text{ for each n= 0, 1, ...}$$

A modified Lax-Wendroff scheme *(Mitchell and Griffiths, 1981; Abramovici et al., 1987; Vafidis, 1988)*, when applied to **Equation (1),** results in:

$$
\begin{cases}
I - \dfrac{p^2}{4}\left[A_{j,m}\left(A_{j+1,m}+2A_{j,m}+A_{j-1,m}\right)+B_{j,m}\left(B_{j,m+1}+2B_{j,m}+B_{j,m-1}\right)\right]+ \\
\dfrac{p^2}{4}\left[A_{j,m}\left(B_{j+1,m}-2B_{j,m}+B_{j-1,m}\right)+B_{j,m}\left(A_{j,m+1}-2A_{j,m}+A_{j,m-1}\right)\right]
\end{cases} U^{n}_{j,m}
$$

$$
+\frac{p}{2}\left\{A_{j,m}\left[I+\frac{p}{2}\left(A_{j+1,m}+A_{j,m}\right)\right]+\frac{p}{2}B_{j,m}\left(A_{j,m}-A_{j,m-1}\right)\right\}U^{n}_{j+1,m}
$$

$$
+\frac{p}{2}\left\{B_{j,m}\left[I+\frac{p}{2}\left(B_{j,m+1}+B_{j,m}\right)\right]+\frac{p}{2}A_{j,m}\left(B_{j,m}-B_{j-1,m}\right)\right\}U^{n}_{j,m+1}
$$

$$
-\frac{p}{2}\left\{A_{j,m}\left[I-\frac{p}{2}\left(A_{j,m}+A_{j-1,m}\right)\right]+\frac{p}{2}B_{j,m}\left(A_{j,m+1}-A_{j,m}\right)\right\}U^{n}_{j-1,m}
$$

$$
-\frac{p}{2}\left\{B_{j,m}\left[I-\frac{p}{2}\left(B_{j,m}+B_{j,m-1}\right)\right]+\frac{p}{2}A_{j,m}\left(B_{j+1,m}-B_{j,m}\right)\right\}U^{n}_{j,m-1}
$$

$$
+\frac{p^2}{8}\left(A_{j,m}B_{j,m}+B_{j,m}A_{j,m}\right)\left\{U^{n}_{j+1,m+1}-U^{n}_{j-1,m+1}-U^{n}_{j+1,m-1}+U^{n}_{j-1,m-1}\right\} \quad (2)
$$

, where p=κ/h. The differencing star of this scheme is shown in **Figure 4.1.** It is a nine-point numerical scheme explicit in the vector U. Given the vector U at a given time, it is a simple matter to compute it at any other time by the above forward time marching process.
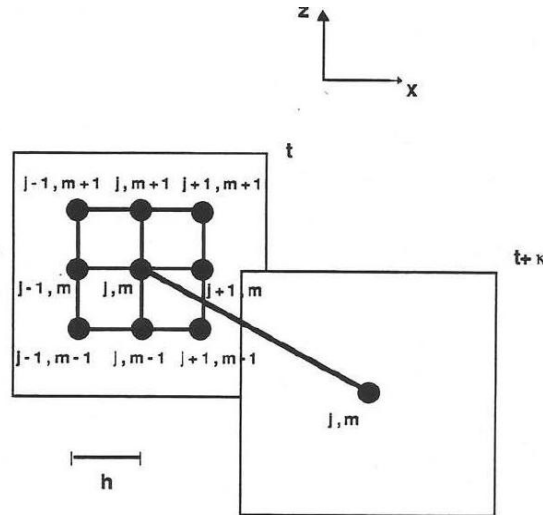
Figure 4.1: *The differencing star for the modified Lax-Wendroff scheme (Vafidis et al., 1992)*

There is also considered another method, based on the concept of splitting in time (*Strang, 1968*). The solution U of **Equation (1)** can be approximated by:

$$U^{n+2} = F_x F_z F_z^+ F_x^+ U^n \tag{3}$$

, where F_x, F_x^+ are one-dimensional difference operators approximating the solution of the one-dimensional equation:

$$\partial_t U(x,z,t) = A\partial_x U(x,z,t) \tag{4}$$

for constant z, while F_z, F_z^+ correspond to a similar partial differential equation with respect to z for constant x. Each operator advances the time parameter by a half-step so that the final output of the combined four operators is two time steps. One advantage of splitting methods is that stability properties are governed by the one-dimensional schemes. Besides, splitting methods have smaller phase error than a wide class of unsplit schemes.

A MacCormack scheme *(Gottlieb and Turkel, 1976)*, applied to **Equation (4)** consists of a predictor:

$$U^{(1)}{}_{j,m} = U^n{}_{j,m} - \frac{p}{6} A_{j,m}(7U^n{}_{j,m} - 8U^n{}_{j+1,m} + U^n{}_{j-2,m}) \tag{5}$$

and a corrector:

$$U^{n+\frac{1}{2}}{}_{j,m} = \frac{1}{2}\left(U^{(1)}{}_{j,m} + U^n{}_{j,m}\right) + \frac{p}{12} A_{j,m}\left(7U^{(1)}{}_{j,m} - 8U^{(1)}{}_{j-1,m} + U^{(1)}{}_{j-2,m}\right) \tag{6}$$

Taken together *Equations (5) & (6)* describe the operator F_x. To define the operator F_z, one replaces the changes in the index *j* by changes in the index *m*. F_x^+ is described by relations:

$$U^{(1)}{}_{j,m} = U^n{}_{j,m} + \frac{p}{6} A_{j,m}(7U^n{}_{j,m} - 8U^n{}_{j-1,m} + U^n{}_{j-2,m})$$

$$U^{n+\frac{1}{2}}{}_{j,m} = \frac{1}{2}\left(U^{(1)}{}_{j,m} + U^n{}_{j,m}\right) - \frac{p}{12} A_{j,m}\left(7U^{(1)}{}_{j,m} - 8U^{(1)}{}_{j+1,m} + U^{(1)}{}_{j+2,m}\right) \tag{7}$$

The Lax-Wendroff scheme is second-order accurate both in time and space, while the MacCormack scheme is second-order in time and fourth-order in space.

4.1.   Elastic Wave Propagation

The basic equation for two-dimensional SH-wave propagation in a heterogeneous isotropic medium, in absence of body forces, is:

$$\rho(x,z)\partial_{tt}u(x,z,t,) = \partial_x(\mu(x,z)\partial_x u(x,z,t)) + \partial_z(\mu(x,z)\partial_z u(x,z,t)) \tag{8}$$

, where u(x, z, t) is the displacement, μ (x ,z) the shear modulus and ρ (x, z) the density. Instead of solving numerically the second-order type hyperbolic wave equation one can use an equivalent first-order system. In matrix form the system is:

$$
\begin{bmatrix} \dot{u} \\ \sigma_{xy} \\ \sigma_{zy} \end{bmatrix} = \begin{bmatrix} 0 & \rho & 0 \\ \mu & 0 & 0 \\ 0 & 0 & 0 \end{bmatrix} \partial_x \begin{bmatrix} \dot{u} \\ \sigma_{xy} \\ \sigma_{zy} \end{bmatrix} + \begin{bmatrix} 0 & 0 & \rho^{-1} \\ 0 & 0 & 0 \\ \mu & 0 & 0 \end{bmatrix} \partial_z \begin{bmatrix} \dot{u} \\ \sigma_{xy} \\ \sigma_{zy} \end{bmatrix}
\tag{9}
$$

, where the dot denotes time derivative and σ_{xy} (x, z, t), σ_{zy} (x, z, t) are the stress components.

The problem of wave propagation when the Earth's response is resolved into components in the horizontal (x) and the vertical (z) directions only. To calculate the elastic response of a model on rectangular (x, z) coordinates, the corresponding first-order system is solved numerically. This system consists of the basic equations of motion in the x- and z-direction.

$$
\rho(x, z)\partial_t \dot{u}(x, z, t) = \partial_x \sigma_{xx}(x, z, t) + \partial_z \sigma_{zz}(x, z, t)
$$

$$
\rho(x, z)\partial_t \dot{w}(x, z, t) = \partial_x \sigma_{xz}(x, z, t) + \partial_z \sigma_{zz}(x, z, t)
\tag{10}
$$

and the stress-strain relations after taking the first time derivatives:

$$
\partial_t \sigma_{xx}(x, z, t) = (\lambda(x, z) + 2\mu(x, z))\partial_x \dot{u}(x, z, t) + \lambda(x, z)\partial_z \dot{w}(x, z, t)
$$

$$
\partial_t \sigma_{xz}(x, z, t) = \mu(x, z)\partial_x \dot{w}(x, z, t) + \mu(x, z)\partial_z \dot{u}(x, z, t)
$$

$$
\partial_t \sigma_{zz}(x, z, t) = \lambda(x, z)\partial_x \dot{u}(x, z, t) + (\lambda(x, z) + 2\mu(x, z))\partial_z \dot{w}(x, z, t)
\tag{11}
$$

, where u(x, z, t) and w(x, z, t) are the displacements in the x- and z-directions respectively, σ_{xx}, σ_{xz}, σ_{zz} the stress components, μ(x, z) and λ(x, z) the Lame parameters, ρ(x, z) the density and the dot denotes time derivative. In this formulation there are no space derivatives of the Lame coefficients.

Equations (10) and (11) can be written in the following matrix form:

$$
\partial_t \begin{bmatrix} \dot{u} \\ \dot{w} \\ \sigma_{xx} \\ \sigma_{zz} \\ \sigma_{xz} \end{bmatrix} = \begin{bmatrix} 0 & 0 & \rho^{-1} & 0 & 0 \\ 0 & 0 & 0 & 0 & \rho^{-1} \\ \lambda+2\mu & 0 & 0 & 0 & 0 \\ \lambda & 0 & 0 & 0 & 0 \\ 0 & \mu & 0 & 0 & 0 \end{bmatrix} \partial_x \begin{bmatrix} \dot{u} \\ \dot{w} \\ \sigma_{xx} \\ \sigma_{zz} \\ \sigma_{xz} \end{bmatrix} + \begin{bmatrix} 0 & 0 & 0 & 0 & \rho^{-1} \\ 0 & 0 & 0 & \rho^{-1} & 0 \\ 0 & \lambda & 0 & 0 & 0 \\ 0 & \lambda+2\mu & 0 & 0 & 0 \\ \mu & 0 & 0 & 0 & 0 \end{bmatrix} \partial_z \begin{bmatrix} \dot{u} \\ \dot{w} \\ \sigma_{xx} \\ \sigma_{zz} \\ \sigma_{xz} \end{bmatrix}
\tag{12}
$$

4.2.   Field Example

The geometry of an initial crosshole experiment conducted by Esso Resources, Ltd., in the Cold Lake, Alberta area is shown in **Figure 4.2**. It consists of one source well and one receiver well separated by 200m. Ten vertical component seismometers were employed that recorded at a rate of 1000 samples/s and the shot was located at a depth 440m. An explosive source that contained high frequency energy up to 500Hz was used, and the records had high signal to noise ratio. Steam was injected from a well located half way between the receiver and the source wells in the Clearwater to mobilize the heavy oils. The perforations were at depths between 442m and 450m. The depths to the interfaces were derived from well log data *(Kanasewich, 1983)*.
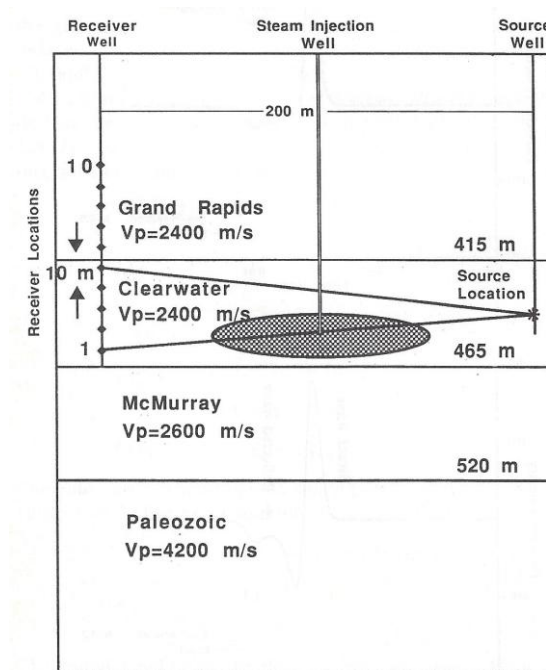
Figure 4.2: *Model geometry for a seismic crosshole experiment. The steam injection well is located halfway between the source and the receiver wells. The shape of the steam zone is not known and is taken to have an elliptical shape with a P-velocity of 1800 m/s (Vafidis et al. 1992).*

The experiment was conducted twice: the first time before steam injection and the second after injecting steam at a pressure of 10 MPa for 48 days. The first 250 ms of the before and after steam injection experiments are shown in **Figure 4.3**, where the seismic signals are rectified in such a way as to allow plotting the *before* records entirely above the zero amplitude baseline and *after* records entirely below it. The original positive parts of the signals are shaded. This display is called BARS (Before/After Rectified Seismic) plots. The amplitudes of the arrivals from the two experiments show significant changes on receivers 2 to 5, and are lower in the after steam traces. Notice the very low amplitudes of the S-waves after injection. Also, clear time delays of up to 2 ms in the P-arrivals and up

to 10 ms in the S-arrivals are observed in the after steam experiment due to propagation through the low velocity steam zone. Reflections from layers below the Clearwater are difficult to identify in the records. Macrides et al. *(1987)* extensively studied this data set and, based on evidence from theoretical and experimental studies *(Tosaya et al., 1984; Nur et al., 1980)*, modeled it with rays and a P-velocity drop of 20% within the steam zone.

Computer seismic wave simulations were carried out for the crosshole experiment employing a high frequency (120 Hz) P-line source whose excitation function is Gaussian-shaped and an S V-line source whose frequency content is up to 60 Hz in accordance to the real experiment. The responses from the P-SV simulations using both types of sources are combined and the vertical component of the particle velocity (***Figure 4.4***) is compared with the real data. Apart from the higher frequency response in the field data set there are also large variations of amplitudes and additional phases. We have found that these can be modeled by introducing more layers both inside and outside the anomalous zone. These complications will not be covered here, so that the focus is kept on the main features of the example. Some minor amplitude differences arise because a line source is being used to model a point source in the field example.

Delays of up to 2 ms are measured after steam injection in the direct P-arrivals for the first five receivers in agreement with the real experiment. Apart from the reflections from the interfaces below the Clearwater that may be clearly observed in the *before* traces, reflection from the top and the bottom of the steam zone are also observed in the *after* traces. SV-converted phases in ***Figures 4.2 and 4.4*** reflected from the top of the Paleozoic formation are present at around 180 ms and show no delays after steam injection. Those phases can be useful for resolving the extent of the steam heated zone in the region between the injector and the receiver wells.

Direct S-waves are recorded in the hole to hole simulations that are delayed in the after steam injection experiment by 5-10 ms for receivers 1 to 3. Those delays are similar to the ones observed in the real experiment and can give useful information concerning the shape and the size of the heated zone. In the synthetic sections the direct S-wave can be completely resolved and this helps to identify it in the real section. The delays on the direct S-arrivals can be modeled by a decrease of P-wave velocity coupled with an increase of Poisson's ratio from 0.36 outside the steam heated zone to 0.4 inside. Notice the reflections *(SSSS)* from the Paleozoic at around 200 ms for receivers 1 to 6. Finally, the converted phase *(SSPP)* from the same interface present at earlier times (120 ms) remain undisturbed after steam injection.
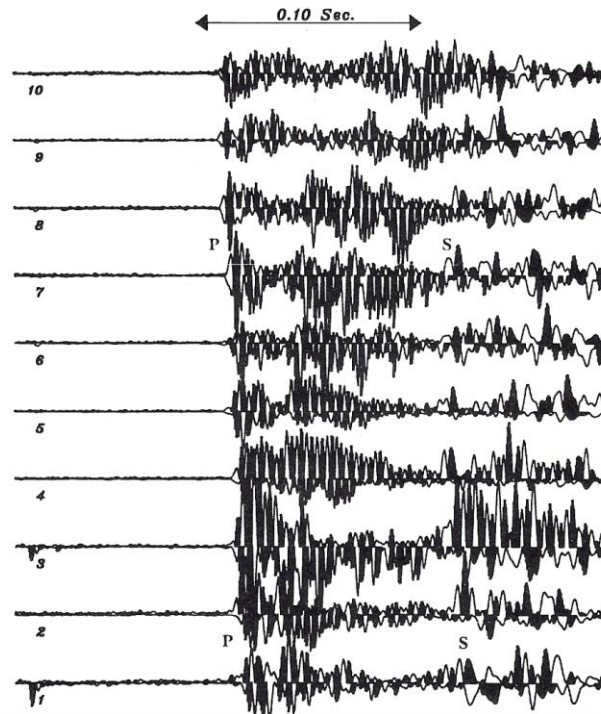
Figure 4.3: BARS plots for a steam injection experiment. The seismic signals are rectified in such a way as to allow plotting the before records entirely above the zero amplitude baseline and after records entirely below it. The original positive portions of the signals are shaded and the original negative parts are unshaded (Vafidis et al. 1992).
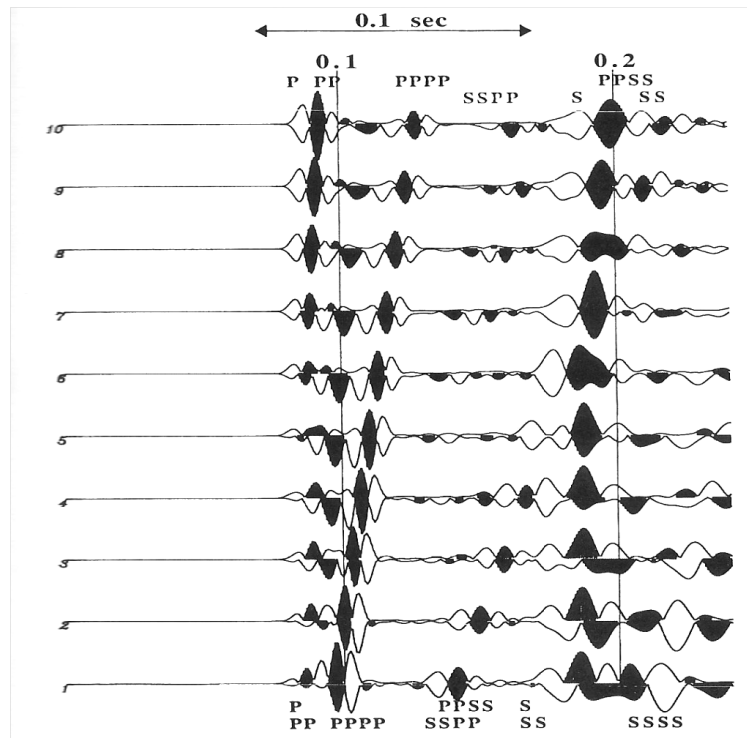
Figure 4.4: BARS plots for a P-SV computer simulation of the cross-hole experiment obtained by summing the P and the SV wave line source results. This shows the vertical component of particle velocity (Vafidis et al. 1992).

CHAPTER 5

Generated Synthetic Seismic Data

For the purposes of creation and processing of the synthetic seismic reflection data, the interface MATLAB™ was used, based on algorithms of the Laboratory of Applied Geophysics of Technical University of Crete for the need of simulation of seismic waves propagation (P-SV) in 2 dimensions with the aid of finite differences method.

5.1. Initial Model

To begin with, given the geologic section where the seismic simulated data refer to, we proceeded to digitization of the section. As a result, each geologic layer of the section can be spatially described through a matrix with x and z coordinates, for the length and the depth respectively.

MATLAB™ interface requires the horizontal extend of model that is equal to 2360m and the total depth 3000m, the minimum S-wave velocity 2100m/s, the dominant frequency of the source that is 20Hz and finally the receiver increment equal to 10m. A free boundary condition has been imposed at the upper surface of the model. Finally, it was supposed that the survey was conducted on land (*Figure 5.1*).

Figure 5.1: *Initial parameters of the model*

The calculated wave field does not only depend on the initial conditions but also on the conditions at the edges of the finite model.

Composite absorbing boundary methods are developed for the numerical simulation of seismic waves. In seismic exploration, two boundary conditions are implemented for wave modeling at the edges of the numerical model: absorbing boundary conditions to mimic an infinite medium and free surface conditions on the top side of the computational domain to represent the air-solid or air-water interfaces which have the highest impedance contrast. There is the assumption that there is no energy deriving outside the computational area and as a result, only outgoing waves must be present near the artificial boundaries *(Virieux et al. 2012)*.

In the modeler used for the synthetic seismic data are embedded absorbing boundary conditions. The calculated wave field does not only depend on the initial conditions but also on the conditions at the edges of the finite model. There are applied field modification approaches, namely the anisotropic filters and the one-way sponge filters. The anisotropic filter method adjusts the propagation direction of the waves, so that they reach the boundary at normal angles. The one-way sponge filter method endows the transition the transition zone with a dissipation mechanism that selectively damps the surface waves *(Dai et al.1994)*. The effectiveness of these boundary conditions is restricted to waves impinging at the artificial boundary at normal angles.*(Figure 5.2)*.
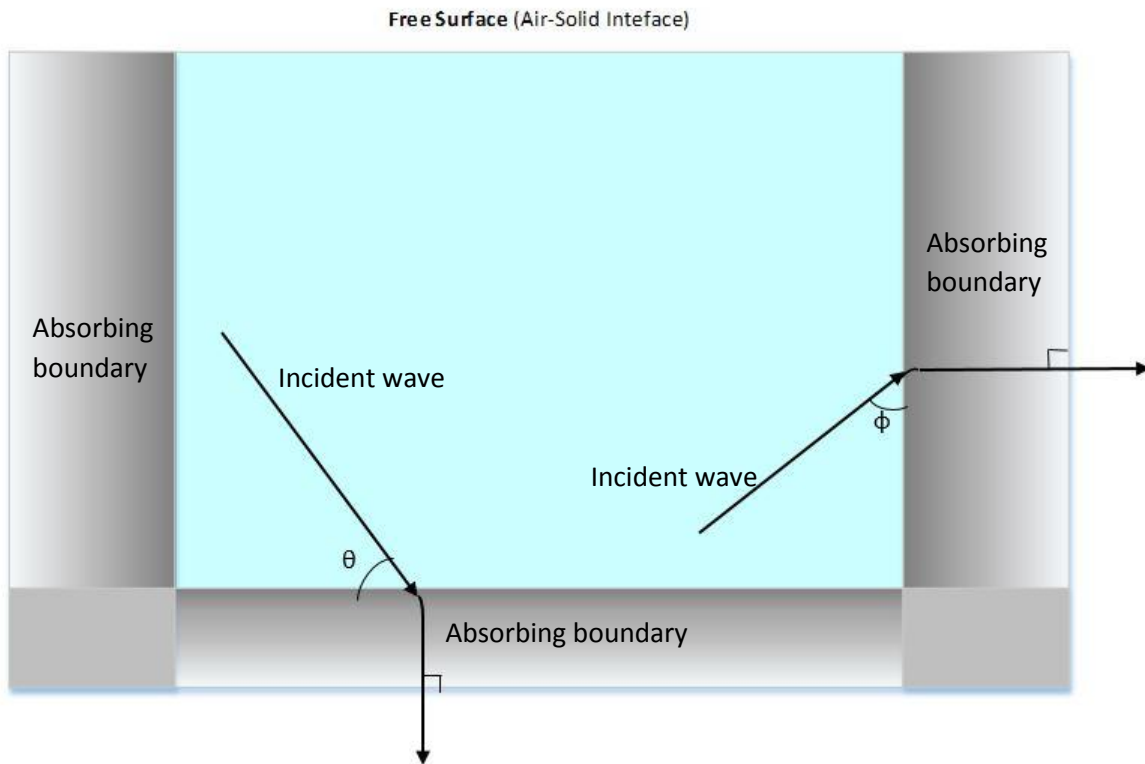
Figure 5.2: Graphical representation of absorbing boundaries
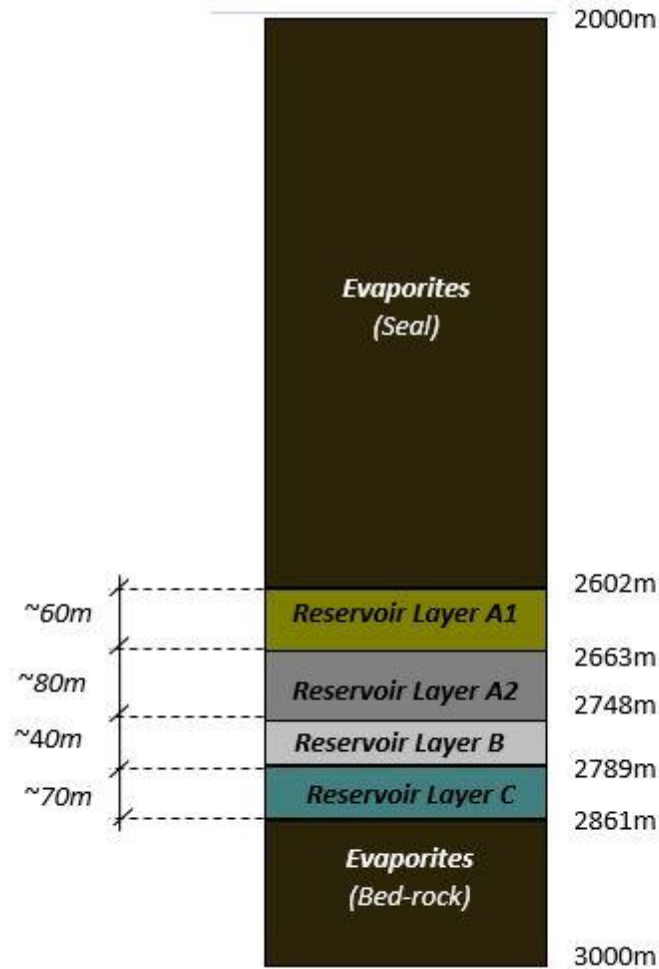
Figure 5.3: Mean depth column of the geologic reservoir model

Figure 5.3 shows a column of the mean depth of each layer of the reservoir model. The first reservoir layer *(A1 reservoir layer)* has a mean thickness approximately 60m, the second one *(A2 reservoir layer)* has a mean thickness almost 80m. The third horizon *(B reservoir layer)* and the fourth one *(C reservoir layer)* have mean thickness approximately equal to 40m and 70m respectively.

Table 5.1 shows P and S wave velocities as well as the density of each layer that were used in the initial model. It is supposed that for the initial stage of the synthetic seismic survey the reservoir is saturated with oil and brine.

Table 5.1: Pre-injection primary (Vp) and shear (Vs) seismic wave velocities and density (ρ).

	Cap-rock (Evaporites)	A1 1st reservoir layer	A2 2nd reservoir layer	B 3rd reservoir layer	C 4th reservoir layer	Bedrock (Evaporites)
V_p (m/s)	4750	4140	3850	3990	3830	4750
V_s (m/s)	3100	2300	2100	2240	2100	2900
ρ (kg/m^3)	2.6	2.4	2.34	2.31	2.28	2.7

The next step of the process refers to the discretization of the layers that comprise the reservoir, as well as the seal rock and the underlying layer beyond the reservoir. The layers are introduced through MATLAB^{TM} as tables that contain coordinates of each one separately. Having introduced a layer, it is required to introduce the seismic velocities of P and S waves and also the density of the layer *(Figure 5.4)*. This process is completed when all the geologic layers and their parameters are inserted in the model *(Figure 5.5)*.
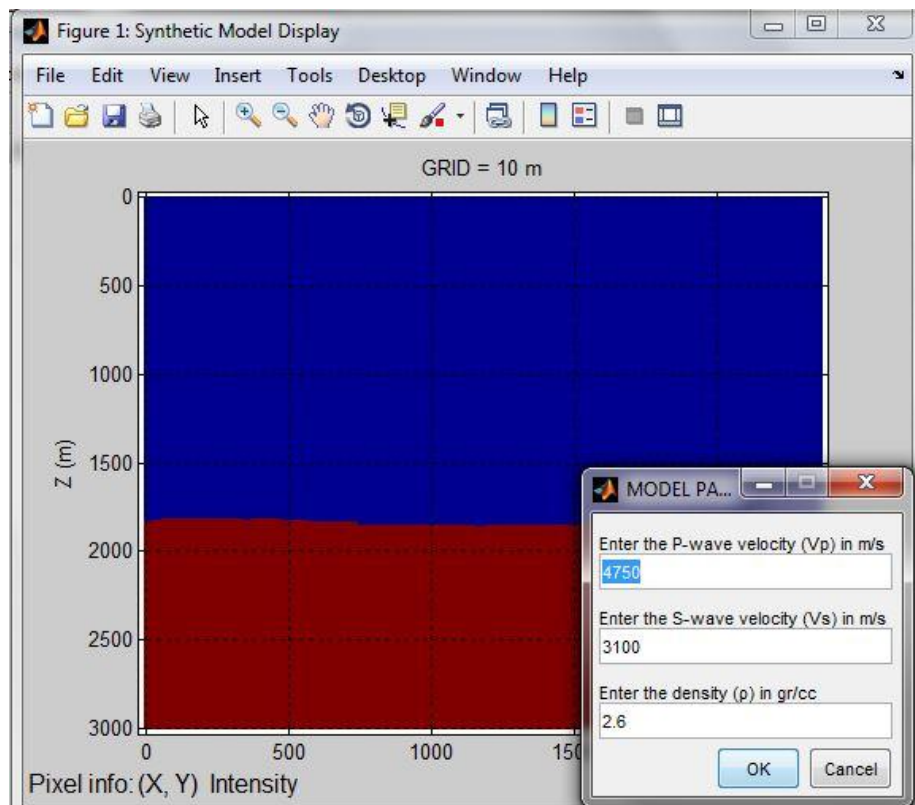
Figure 5.4: The first introduced interface of the model with the corresponding parameters.
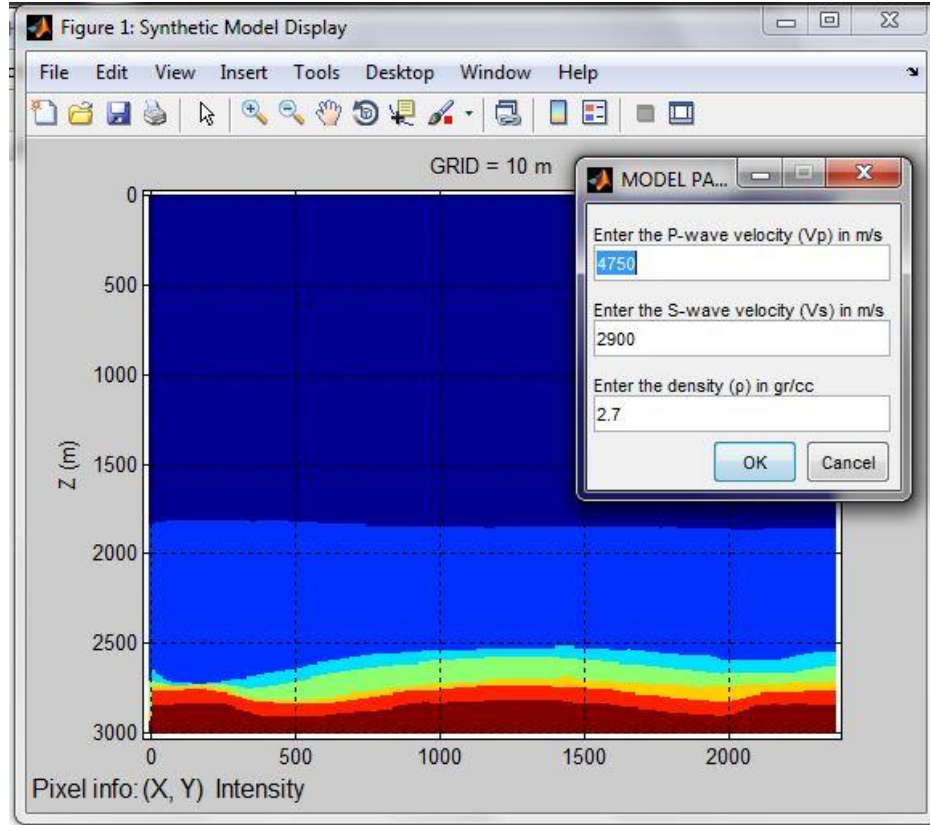
Figure 5.5: *The last introduced layer of the model with the corresponding parameters*

The following step of the simulation process refers to the introduction of the receivers' and the sources' geometry. For this model, there were used 59 shots and 237 geophones. The first shot is located on the 10m spot of the seismic line and the shot increment is 40m, which means that the shots are conducted every 40m. The shots are also located 15m deep. The receiver's increment is 10m. It should be mentioned that the geophones do not have a stable distance with the shot. The geophones remain in stable positions to all the extent of the seismic section, while the shots change positions every 40 m (***Figure 5.6, 5.7***).

It should be mentioned that there is a restriction, concerning the spots that the shots are placed. Specifically, the sampling interval is equal to 1ms, while the time step is equal to 0.5ms. The grid of the model is calculated through the following formula:

$$Grid = \frac{V_{Smin}}{15*f} = \frac{2100}{15*20} = 7 \qquad\qquad (13)$$

The maximum calculated value of the grid is equal to 7. The dimensions of each grid cell are defined through the spacing of the nodes in x and z axis and as a result they are equal to Δx = Δz = 5m.
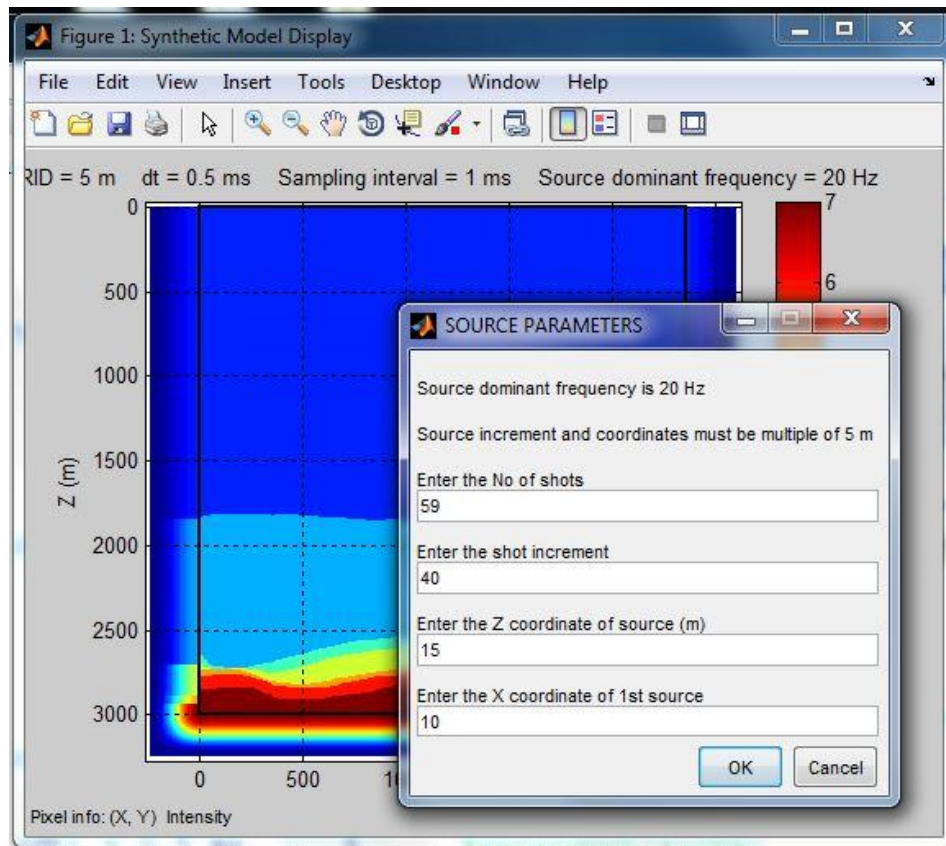
Figure 5.6: Source Parameters
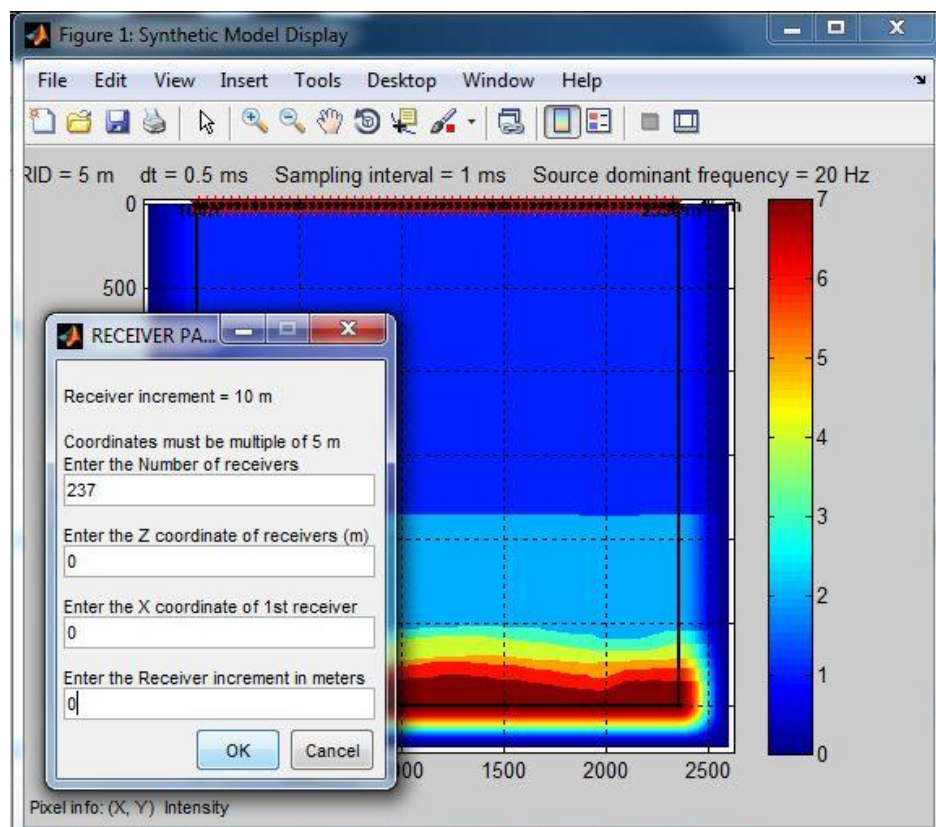
Figure 5.7: Receiver parameters

Finally, it is required the total record length, in other words, the maximum two-way travel time that is needed for the signal to travel from the first shot up to the last receiver of the seismic line. For the above calculation is needed the average velocity. The average velocity of wave propagation from the shot to the geophone is equal to the depth of the geophone below the shot, divided by the measured travel time *(The Leading Edge, 1993)*:

$$a_n = \frac{\sum_{j=1}^{n} d_j}{\sum_{j=1}^{n} t_j} = \frac{\sum_{j=1}^{n} a_j t_j}{\sum_{j=1}^{n} t_j} \qquad (14)$$

where,

- τ_j: *two-way travel time*
- α_n : *the interval velocity of each layer*
- d_j : *the total depth of each layer*

The two-way travel time of a seismic signal to travel up to the last reservoir layer is calculated by:

$$t^2(x) = t^2(0) + \frac{x^2}{Vmean^2} \qquad (15)$$

where,

- *t(0): two-way travel time that corresponds to zero offset (vertical two-way travel time)*
- *x: maximum offset*
- V_{mean}: *mean Vp (compressional) velocity*

As a result, the mean Vp velocity is equal to 4,678 m/s. The maximum offset between the first shot and the last receiver of the seismic line is equal to 2,350m, since the first shot is accomplished at the first 10m of the survey line. Factor t(0) is the zero offset two-way travel time and can be calculated through the following formula:

$$t(0) = 2\frac{Depth}{V_{mean}} \qquad (16)$$

Based on the maximum calculated travel time we set the record length equal to 2,000ms, by adding a safety margin to the primarily calculated time. Additionally, it is required the spline interval that is set equal to 50m. The spline interval value defines the spacing where measurements are taken and as a result the points of the section that will demonstrate seismic traces *(Figure 5.8)*.
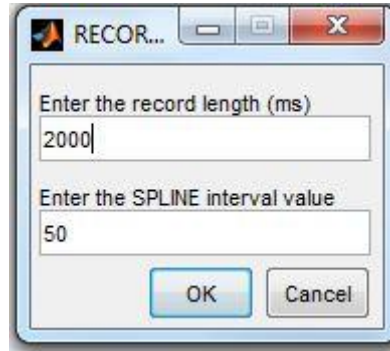
Figure 5.8: Record Length and spline interval value

In *Figure 5.9* a representation of the layers of the reservoir model is shown, with a spline interval equal to 50.
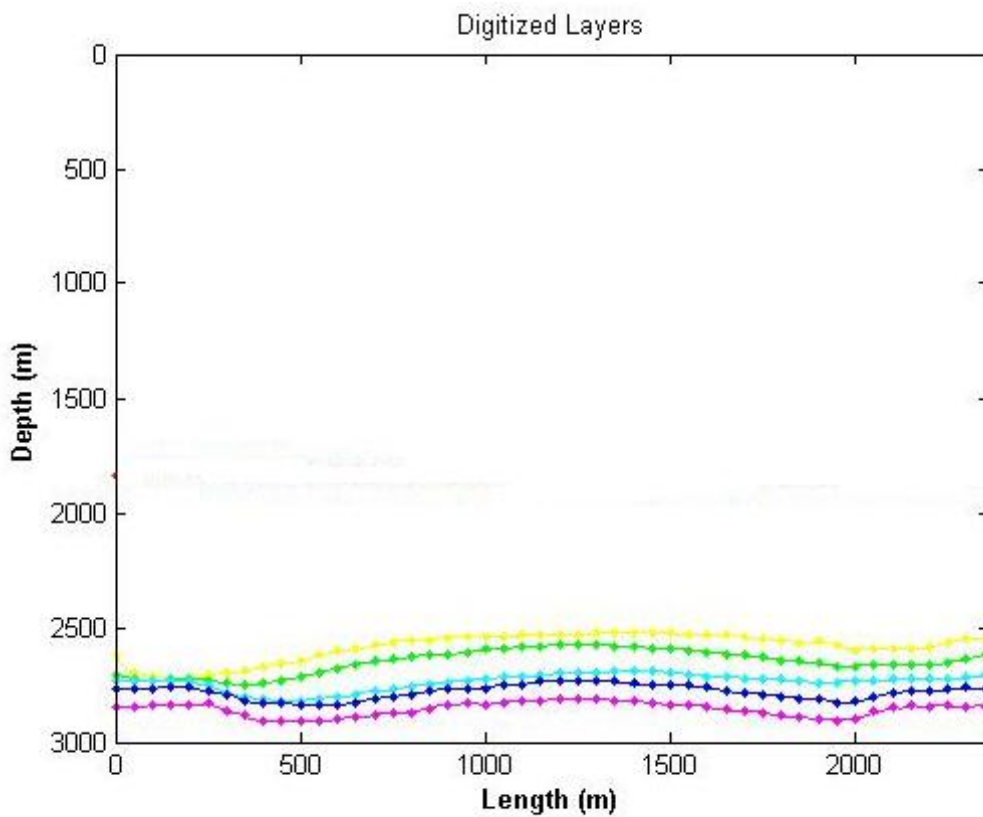
Figure 5.9: Digitized layers of the model with spline interval equal to 50m as a function of depth.

Through cubic interpolation, with time interval equal to 0.001ms, there are available data points not only for the times that correspond to the reservoir layers but for all the time instances from 1ms up to 2,000ms *(Figure 5.10)*.

The general idea of spline is that on each interval between data points represent the graph with a simple function. Using cubic functions the curves would be smooth at the data points by matching up the derivatives. In fact, the goal of cubic spline interpolation is to get an interpolation formula that is continuous in both the first and second derivatives, both within the intervals and at the interpolating nodes.
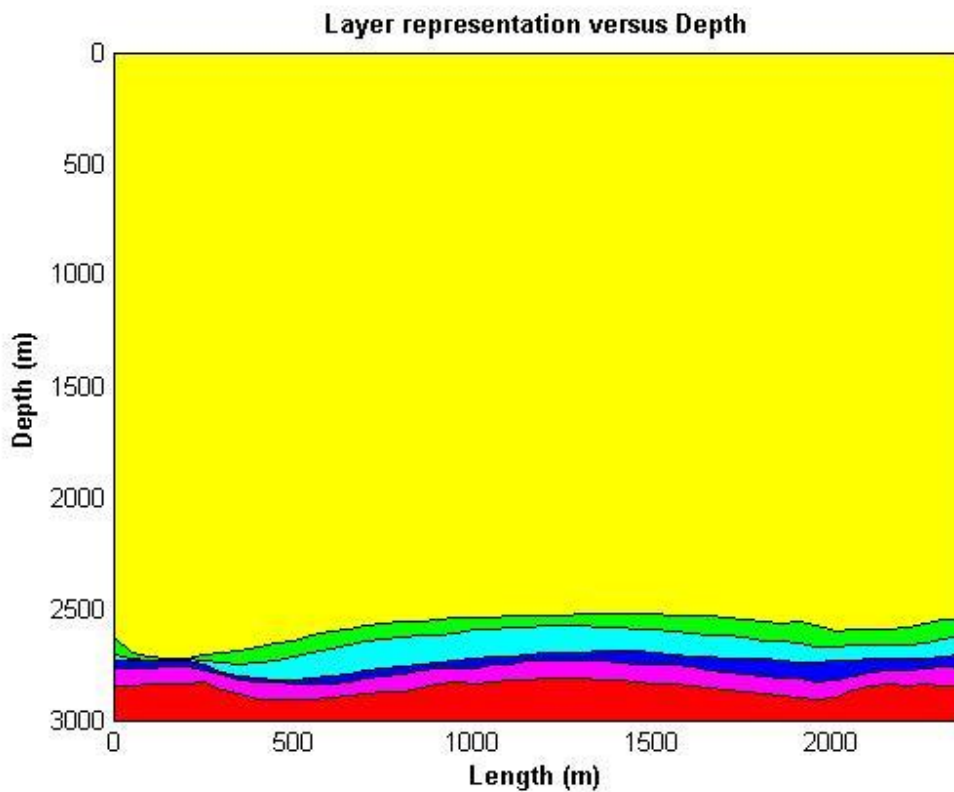
Figure 5.10: Horizontal distance of the layers as a function of two-way travel time.

Figure 5.11 shows the same reservoir model as *Figure 5.10*, but with respect to depth. Time has been converted to depth for every layer, through formula (15).
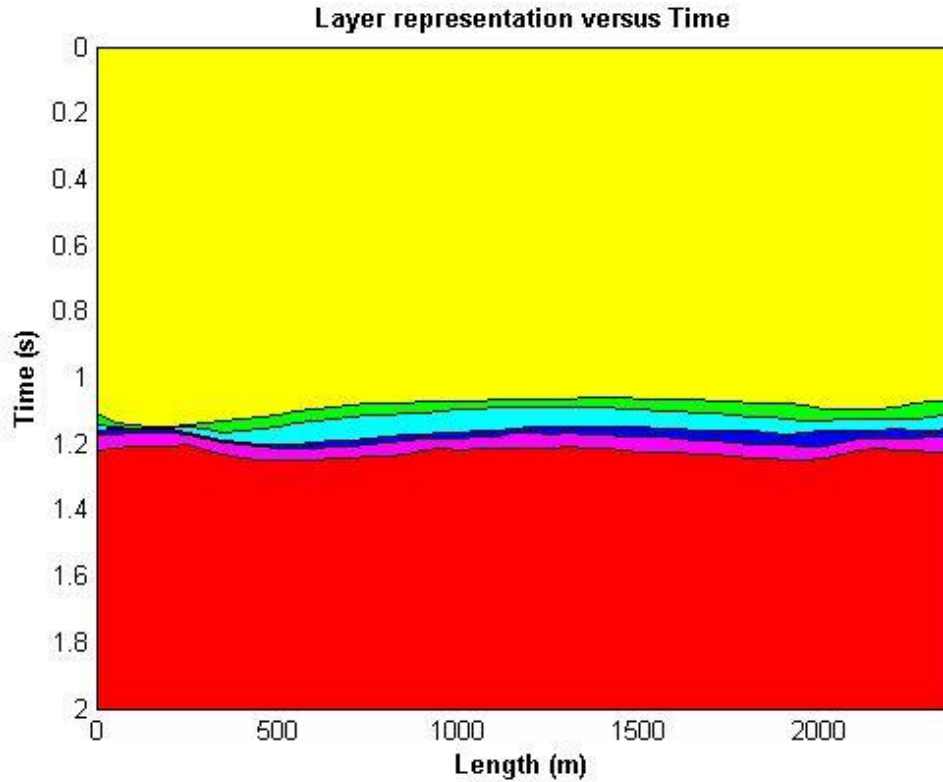
Figure 5.11: *Horizontal distance of layers as a function of two-way travel time.*

5.2. Steam Injection Model

The above procedure was also adopted for the creation of synthetic seismic data in the case of the steam injection. All the layers that comprise the reservoir are injected with steam, through a well that is assumed that is located in the middle of the geologic section. At a final step, there is made the assumption that all the layers among the reservoir are filled with steam. For simplification the final brine saturation equals 50%, while the steam saturation is also equal to 50%.

Due to the injection process, there is a differentiation mainly on the values of primary wave seismic velocities and also on those of the density. The shear wave velocity remains almost constant *(Oilfield, Spring 1999).* ***Figure 5.12*** shows that even the slightest amount of steam causes P-wave velocities to decrease, while S wave velocities do not show any difference in their magnitude.
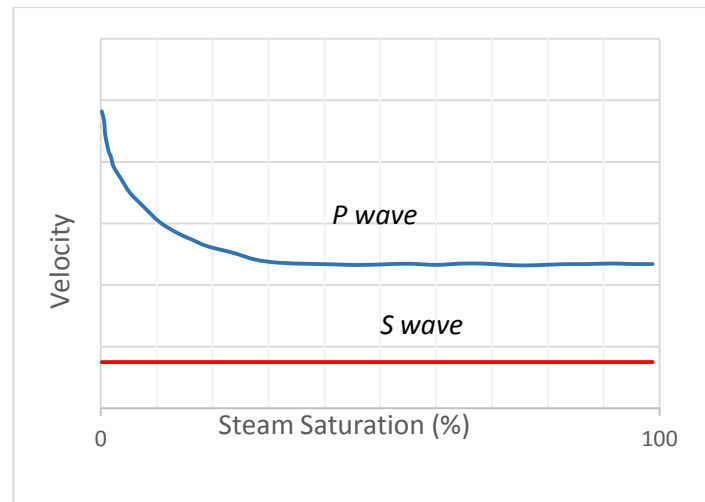
Figure 5.12: *P and S wave velocities as a function of steam saturation (%).*

The calculations of P wave velocity as well as density were based on the results of a seismic reflection monitoring survey over a thermally enhanced oil recovery site in Alberta, Canada *(Tsingas, 1989).* In this case study, the same reduction rates are considered for both in velocities and density that were used in the already mentioned seismic survey in Alberta, Canada. As a result, P wave velocity has a reduction of 15%, density is 10% reduced, while S wave velocity is slightly increased 5%.

The seismic velocities and density of each layer that result from the steam injection process are shown in **Table 5.2**.It should be mentioned that only the reservoir layers face these changes and not the cap rock or the bedrock formations, because only the reservoir layers participate in the injection process and as a result, only these layers are affected by the injection.

Table 5.2: *Post-injection primary (Vp), shear (Vs) seismic wave velocities, density (ρ) of each layer*

	Cap-rock (Evaporites)	A1 1st reservoir layer	A2 2nd reservoir layer	B 3rd reservoir layer	C 4th reservoir layer	Bedrock (Evaporites)
V_p (m/s)	4750	3519	3273	3392	3256	4750
V_s (m/s)	3100	2415	2205	2352	2205	2900
ρ (kg/m³)	2.6	2.16	2.10	2.07	2.05	2.7

CHAPTER 6

Processing of Pre-Injection Seismic Reflection Data

6.1.   Introduction

Among many other geophysical surveying techniques, seismic reflection is the most widely used and widespread geophysical technique. Seismic reflection data can be processed to reveal details of geological structures on scales from the top ten of meters of the Earth's crust to its inner core *(Yilmaz, 2001).* Part of its success lies in the fact that the raw seismic data is processed to produce seismic sections, which are images of the subsurface structure. Seismic processing refers to the manipulation of measured data, in order to obtain an accurate image of the subsurface. In fact, the main problem is that the information that is measured at the surface is a function of time and that it should be mapped to the correct position in depth in the subsurface. This means that reflection energy has to be repositioned, which is called migration.

A seismic trace represents a combined response of a layered ground and a recording system to a seismic source wavelet. Assuming that the pulse shape remains the same as it propagates through such layers, the resultant seismic trace may be considered as the convolution of the input impulse with a time series, known as reflectivity function, which is composed of spikes. Every spike has an amplitude related to the reflection coefficient at a boundary and a travel-time equivalent to the two-way reflection time from the surface up to that boundary. Additionally, the reflection time series represents the impulse response of the layered subsurface, which is basically the output for a spike input *(Figure 6.1)*.
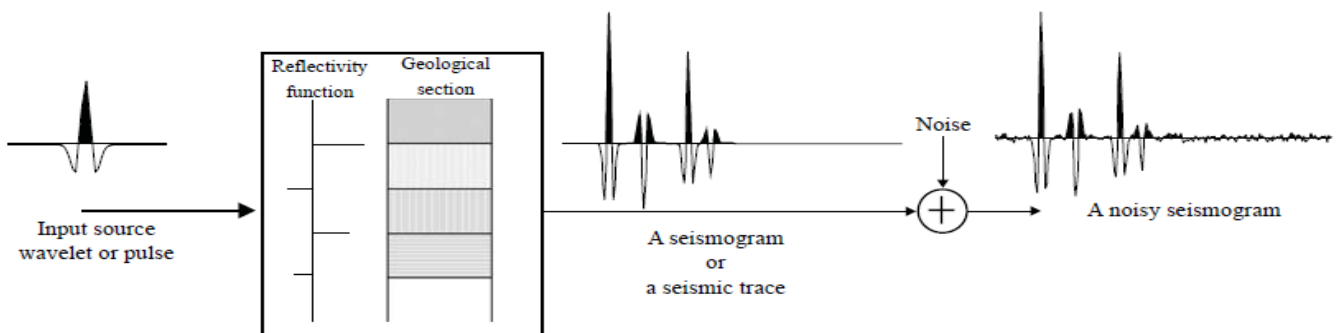
Figure 6.1: Convolution seismic data model. A seismic pulse is convolved with the reflectivity function to get a seismic trace. The reflectivity function is related to the geological section of the subsurface through the reflection coefficient of each geological boundary and the two-way travel time.

With seismic processing there are many physical processes that have to be taken into account. Firstly, we only look at reflected energy, not at critically refracted waves, surface waves, etc. of course, these types of waves contain much information of the subsurface, but these waves are treated as noise. That information is indeed used indirectly in reflection seismic via determining static corrections, but in the seismic processing itself, this information is thrown away and thus treated as noise.

Due to many factors, unwanted waves such as surface waves, corrupt the seismic records with noise. As a consequence, seismic traces generally are presented with a complex appearance and their reflection events are often not recognized without the application of suitable processing techniques.
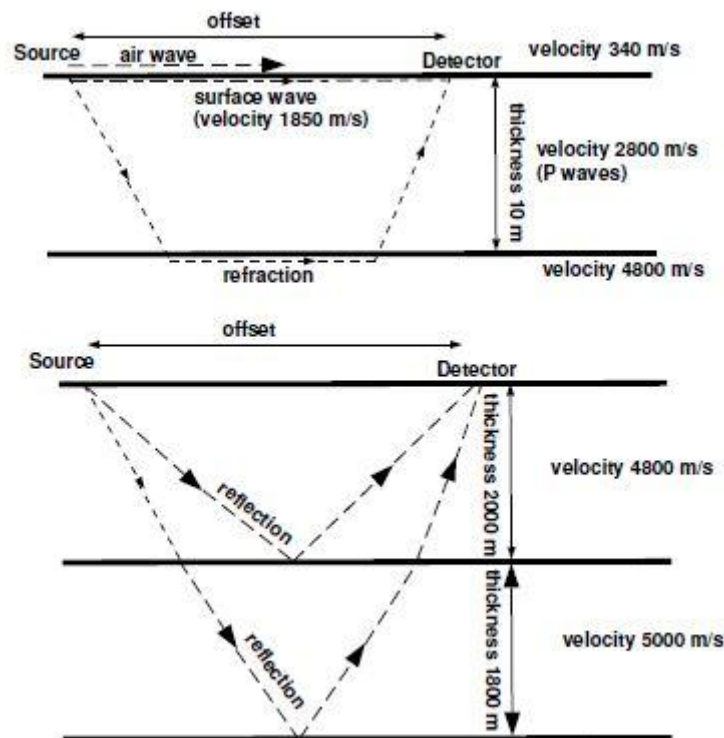
Figure 6.2: *Field seismic shot model (TU Delft, 2003)*

Each layer of any geologic model has a specific density ρ and a velocity v. The product of velocity and density is a material property of the layers and is known as acoustic impedance *(Onajite 2014)*. The amount of energy reflected is a function of acoustic impedance, which is the product of the density of the beds and the velocity of the sound waves. Seismic waves are mechanical disturbances that travel through the Earth at a speed which is governed by the acoustic impedance of the medium. The acoustic impedance is defined as the product of velocity and rock's bulk density. When a seismic wave is travelling through the Earth encounters an interface between two different materials, which they also have different acoustic impedances, some of the wave energy is reflected from the interface and some is refracted through the interface. Basically, the reflection seismics consist of generating seismic

waves and measuring the time for these waves to travel from the source, reflect off an interface to be detected by an array of receivers at the surface. *(Annetts et al., 2012)*

The coefficient for reflection (R) is then:

$$R = \frac{\rho_2 V_2 - \rho_1 V_1}{\rho_2 V_2 + \rho_1 V_1}$$

(16)

, where ρ_1 and ρ_2 are the densities of the two rocks, and V_1, V_2 their respective velocities. The greater difference in density and velocity, the greater the amount of energy which will be reflected. On a seismic section, beds which have greatly contrasting acoustic impedances stand out as strong reflectors. This makes it possible to map characteristic rock boundaries. If there is gas instead of water a rock, the velocity will be considerably reduced. The velocity of sound in gas is much lower than it is in liquid, depending on composition, temperature and pressure. The boundary between gas-bearing and water-bearing rocks may produce a strong reflection because there is a large difference in impedance between the two layers.

Another important assumption in seismic processing is that the earth is not elastic medium, but acoustic. In conventional processing, we mainly focus at P-wave arrivals. The conventional way of processing is to obtain an image of the primary P-wave reflectivity image. All other arrivals/signals are treated as noise. Multiples are treated as noise (as opposed to P-waves): refractions are treated as noise. Therefore, we can define the signal-to-noise-ratio as:

$$\frac{S}{N} = \frac{Signal}{Noise} = \frac{Primary\ Pwave\ reflection\ energy}{All\ but\ Primary\ Pwave\ reflection\ energy}$$

(17)

It can be seen now that the main goal of the processing of seismic data is to cancel out and/or remove all the energy which is not primary P-wave reflectivity energy, and "map" the reflectivity in depth from the time-recordings made at the surface.

There are three primary stages in processing seismic data. In their usual order of application, they are:

1. Deconvolution
2. Stacking
3. Migration
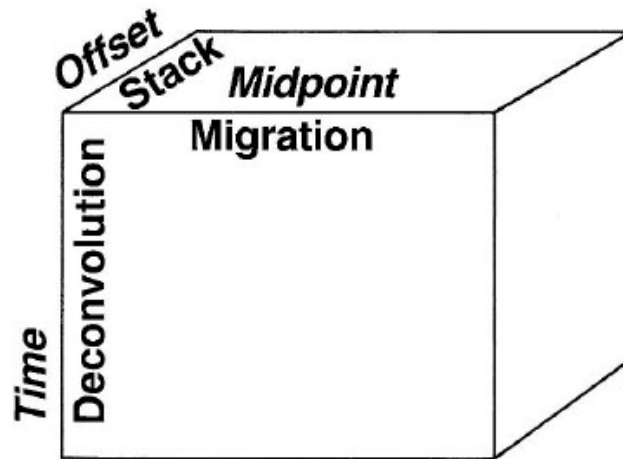
Figure 6.3: *Seismic data volume represented in processing coordinates – midpoint-offset-time (Yilmaz, 2001)*

Since the introduction of digital recording, a routine sequence in seismic data processing has evolved. This basic sequence now is described to gain an overall understanding of each step. There are three primary steps in processing seismic data – deconvolution, stacking and migration, in their usual form of application. **Figure 6.3** represents the seismic data volume in processing coordinates – midpoint, offset and time. Deconvolution acts along the time axis *(Yilmaz, 2001)*. It removes the basic seismic wavelet (the source time function modified by various effects of the earth and recording system) from the recorded seismic trace and thereby increases temporal resolution. Deconvolution achieves this goal by compressing the wavelet. Stacking also is a process of compression (velocity analysis and static corrections). In particular, the data volume in **Figure 6.3** is reduced to a plane of midpoint-time at zero offset (the frontal face of the prism) first by applying normal move-out correction to traces from each CMP gather, then by summing them along the offset axis. The result is a stacked section. Finally, migration commonly is applied to stacked data. It is a process that collapses diffractions and maps dipping events on a stacked section to their supposedly true subsurface locations. In this respect, migration is a spatial deconvolution process that improves spatial resolution *(Yilmaz, 2001).*

6.2.   Common Midpoint Gathers

The data are firstly transformed from shot-receiver to midpoint-offset coordinates. This is CMP sorting, which requires field geometry information. A commonly way of sorting the data is in *common-midpoint gathers*.
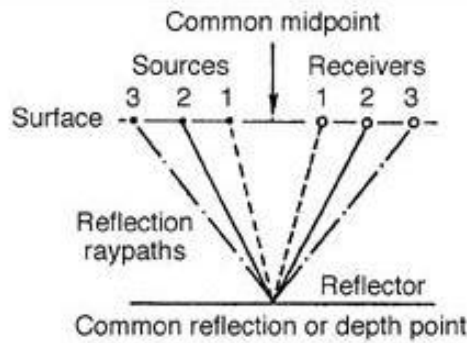
Figure 6.4: Common midpoint (CMP) (Schlumberger Oil Glossary)

A mid-point is defined as the mid-point between source and its equivalent receiver position. Each individual trace is assigned to the midpoint between the shot and the receiver locations associated with that trace. The set of traces recorded from different source-receiver pairs that have the same common midpoint (CMP) is called a CMP gather. All the reflections measured at the different offsets in a CMP gather carry information on the same subsurface points (below the midpoint position).
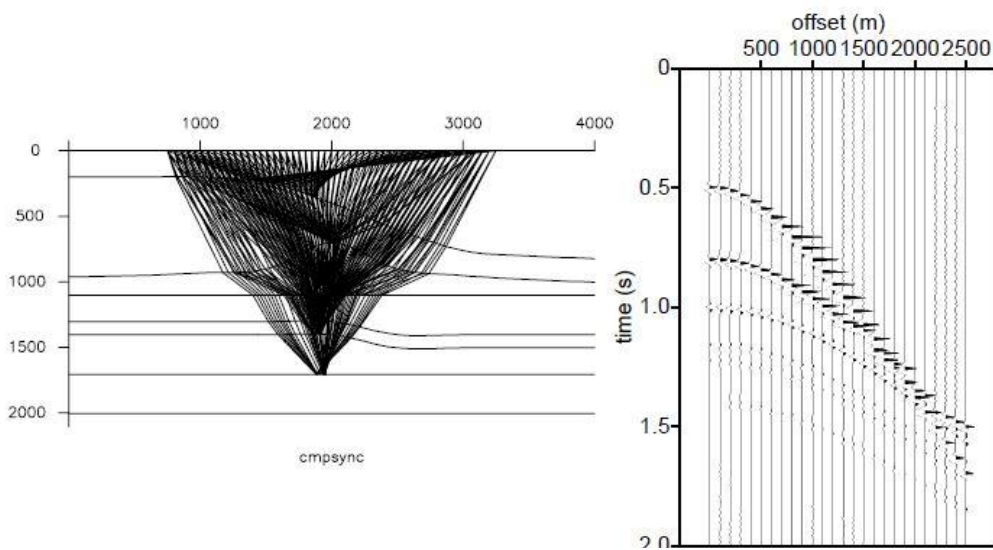
Figure 6.5: Common midpoint gather (TU Delft, 2003)

A Common Midpoint Gather chart of the 100th CMP which is located at the 495th meters of the seismic survey line is shown in *Figure 6.6.* It should be mentioned that the larger reflection amplitudes are confined to shallower times at increasingly higher frequency bands *(Oz Yilmaz, 2014).*
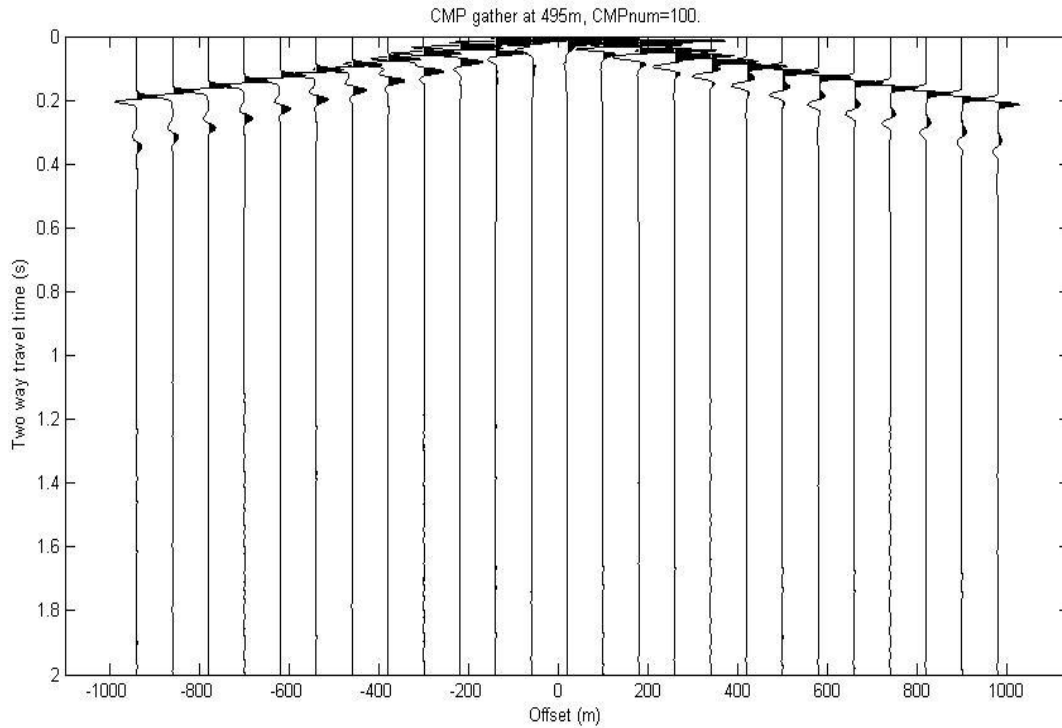
Figure 6.6: *Common Midpoint Gather 100, located at 495m of the seismic section.*

6.3.   Geometrical Spreading (Spherical Divergence)

As the acoustic wave emitted by the seismic source travel through the subsurface, its energy expands in all directions like a sphere *(Onajite 2014)*. All the energy initially contained in the seismic source is spread out over a wider area as time increases. This causes loss of energy in the seismic signal and results in a decrease in the amplitude of the source wavelet and it referred to as spherical divergence. By definition, spherical divergence is the apparent loss of energy from a source wavelet as it propagates through the subsurface. Spherical divergence decreases energy with the square of the distance *(Onajite 2014)*.
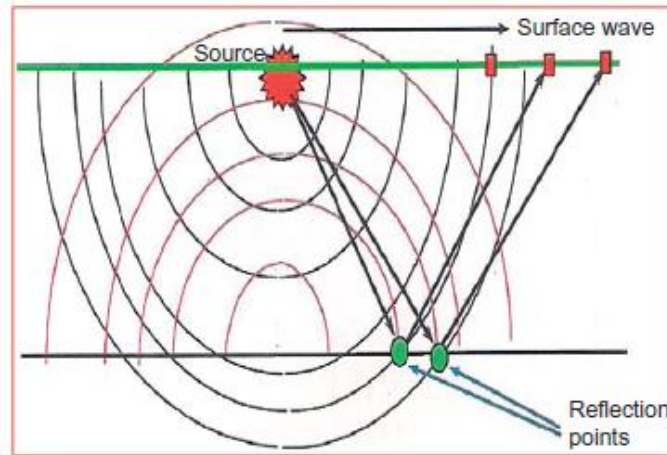
Figure 6.7: *Spherical Divergence* (Onajite 2014)

In a constant velocity medium, amplitude losses caused by geometrical spreading can be corrected by multiplying by time t, but rock velocities are not constant and the rate at which seismic energy expands depends on the velocity of the rock through which it is passing through. So actual wave fronts are not spherical, and their area increases at a faster rate than spherical divergence *(Onajite 2014).*

True amplitude processing are the steps used in seismic processing to compensate for attenuation, spherical divergence and other effects by adjusting the amplitude of the data. The goal is to get the data to a state where the reflection amplitudes relate directly to the change in rock properties giving rise to them *(Onajite 2014).*

The effect of geometrical spreading correction on a random trace of a CMP is shown in ***Figure 6.8.*** With red color is presented the seismic signal after geometrical spreading correction. It is profound that the amplitudes are reinforced. On the other hand, before geometrical spreading correction, the amplitudes are comparatively low, that finally are almost described by a straight line.
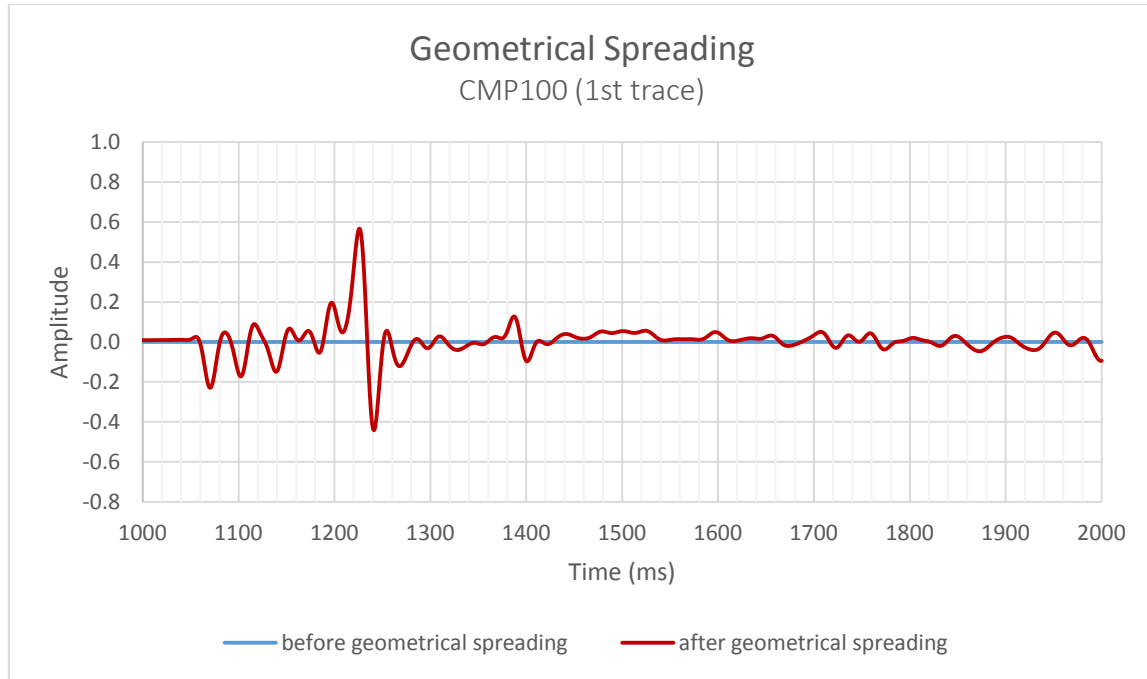
Figure 6.8: *Effect of geometrical spreading correction on the first trace 100TH CMP.*
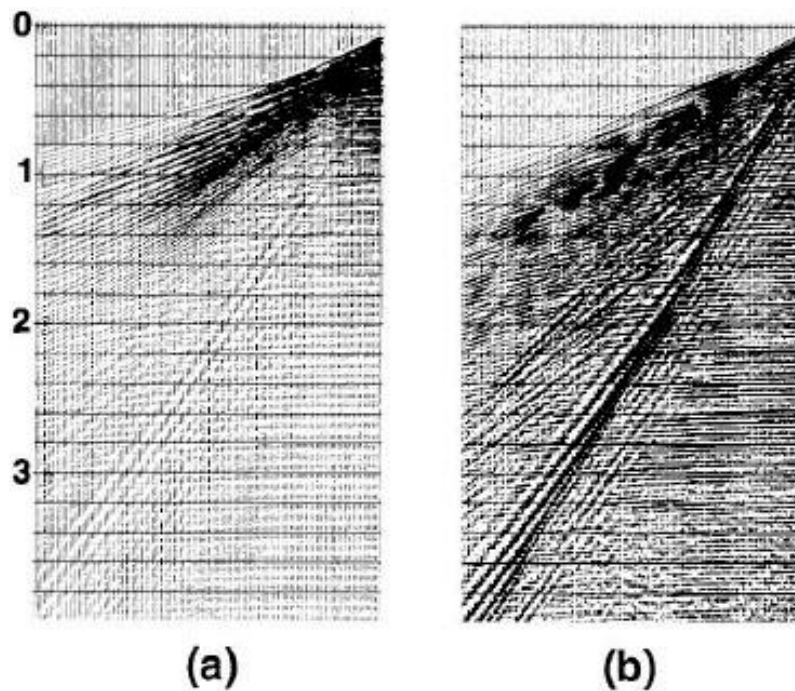
Figure 6.9: *(a) A raw field record from a marine survey. Before correcting for geometric spreading, refraction and guided wave energy dominate the record. (b) After the geometric spreading correction, while reflection amplitudes have been restored, multiples and coherent noise also have been boosted (Yilmaz, 2001).*

Figure 6.10 illustrates a CMP gather plot after geometrical spreading correction. It refers to the 100th CMP of the seismic line, which is located at the 495m of the section. It can be clearly seen that reflections have been brought up in strength.
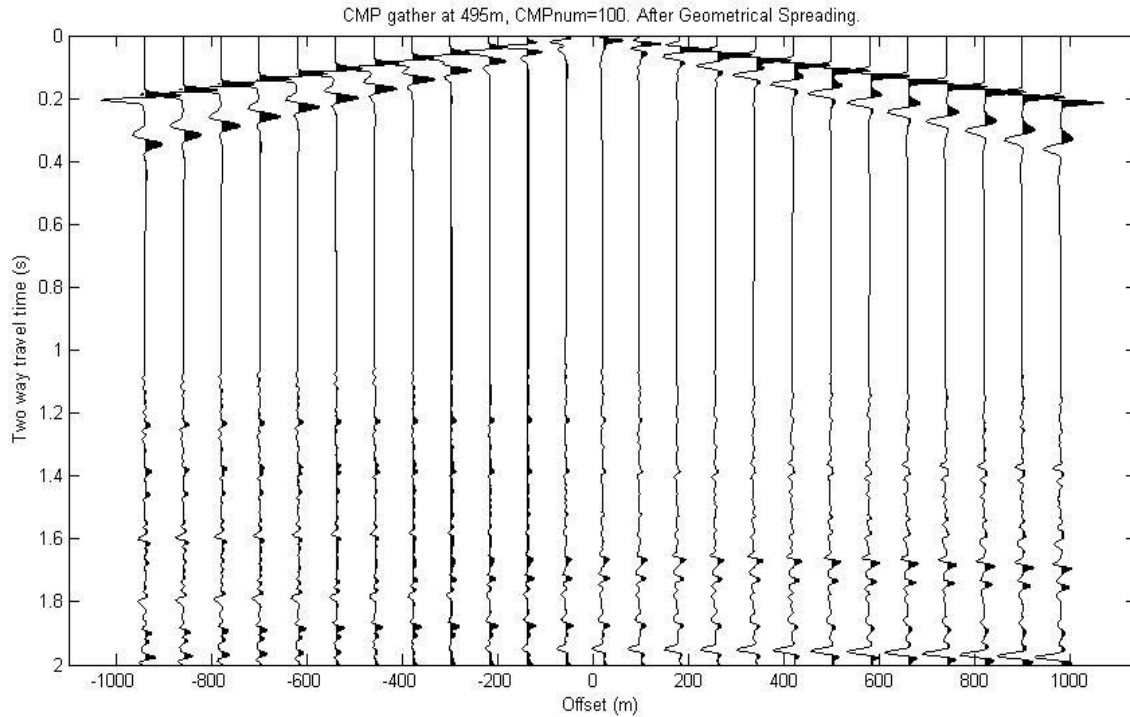
Figure 6.10: CMP gather 100 at 495m of the seismic section after geometrical spreading correction.

6.4.   Normal Move-Out (NMO) Correction

The most important physical parameter needed for obtaining an accurate image of the subsurface, is the velocity of the medium. The record of the data at the subsurface are based in time and we try to obtain an image of the subsurface in depth. The link between time and depth is of course the wave velocity, which varies in the earth from position to position (earth is an inhomogeneous medium). With NMO there is interpolation of the data.

The velocity field is used in normal move-out (NMO) correction of CMP gathers. The events are virtually flattened across the offset range; i.e., the offset effect has been removed from travel times. However, as a consequence of move-out correction, traces are stretched in a time-varying manner, causing their frequency content to shift toward the low end of the spectrum. This frequency distortion lowers the dominant frequency via a stretching of the dominant period *(Yilmaz 2001)*. NMO stretch is an artifact of NMO correction. Frequency distortion increases at shallow times and large offsets. To prevent the relegation of especially shallow events, the distorted zone is deleted (muted) before stacking. Finally, a CMP stack is obtained by summing over the offset. *(Behera et al., 2010)*
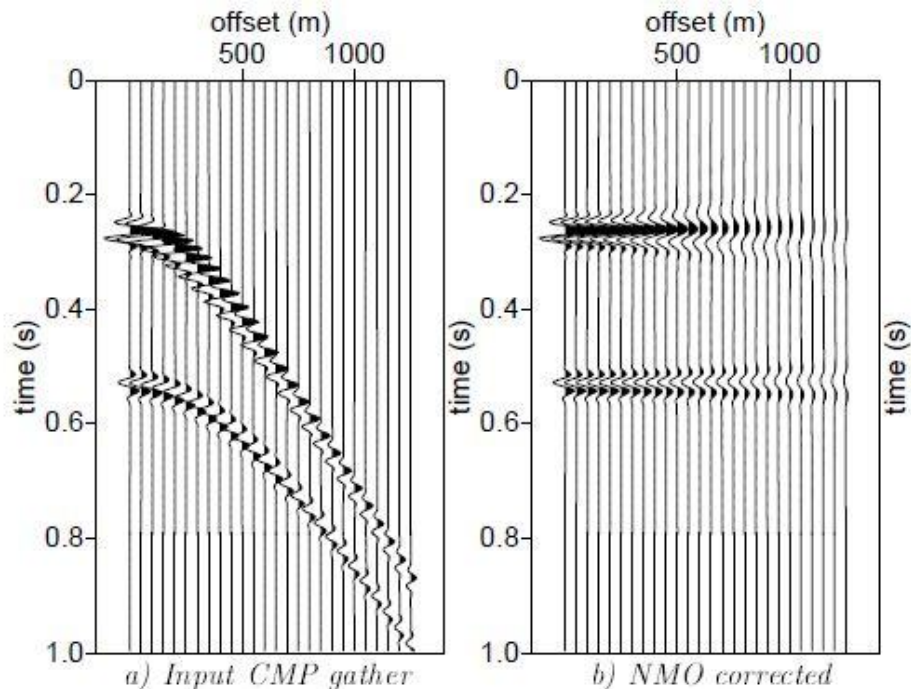
Figure 6.11: *a) CMP gather with two reflections b) CMP gather after NMO correction (TU Delft, 2003).*
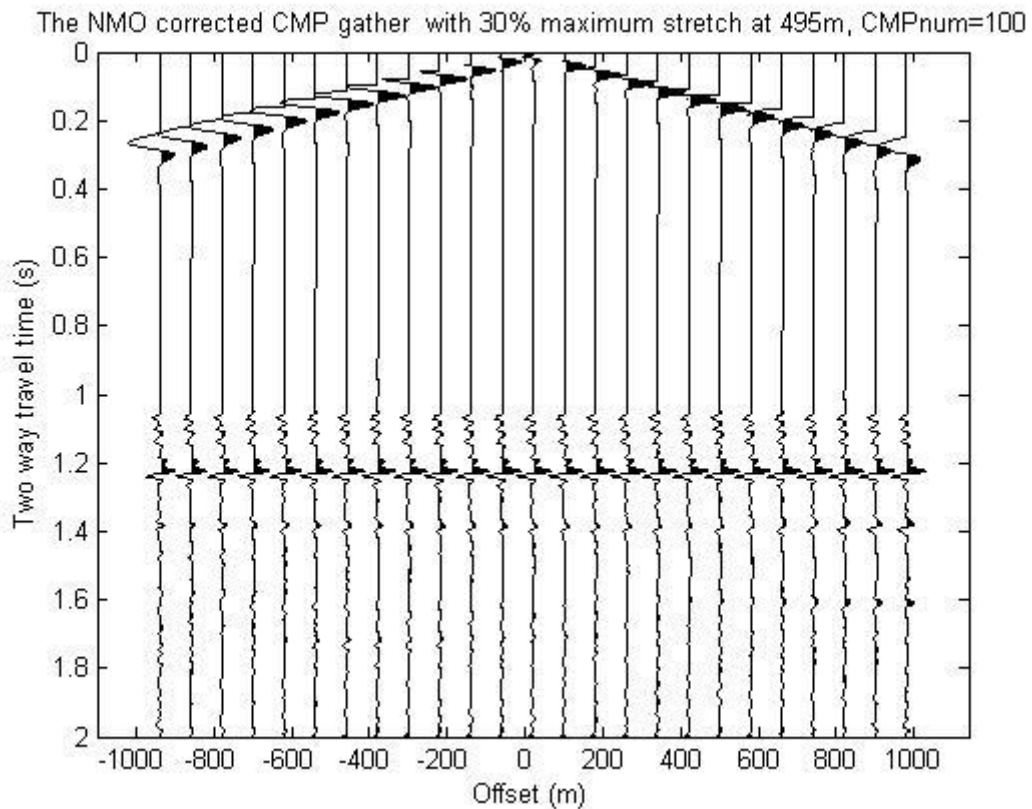
Figure 6.12: *CMP100 after NMO correction with 30% maximum stretching.*

6.5.   Velocity Analysis

In addition to providing an improved S/N ratio, multifold coverage with nonzero-offset recording yields velocity information about the subsurface. Velocity analysis is performed on selected CMP gathers or group of gathers. The output from one type of velocity versus two-way zero-offset time. These numbers represent some measure of signal coherency along the hyperbolic trajectories governed by velocity, offset and travel time. *(Yilmaz, 2001)*

For determining average velocities and interval velocities, the most accurate method is in well velocity (sonic) logging and well shooting. Seismic data, on the other hand, provide an indirect measurement of various types of velocities. This processing step focuses on three main types of velocity:

- The interval velocity (Vi): the estimated velocity of a layer between two reflectors.
- The stacking velocity (Vst): the velocity determined from the reflection move-outs and used in stacking common-mid-point (CMP) records. The correct stacking velocity is that which removes NMOs most efficiently, converting a hyperbolic reflection into a line-up of arrivals and gives maximum summed amplitudes after NMO correction.
- The root-mean-square velocity (V$_{RMS}$)

Root-mean-square velocity (V$_{RMS}$) is described by **Equation (18):**

$$V_{rms}^2 = \frac{\sum\limits_{i=1}^{n} V_i^2 t_i}{\sum\limits^{n} t_i}$$

(18)

, where t$_i$ is the zero-offset two way travel time in each layer.

The RMS velocity is that of a wave through sub-surface layers of different interval velocities along a specific ray path. RMS velocity is higher than average velocity. For horizontal layers, or gently dipping layers, NMO and stacking velocities are equal to the RMS velocity. However, stacking velocities differ substantially from the RMS velocities in areas with large lateral variations in velocity *(Yilmaz, 2001)*.

Velocity estimation requires the data recorded at nonzero offsets provided by common-midpoint (CMP) recording. With estimated velocities, we can correct for nonzero offset and compress the recorded data volume (in midpoint-offset-time coordinates) to a stacked section. Travel time as a function of offset from a series of plane horizontal isovelocity layers is approximated by a hyperbola.

This approximation is better at small offsets. By making the small-spread approximation, V_{RMS} can be calculated as follows *(Yilmaz 2001)*:

$$t^2(x) = t^2(0) + \frac{x^2}{Vrms^2} \qquad (19)$$

, where

> ➤ *x: Distance (offset) between the source and receiver positions*
> ➤ *V_{RMS}: RMS velocity down to the reflector on which depth point D is situated*
> ➤ *t(x): Travel time along ray path SDR and t(0) : Twice the travel time along ray path MD*
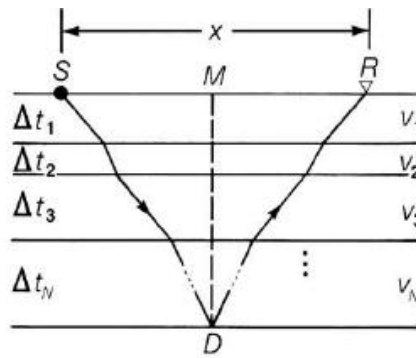
Figure 6.13: *Horizontally layered earth model (Yilmaz 2001)*

The estimated stacking or RMS velocities are employed for the calculation of the interval velocity. The velocity of seismic waves within the nth layer, α_n, is estimated from Dix equations *(Yilmaz 2001):*

$$a_n^2 = \frac{V_n^2 T_n(0) - V_{n-1}^2 T_{n-1}(0)}{T_n(0) - T_{n-1}(0)} \qquad (20)$$

, where

> ➤ *α_n: interval velocity*
> ➤ *V_n :root-mean-square velocity to the second reflector*
> ➤ *V_{n-1}: root-mean-square velocity to the first reflector*
> ➤ *T_n: the zero offset two-way travel time to the second reflector*
> ➤ *T_{n-1}: the zero offset two-way travel time to the first reflector*

The RMS velocities of the model are presented in **Figure 6.14**. The creation of this chart was based on linear interpolation method, with time interval equal to 0.001ms. As a result, there are created data

not only for times that correspond to the existing layers, but there are data for the whole record length of the survey (2,000 ms).
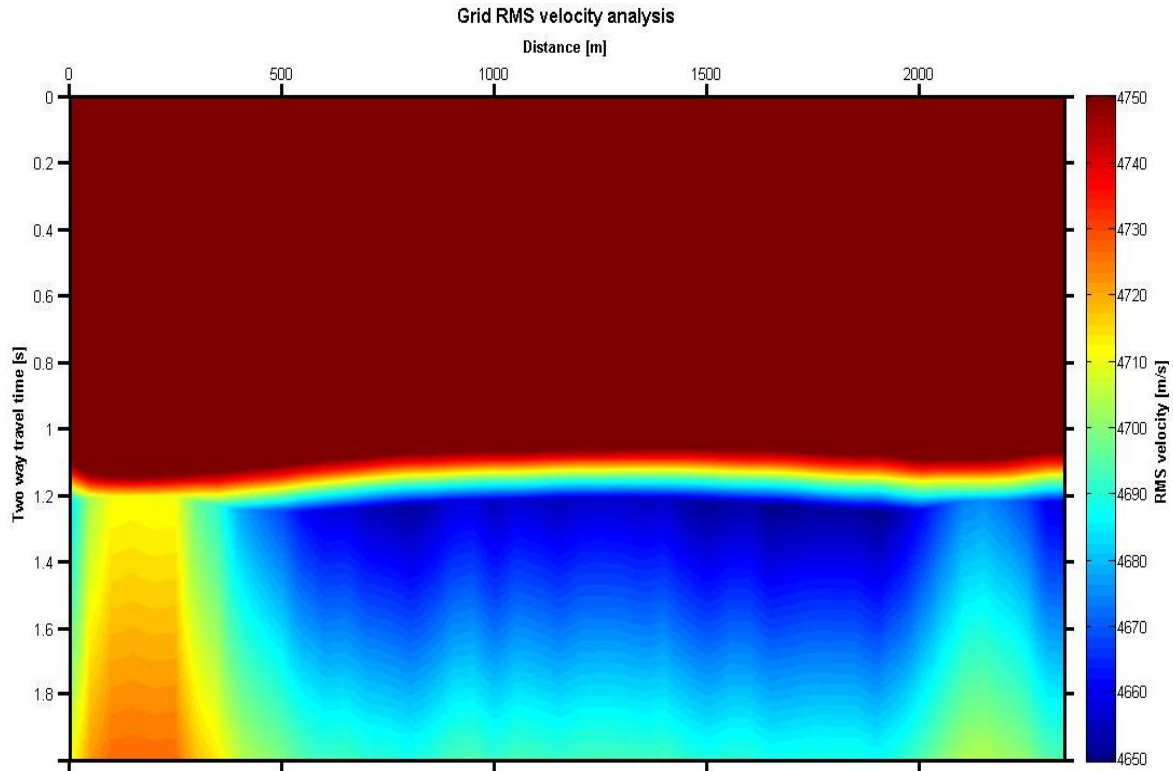
Figure 6.14: *RMS velocities of the synthetic model*

6.6.   Stacking

Stacking is the process whereby traces are summed to improve the signal-to-noise ratio, reduce noise and improve seismic data quality. Traces from different shot records with a common reflection point, such as common midpoint data (CMP), are stacked to form a single trace during seismic processing. Stacking reduces the amount of data by a factor called the fold *(Figure 6.15)*. In CMP stack, noise is attenuated by adding all the geophones output with the same reflections' point but different random noises *(Onajite 2014).*

The three shots and geophones in ***Figure 6.2*** have the same reflection point, recorded with the noise observed at different times and at different places because the shots are taken at different times. Since the shots to geophones distances are different, the surface wave is different as well. By adding together the reflected signal obtained from one shot to the corresponding geophone, the geophysicists build up the reflections and suppress both random noise and surface wave *(Onajite 2014).*
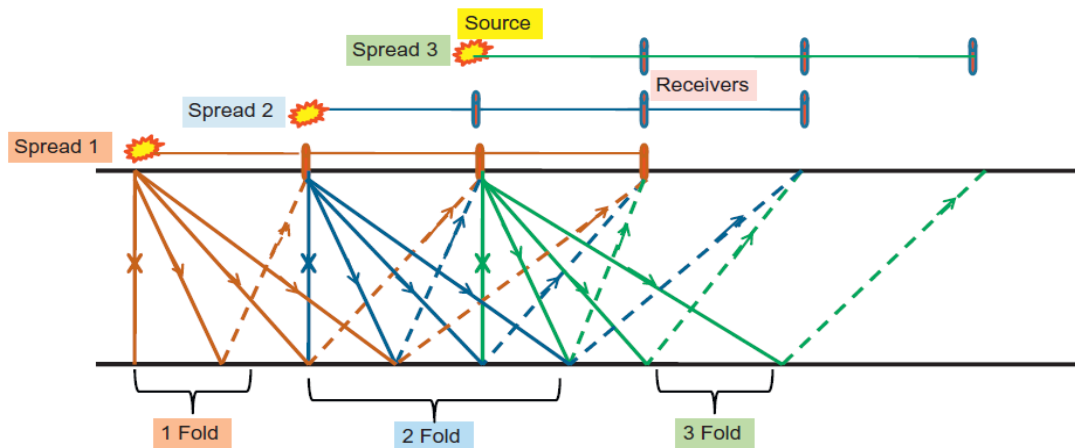
Figure 6.15: *Conceptualized seismic configuration (Onajite 2014)*

A characteristic of seismic data as obtained from the exploration of oil and gas, is that they generally show a poor signal-to-noise-ratio, not only due to coherent events such as surface waves, but also due to uncorrelated noise. Often, only the strong reflectors show up in raw seismic data. With stacking the NMO-corrected traces are added in a CMP gather to give one output trace. Although the signal to noise ratio is improved by stacking, there are also introduced some distortions (NMO stretch and the approximation in root-mean-square velocity). Therefore, by adding traces, resolution is lost. A stacked section simulates a zero offset section, but with much better signal to noise ratio. It should be mentioned, that with stacking the data volume is decreased. The amount of data reduction is the number of added traces in a CMP gather.
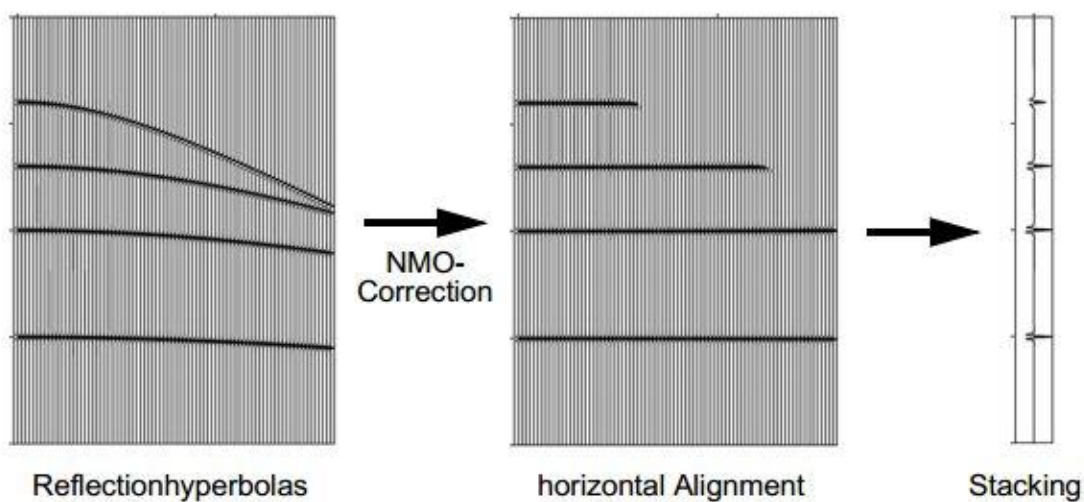
Figure 6.16: *(a) Recorded seismic traces, (b) Normal Move-Out Corrected traces c) Stacked trace (TU Delft, 2003).*

The resulted stacked section of CMP gathers is shown in ***Figures 6.17.*** With the yellow dashed line is denoted the upper reservoir horizon while with the red line is mentioned the lower horizon. The same stacked section but within a narrower time window from 1,000 ms up to 1,400 ms is illustrated in ***Figures 6.18***. In this section there is a more detailed description of the reservoir, where the upper and the last layer of the reservoir can be clearly discriminated. For two reflections, one from the top and one from the bottom of a thin layer, there is a limit on how close they can be, yet still be separable. This limit depends on the thickness of the layer and is the essence of the problem of vertical resolution *(Yilmaz 2001)*.

The dominant wavelength of seismic waves is given by:

$$\lambda = \frac{u}{f}$$

(21)

, where

 ➢ *u: the seismic velocity (m/s)*
 ➢ *f: the predominant frequency (Hz).*

Since wavelength determines resolution, deep features must be thicker than the shallow features to be resolvable. In this case, dominant frequency equals 20Hz, while the minimum velocity of the model is equal to 3830m/s. As a result, the minimum wavelength that is required in order to resolve better all the reservoir layers is 191.5m. There is a lower limit to the thickness that can be tracked, which corresponds to the half wavelength of the seismic waves and in this study equals 95m. The thickness of the reservoir layers is lower than calculated value based on the applied frequency and this results to poor resolution.

The upper as well as the lower layer of the reservoir model are better described in the seismic sections, since they appear as strong reflectors due to high contrast in seismic velocity and density with their neighboring formations (evaporites). The upper layer corresponds to time equal to 1,100ms, while the last reservoir layer is found at approximately 1,250ms. Both these reflections delineate the reservoir and are mentioned with yellow and red lines respectively in the seismic sections.

Apart from the main reflections that correspond to the upper and lower reservoir layers, in the seismic sections appear some side reflections that do not constitute real horizons. These reflections may are caused due to the complex geometry of the reservoir layers at the edges of the model.

Figure 6.17: Stacked sections of CMP gathers before steam injection

Figure 6.18: Stacked sections of CMP gathers before steam injection for a time window 1000ms up to 1400 ms

6.7.   Migration

Although time effects are removed with NMO correction, this does not mean that the wave effects are removed. Migration deals with a further removal of wave phenomena in order to arrive at a section which is a better representation of the subsurface. After the NMO correction and stacking, there are still diffractions in the stacked section. Also, dipping reflectors will not be positioned at their right place and will not show the true dip. In other words, dipping events then are moved to their true subsurface positions and diffractions are collapsed by migrating the stacked section using the medium velocity.

Migration can be performed in a number of different domains such as time, frequency, space and wavenumber. Also, it can be performed before or after stacking the recorded seismic data.

Time migration is the repositioning of the reflected seismic data from their apparent reflection point to their true reflection points in space and time.

6.7.1. Kirchhoff Migration

In Kirchhoff migration, the important parameters are the aperture width used in summation and the maximum dip to migrate*.* The Kirchhoff migration uses integration to solve the wave equation. The Kirchhoff migration method uses geometry and Huggen's principle to collapse diffraction and reposition the recorded data *(Yilmaz 2001)*. It considers the apex of the diffraction curve as the location of the true reflection point *(Figure 6.19)*.
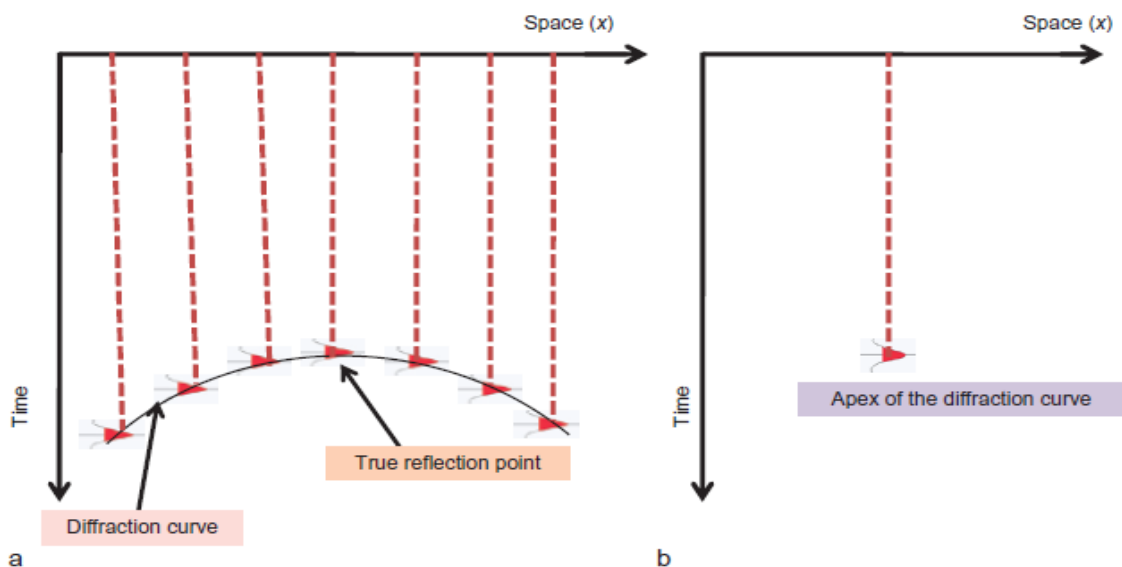
Figure 6.19: (a) Amplitude on the diffraction curve which resulted from the formation termination point and (b) amplitudes summation along the diffraction curve (Onajite, 2014).

Kirchhoff migration collapses diffraction by summing the amplitudes along the diffraction curve and placing the sum at the true reflection point (the apex of the diffraction curve). This will put the energy belonging to the diffractor as its correct position onto the migrated trace. This process is done for every migrated trace, and the input consists of the unmigrated section. *(Onajite, 2014)*

The MATLAB function that is used for Kirchhoff migration is called **kirk**, which is a simple post-stack Kirchhoff migration routine.

<div align="center">function [arymig, tmig, xmig] = kirk (aryin ,aryvel, t ,x)</div>

Where the inputs are:

- *aryin: matrix of zero offset data. The stacked data was used.*
- *aryvel: RMS velocity matrix with same dimensions as the above matrix aryin*
- *t: time interval*
- *x: location of CMPs*

And the outputs are:

- *arymig: the output migrated time section*
- *tmig: t coordinated of migrated data*
- *xmig: x coordinated of migrated data*

Figures 6.20 and *6.21* illustrate the resulted migrated sections through Kirchhoff migration processing. Figures 6.21 shows the Kirchhoff migrated section at a narrower time window that corresponds to times from 1000ms up to 1400ms, for a better view of the reservoir layers. The resolution of this section, especially within the reservoir layers, is not adequate.

With the dashed colored lines the upper and the lower reservoir horizons are mentioned respectively.
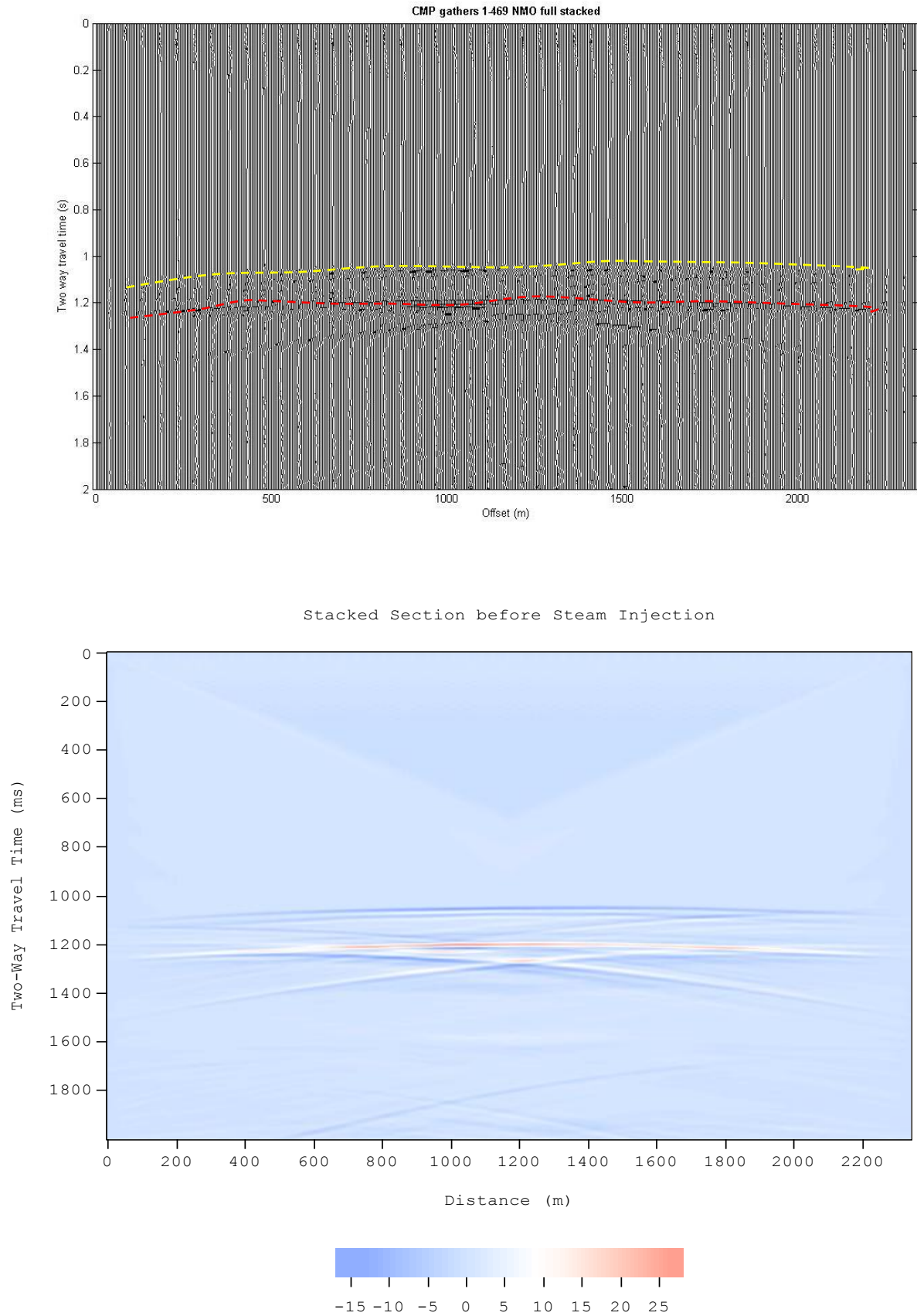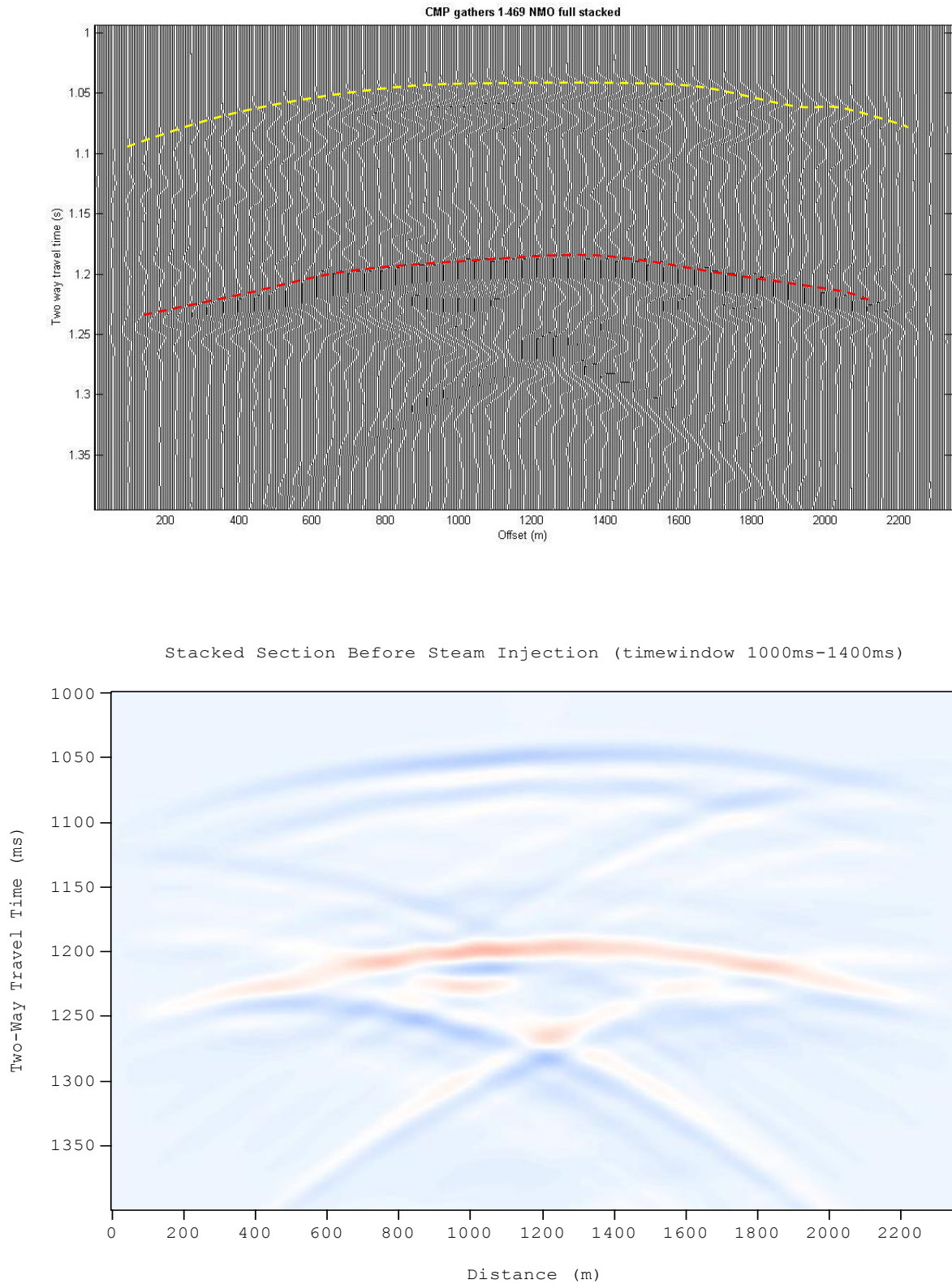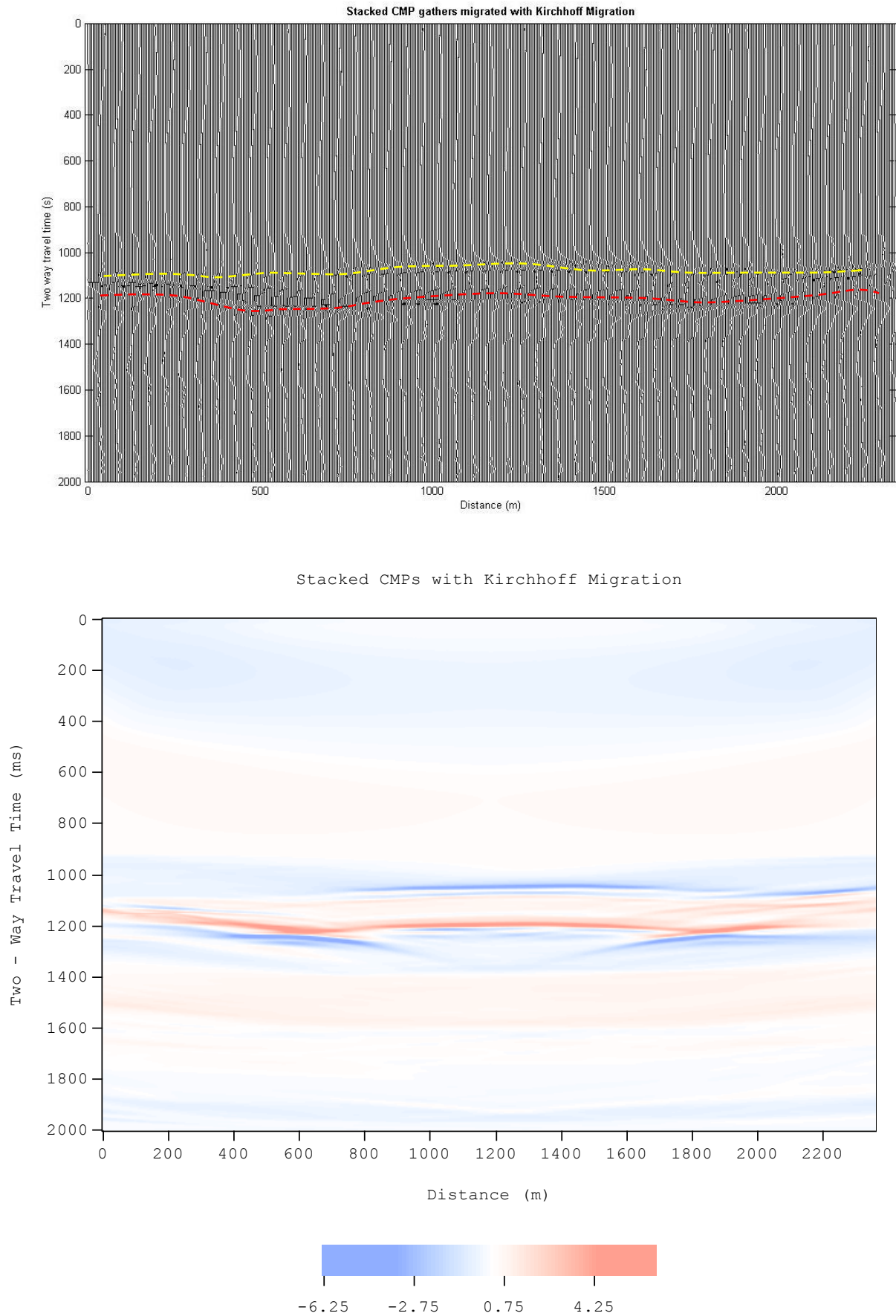
Figure 6.20: Kirchhoff migrated sections of CMP gathers before steam injection
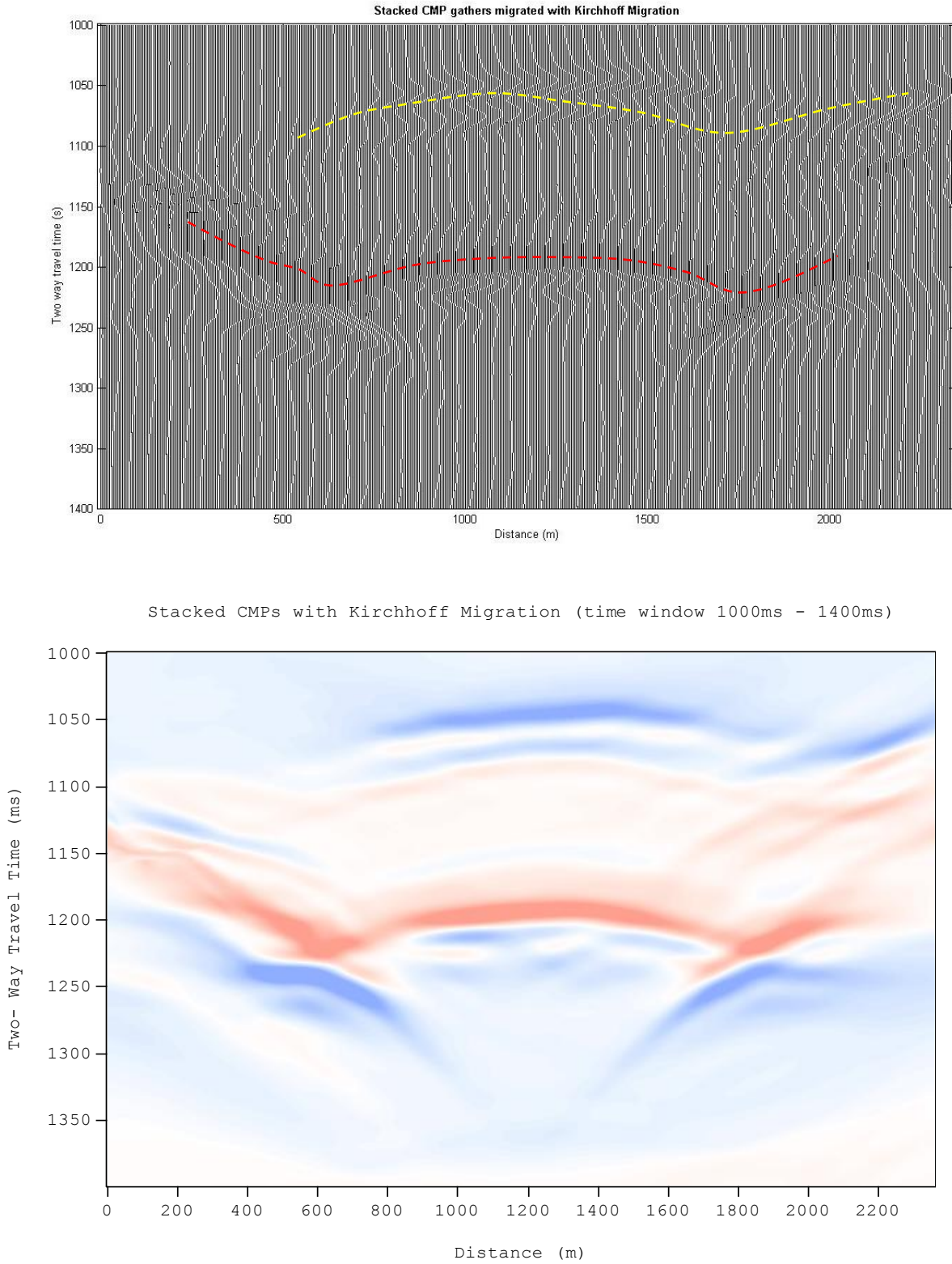
Figure 6.21: *Kirchhoff migration of CMP gathers before steam injection for a timewindow 1000 ms up to 1400 ms*

6.7.2. Finite – Difference Migration

The second time migration method uses differentiation in order to obtain a solution to the wave equation and is generally known as finite-difference methods. Finite – difference also known as downward continuation migration maps the diffraction curve *(Onajite, 2014)*. Recorded at one depth to another as if it were recorded at the new depth and predicts the change in the waveform produced by the change in depth.

In other words, finite – difference migration extrapolates input data (CMP stack sections or pre-stack) using finite increments of depth and predicts what the data would look like at the new depth. It should be noted that finite – difference migration is not sensitive to velocity variations as Kirchhoff migration method. The finite – difference migration can accommodate minor lateral velocity variations. Finite – difference migration method can handle data with small lateral velocity variations and can also handle data with low signal-to-noise ratio. *(Onajite 2014).* Kirchhoff migration cannot handle seismic data with low signal-to-noise-ratio and data with lateral velocity variation.

The MATLAB^TM function that is used for finite difference migration is called ***fd15mig*** and is a 15 degree finite difference migration routine. Finite differences can be used to implement both steep dip depth migration solutions and dip-limited time migration solutions. These latter are usually referred to as the *15 degree* and *45 degree* assumptions. The 15 degree equation is generally considered good up to 35 degrees dip.

function [arymig, tmig, xmig] = **fd15mig** (aryin, aryvel, t ,x, dtau)

Where the outputs are:,

- ➢ *aryin: matrix of zero offset data. The stacked data was used.*
- ➢ *aryvel: RMS velocity matrix with same dimensions as the above matrix aryin*
- ➢ *t: time interval*
- ➢ *x: location of CMPs*
- ➢ *dtau: a scalar that indicates the step length in time in milliseconds.*

And the inputs are:

- ➢ *arymig: the output migrated time section*
- ➢ *tmig: t coordinated of migrated data*
- ➢ *xmig: x coordinated of migrated data*

Stacked CMP gathers migrated with Kirchhoff Migration

Stacked CMPs with Finite Difference Migration
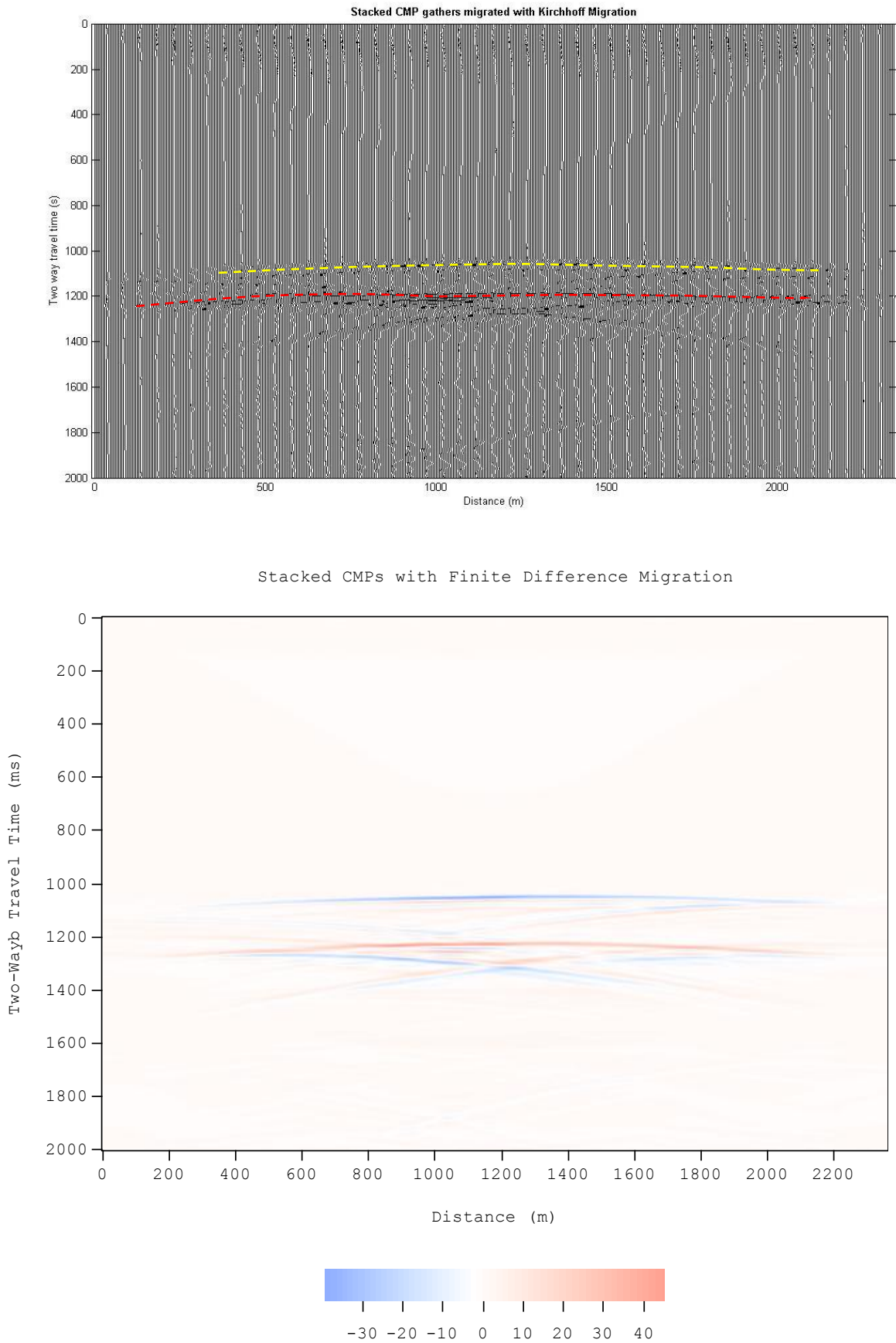
Figure 6.22: *Finite difference migrated sections of stacked CMP gathers.*

Stacked CMPs with Finite Difference (time window 1000ms - 1400ms)
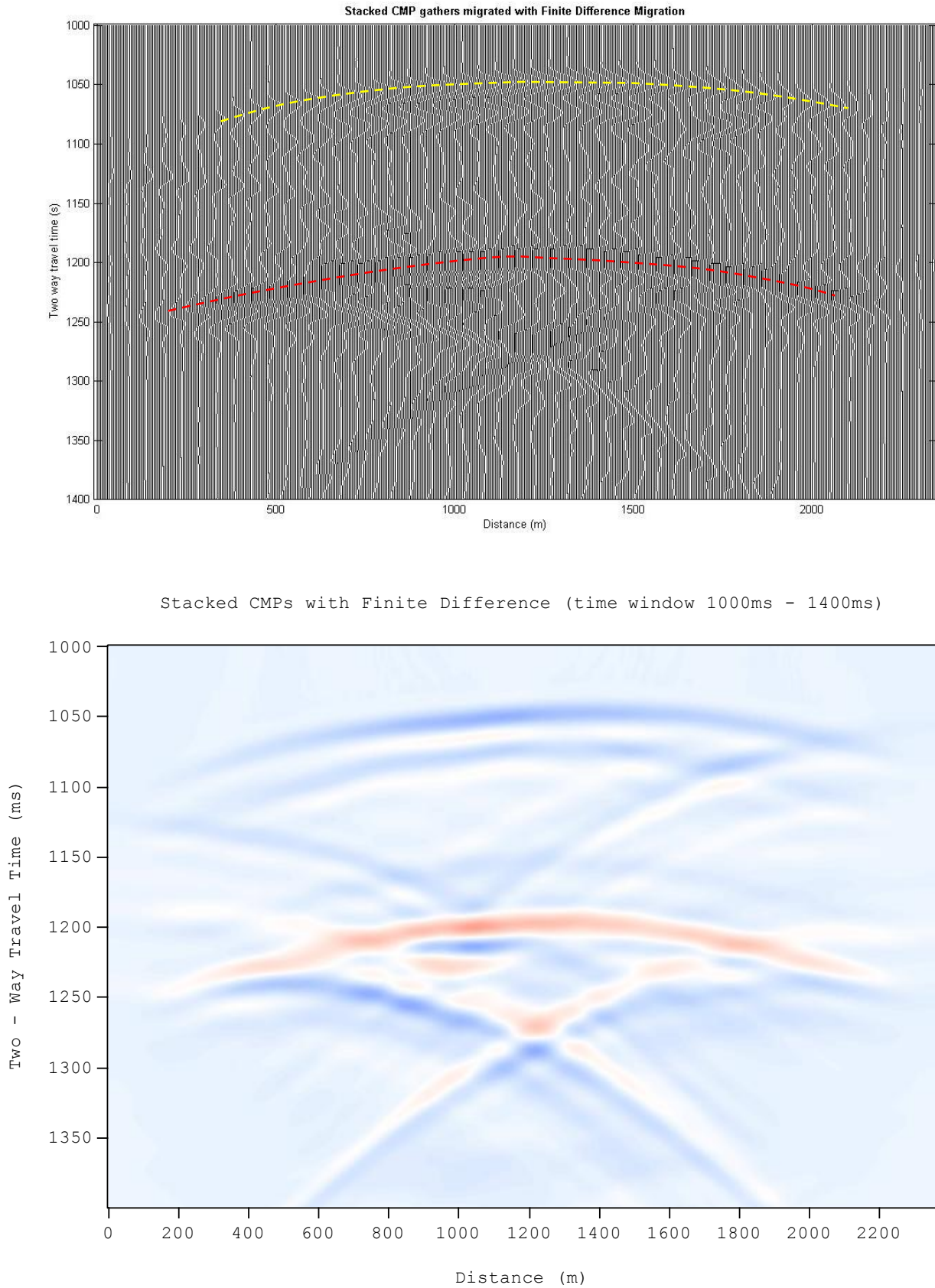
Figure 6.23: Finite difference migrated sections of stacked CMP gathers for a time window 1000 ms up to 1400 ms

Figures 6.22 and *6.23* show the resulted migrated sections through finite differences migration processing. *Figure 6.23* refers to a narrower time window and for this reason depicts the reservoir with more detail. The upper and the last horizons of the reservoir model appear at the same two-way travel times in the seismic sections as in the stacked sections (*Figure 6.17* and *6.18*).Finite difference migration results in a better depiction of the reservoir than Kirchhoff migration.

Finally, it should be mentioned that all the processing was conducted to an input file of an SEG-Y file format, derived from the seismic simulation process. SEG-Y is an internationally recognized format developed by the Society Exploration Geophysicists (SEG) for storing geophysical data, particularly in the seismic industry. An SEG-Y file comprises of data traces (which contain the actual seismic records). Typically, contains all the traces which recorded a given source and is usually referred to as a shot gather, or the file may contain traces from a single receiver recorded from a large number of sources and is known as a receiver gather. Each trace within the gather is limited to 32767 samples.

CHAPTER 7

Post Injection Results of Seismic Processing and Time-Lapse Results in Prinos Field

The time lapse method is used to ascertain if the surface reflection seismic method is capable of detecting changes in the reservoir due to steam injection in a layered sandstone reservoir. Time-lapse monitoring is comprised of a baseline survey, recorded before the onset of the steam injection process and refers to initial reservoir conditions (even before the onset of primary production) when the reservoir is fully saturated with brine and oil and a monitor survey recorded after a period, when the whole reservoir is half saturated with brine and oil and the remaining half with steam. The objective of time-lapse seismic monitoring is to conceive injection induced changes within the reservoir. Ideally, through a time-lapse monitoring survey, there should be identified areas saturated with steam or even regions that are not stimulated by the injection process.

To aid in the time-lapse interpretation, a difference in volume was produced through the subtraction of the baseline initial data from the post-injection data, producing a third dataset comprised of traces that are different between surveys *(Kelly, 2012).* Difference in volumes form the foundation for time-lapse analysis, ideally integrated with reservoir characterization, geological modeling and reservoir production *(Johnston 1997).*

Figure 7.1 illustrates the first seismic trace of the 100th CMP before and after the steam injection process for a time window 1,000ms up to 1,600ms. It should be mentioned that the seismic signal has undergone no processing and consequently all the amplitudes have their original magnitude. Post-injection seismic signal presents higher amplitude values than the pre-injection one. Approximately at 1,100ms the two-way travel time of the upper reservoir layer appears. The amplitudes in the post injection case are higher, while there is mentioned no time delay between these two signals at this time period that refers to the upper reservoir layer (approximately 1070 ms). This lack of time shift on that layer happens due to the fact that the travel time of the upper layer remains unaffected by the steam, since the seismic wave travels through the underlaying layers before being reflected and these layers are not steam injected. From 1,200ms up to 1,300ms approximately there are observed peaks of amplitude that correspond to the reflections of the lower reservoir horizon. Due to the injected steam in the reservoir formations, a time delay is caused between these two signals. The

compressional velocity in the case of steam-bearing layers is lower than that of the initial case. As a result, more time is needed for the seismic signal to travel through formations that contain steam.
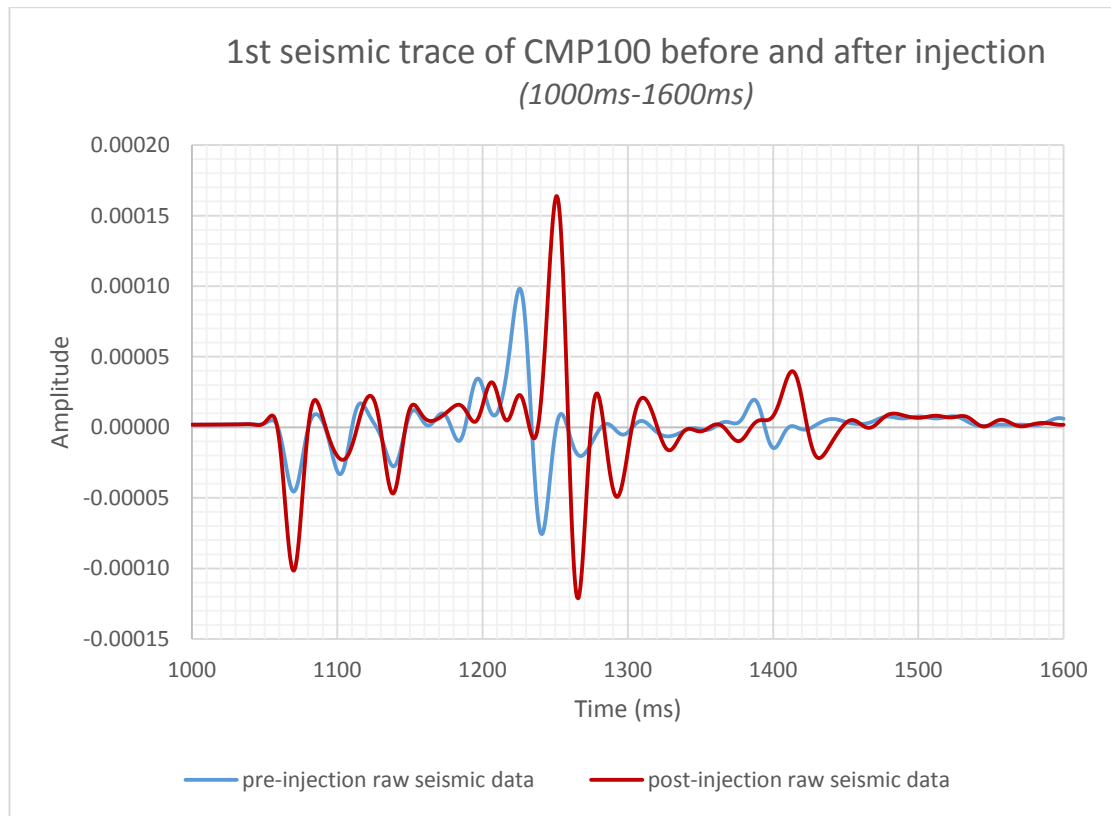
Figure 7.1: *Seismic trace of CMP100 before and after the steam injection process.*

7.1.   Post Injection Results

For the post-steam injection process was followed the same processing as for the baseline survey *(Figure 7.2)*. The baseline survey is useful in order to delineate the pre-injection reservoir geometry. The only difference is that in the post-injection case only the finite difference method was applied. In this case, with the predominant frequency that equals 20Hz, is not achieved good resolution of the layers within the reservoir, which means that the signal is comparatively low in order to discriminate layers with such thickness. Additionally, there is indeed lateral velocity variation between the layers of the reservoir.
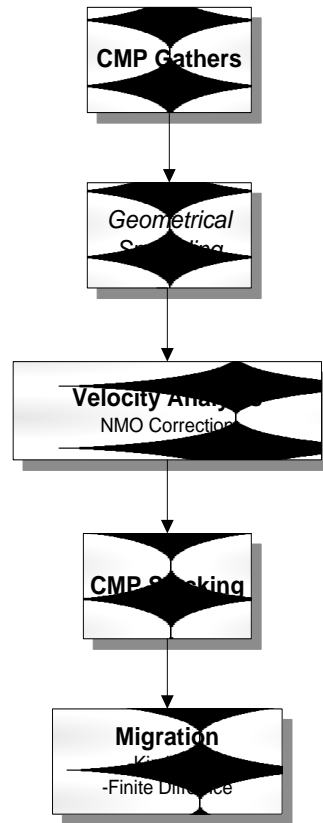
Figure 7.2: *Steps of seismic processing procedure*

As it is already mentioned in **Chapter 5 – Generated Synthetic Seismic Data,** the compressional and the shear wave velocities as well as the density of each layer were calculated based on the results of a survey over a steam injection process that was conducted in Alberta, Canada *(Tsingas, 1989).* Based on the changes on magnitude of velocities and density of that survey, we implement the same reduction both in the compressional wave velocity (15%) and in the density (10%) of each layer of the reservoir. The shear wave velocity appears to be slightly increased (5%).

The stacked section of the CMP gathers based on the post-injection seismic data is shown in **Figure 7.3** The same stacked section but in a greater magnification, due to the smaller time window, is illustrated in **Figure 7.4**. This section provides a better image of the reservoir and basically a better discrimination of the upper and the last layer of the reservoir model. For the post-injection processing there was only followed the finite-difference migration. In **Figure 7.5** and **7.6** the migrated results are presented.

The resulted figures both from stacking and also form migration process, provide us with almost the same information concerning reservoir's geometry. This means that the upper layer of the reservoir can be recognized at the area of 1,050 ms of two-way travel time with negative amplitudes, while the last layer is almost identified at 1,250 ms two-way travel time.
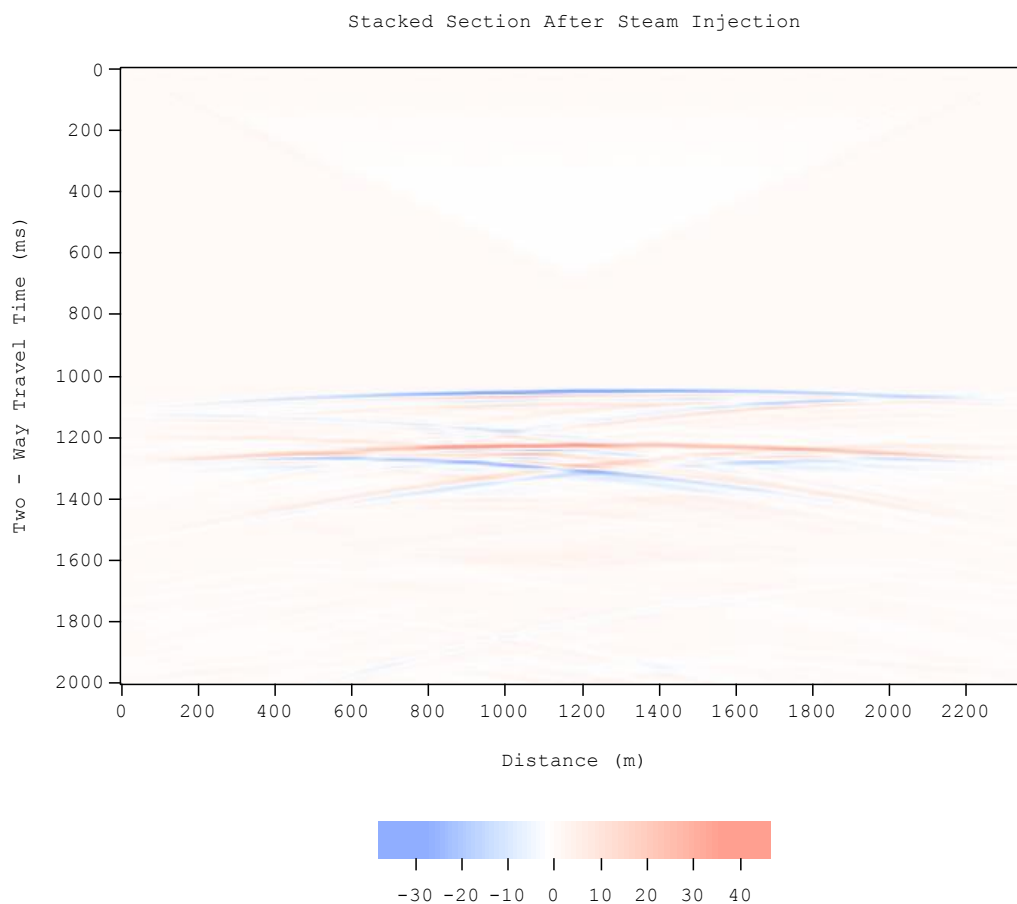
Figure 7.3: *Stacked CMP gathers of the post-injection seismic data*
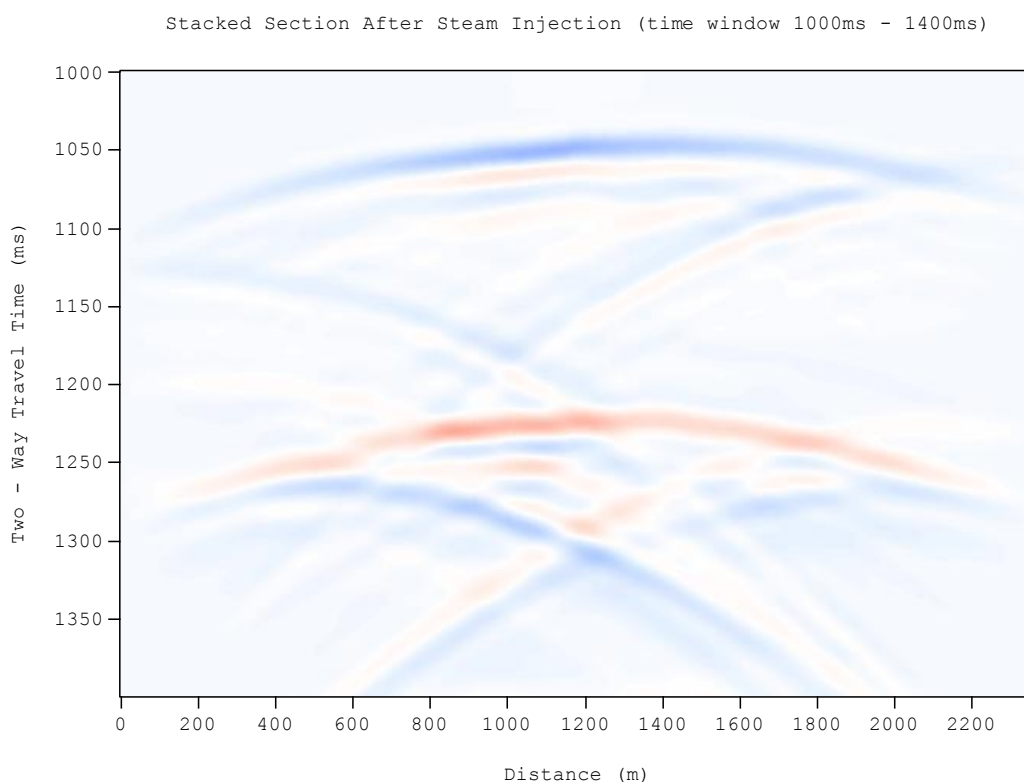
Figure 7.4: *Stacked CMP gathers of the post-injection data for a time window 1000 ms up to 1400 ms*

Stacked CMPs with Finite Difference Migration (After Steam Injection)
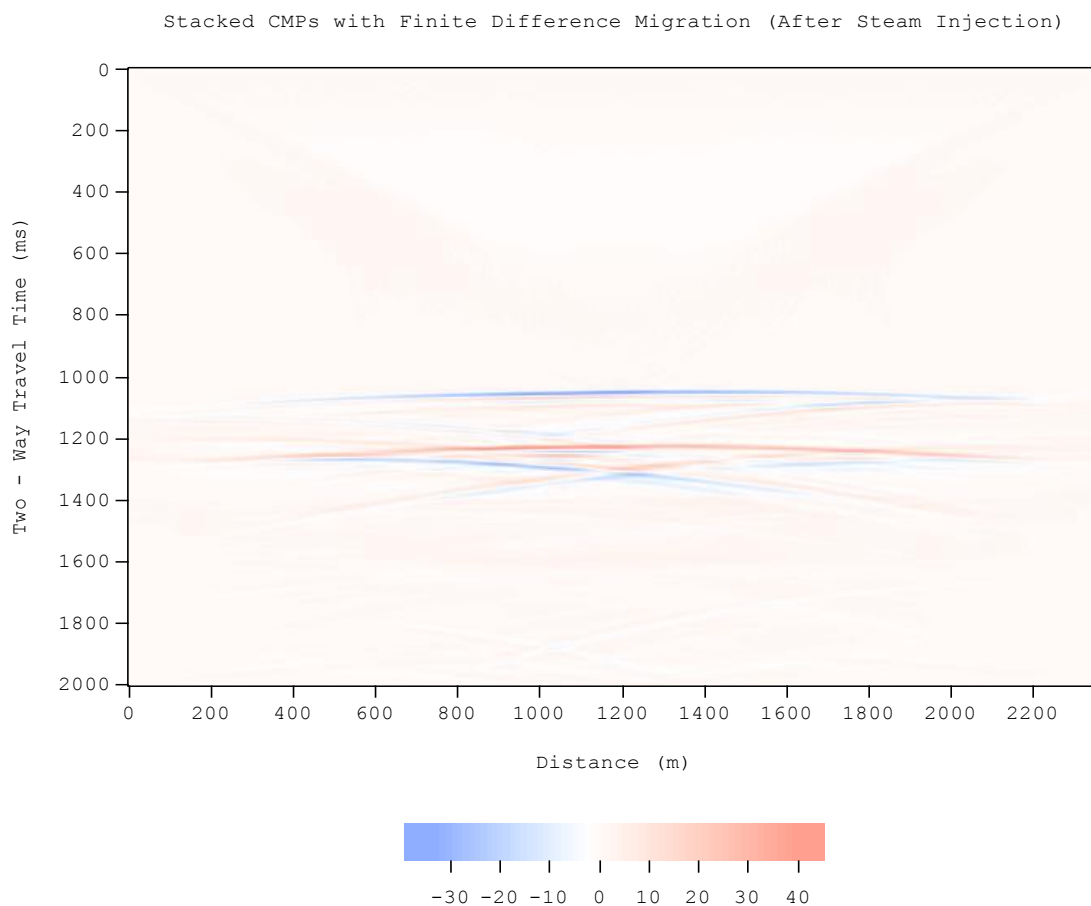
Figure 7.5: *Finite difference migration of stacked post-injection CMP gathers.*

Stacked CMPs with Finite DIfference Migration After Steam Injection (time window 1000ms-1400ms)
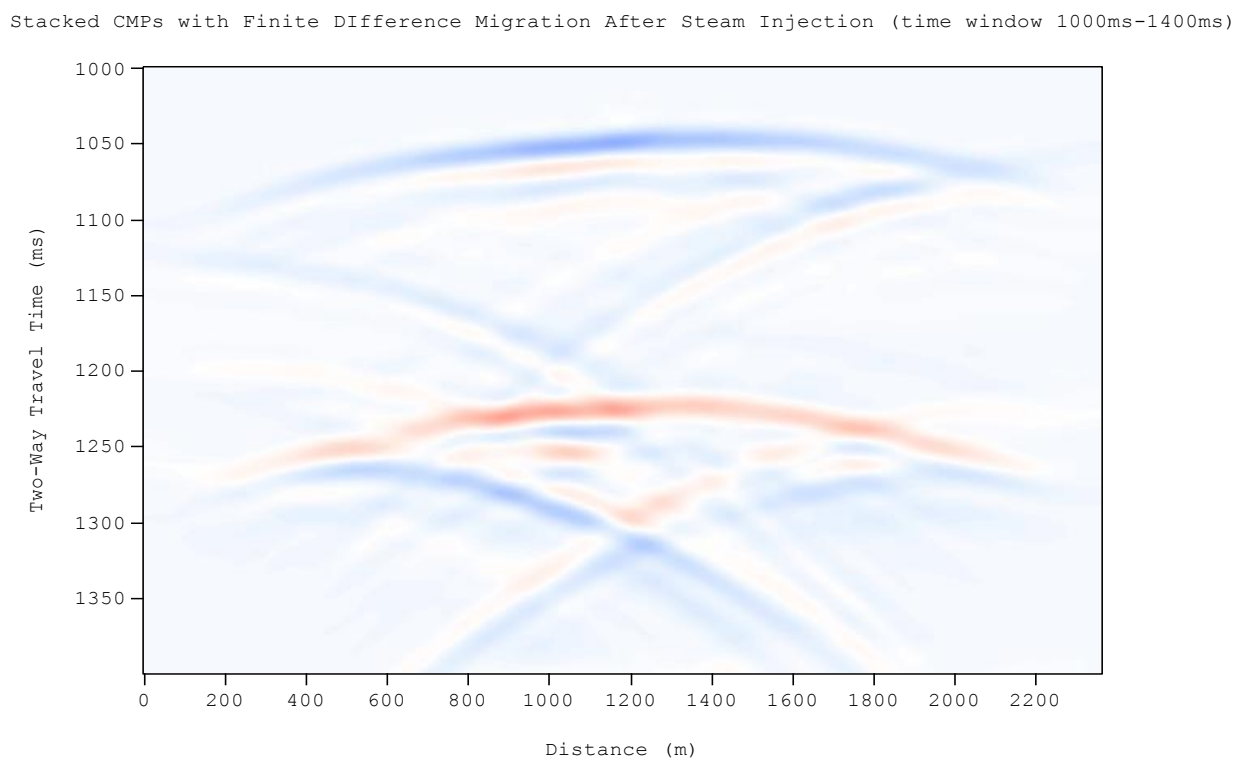
Figure 7.6: *Finite difference migration of stacked post-injection CMP gathers for a time window 1,000 ms up to 1,400 ms*

7.2.   Time – Lapse Imaging Results

Time Lapse of Steam Injection (Difference in stacked sections-time window 1000ms-1400ms)
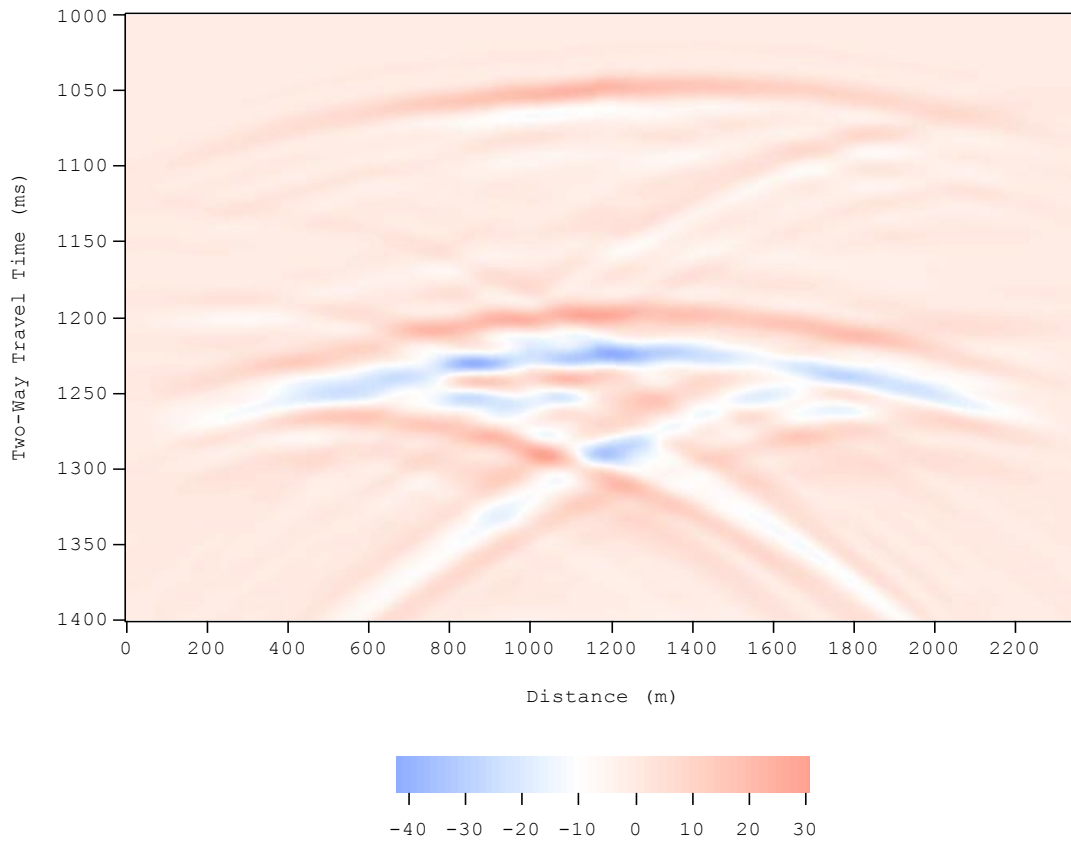
Figure7.7: *Difference in stacked sections (pre and post injection stacked sections) for a time window 1,000ms up to 1,400ms*

Time-Lapse of Steam Injection (difference in Fin.Diff. migrated sections - time window 1000ms-1400ms)
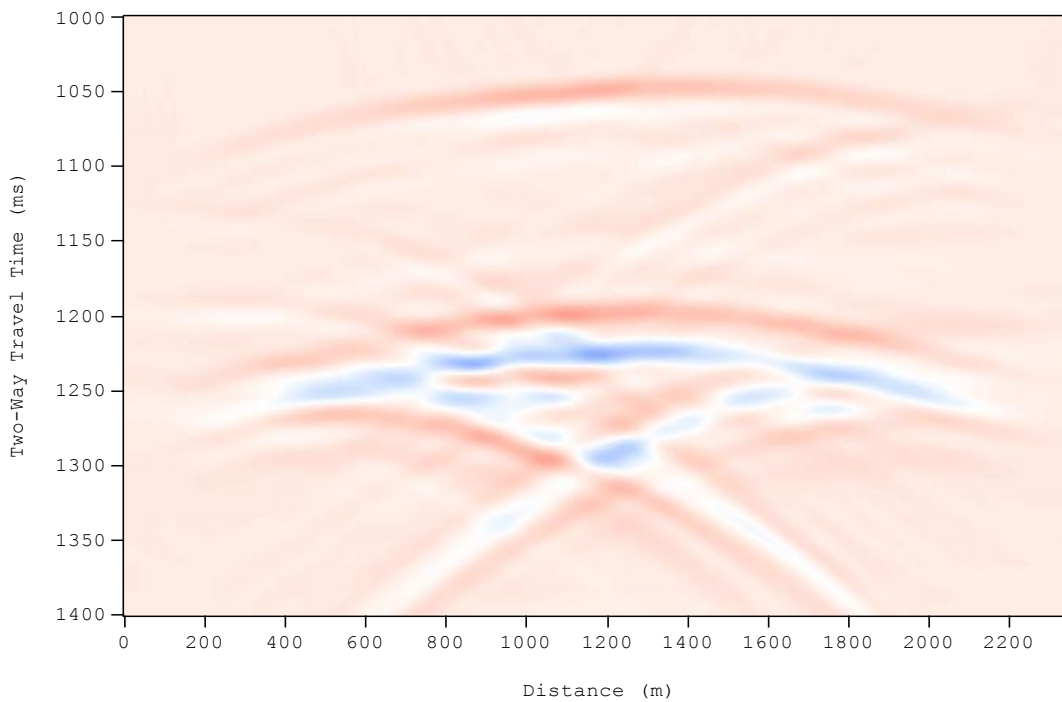
Figure 7.8: *Difference in finite difference migrated sections for a time window 1,000ms up to 1,400ms*

The difference of stacked and also of migrated sections is shown in ***Figures 7.7 and 7.8***. It can be mentioned that there is no any basic difference between these two sections, as there is also no basic difference between the stacked and the migrated sections that were presented previously ***(Figures 7.4 and 7.6)***.

In the difference seismic sections ***(Figures 7.7 and 7.8)*** there are also easily determined the upper and the last layer of the reservoir model. The main target of the difference sections is to determine the position of the steam face, while the reservoir is half saturated with steam. This cannot be clearly seen from these sections due to poor resolution within the reservoir layers. It can be easily observed that there are still strong side reflections underneath the reservoir model. These reflections are profound, due to their shape and geometry. These are artifacts probably created due to the sensitivity of the algorithm to the more complex geometry of the layers at the edges of the model.

As far as the lower reservoir horizon refers, in the time-lapse seismic sections is captured with two reflections of high amplitudes. This happens due to the time shift that occurs in this layer due to steam-bearing reservoir layers ***(Figure 7.7*** and ***7.8)***.

Due to steam injection, the seismic velocity is expected to be reduced and as a result the two-way travel time for each layer to be increased. In order to testify whether the steam is fully positioned to all the extent of the reservoir layers, we proceeded to the calculation of the time delay (time lag) of two-way travel time of the last reflector of the reservoir between the pre and post injection process ***(Figure 7.9)***. This calculation was mainly based to the two-way travel times that refer to the last layer, since the two-way travel times of the upper layer do not seem to be affected by the injection process. To the post-injection results, boundaries above the reservoir should remain unchanged across the survey, since steam injection is performed to the layers below. Boundaries beneath the reservoir and specifically the last reservoir horizon, exhibits velocity pushdown (time lag) since steam has a lower acoustic velocity than brine. Thus, the last horizon can be used to measure the growth of pushdown and to check whether the steam has been extended across the entire reservoir.
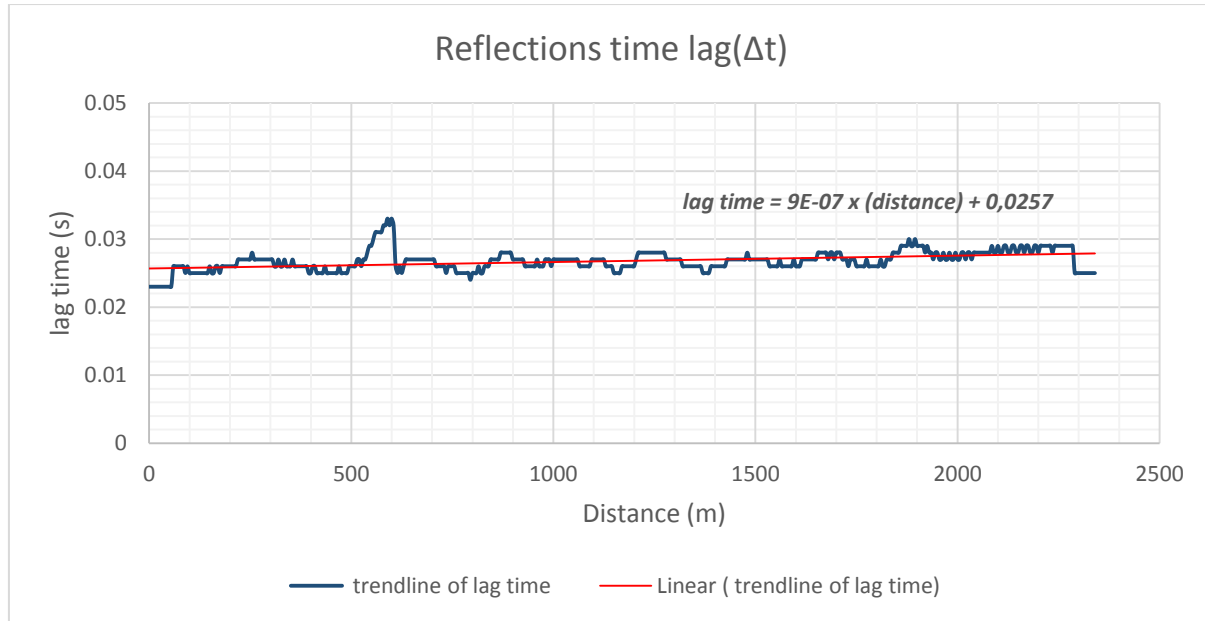
Figure 7.9: *Lag time of the last reservoir layer (Layer C) due to steam injection process.*

The time delay is nearly described by a straight line for all the extent of the reservoir and is approximately equal to 26ms. As a result, it can be concluded that the steam face is finally extended all over the reservoir to all four layers, despite the fact that it cannot be clarified by the seismic difference sections.

Generally, velocity pushdown for the last layer provides a useful estimate of the steam distribution within the reservoir. Pushdown arises because steam-bearing sandstone has significantly lower acoustic velocity than brine-bearing sandstone.

CHAPTER EIGHT

Conclusion and Recommendations

8.1. Conclusion

This thesis refers to the creation and processing of synthetic seismic reflection data in order to monitor a steam injection process in Prinos field, through time lapse imaging. The main target of this thesis was to determine whether surface seismic reflection data are capable of detecting the steam front of an injection process in a layered sandstone reservoir. Time lapse 2D seismic surveys are employed to monitor reservoir changes between post injection data (baseline survey-initial reservoir conditions) and repeated after the reservoir is fully stimulated by the steam injection process (monitor survey).

Time lapse seismic monitoring is considered to detect reservoir changes, observed through a subtraction between the baseline data and the monitor data. Seismic wave velocity depends on porosity, pore fluid, consolidation, temperature and finally pressure. A variation in these parameters will finally result in changes in the velocity, which is observable in the post-injection data. The seismic changes that are finally investigated through a time-lapse experiment are time delays of two-way travel time, amplitude changes and changes in acoustic impedance. Through a steam injection process, seismic velocity, density and finally acoustic impedance decrease.

For numerical simulation of the propagating P waves through the layered reservoir, the finite difference method was used. For the generation of the synthetic seismic reflection data a geological section in Prinos field was selected. The reservoir consists of layered sandstone, while the cap rock formations as well as the bedrock consist of evaporites. All the parameters that are related to the geometry and the set-up of the seismic simulation process are mentioned in *Table 8.1*. The simulated seismic survey refers to a surface seismic array that consists of shots buried 15m below the surface, with a shot interval equal to 40m and receivers placed in stable positions that cover all the extent of the seismic section. The receivers are placed on the surface and the distance between them is 10m.

The predominant frequency that is followed for both synthetic seismic surveys is 20Hz. The typical recorded seismic frequencies are in the range of 5-100Hz. High frequency and short wavelengths provide better vertical and lateral resolution. However, there is a practical limitation in generating

high frequencies that can penetrate large depths. The Earth behaves as a natural filter removing the higher frequencies more readily than lower frequencies (absorption effect).

Firstly, there is an assumption that before the EOR steam injection process the reservoir is fully saturated with brine and oil. For EOR purposes, it is assumed that the reservoir contains crude oil which has an average density range between 0.79g/cc to 0.97 g/cc. The typical density range for brine (NaCl) is 1g/cc to 1.19 g/cc. Moreover, steam density at 350 °C and 2500psia (steam injection conditions) is about 0.58 g/cc and as a consequence there is a difference in magnitude between steam and oil-brine densities.

Table 8.1: Parameters for the generation of the seismic reflection data

Dominant frequency *(Hz)*	20
horizontal extent *(m)*	2360
vertical extent *(m)*	3000
Grid *(m)*	5
minimum offset *(m)*	10
maximum offset *(m)*	2350
Receiver interval *(m)*	10
Number of receivers	237
Receiver depth *(m)*	0
Receiver increment *(m)*	0
x coordinate of 1st receiver *(m)*	0
Shot Interval *(m)*	40
Number of shots	59
Shot depth *(m)*	15
x coordinate of 1st shot *(m)*	10
CMP interval *(m)*	5
Number of traces	13983
fold of coverage	30
number of CMPs	469
sampling interval (ms)	0.001
record length (ms)	2000

The time lapse process is mainly oriented to the last step of the steam injection project, when all the reservoir layers are totally stimulated by steam and consequently all the layers are 50% saturated with steam and 50% saturated with brine and oil. For the post-injection synthetic seismic data, modified seismic velocities and densities are used for all the layers that are influenced by the injection project. Based on a monitoring survey that was conducted in Alberta, Canada over a steam injection

project *(Tsingas, 1989)*, there were followed the same reduction rates both in velocity and the density of each reservoir layer. If the pores are filled with steam instead of liquid (water/oil), the velocity reduction will be great because the sound travels much more slowly in steam than through reservoir liquids. As a result, in this thesis, the compressional wave velocity faces an average reduction equal to 15% while the densities are also reduced by 10%. Finally, the shear wave velocities have a slight increase almost 5%.

Both the baseline and the monitor data were treated with identical processing due to the needs of repeatability among the two surveys. The first processing step refers to the common-midpoint (CMP) sorting, where all the reflections recorded at the different offsets in a CMP gather carry information on the same subsurface points (below the midpoint position). The second step refers to the geometrical spreading correction, where enhancement of the amplitudes of each trace is carried out. The next step of processing refers to the NMO correction, where all the reflection events are flattened. With velocity analysis all the RMS velocities of the reservoir model were calculated as a function of depth, while the traces of the same CMP gather are stacked together, formulating in this way one single trace. Through this process the signal-to-noise ratio is improved and as a result this has a positive impact on the seismic data quality. Finally, the last step of processing refers to migration, where ideally all the dipping effects that still exist in the stacked section are transferred to their real position. Nevertheless, migration did not seem to result in any improved seismic sections, while the resulting sections are quite similar with those of the stacking process. Due to this reason, only the stacked data of pre- and post-injection survey were used for the time lapse sections.

In post-injection data differences are observed mostly in amplitudes and also in terms of two-way travel times. Due to contrasting acoustic impedances between the reservoir formations and the evaporite formations, the upper and the lower reservoir horizons stand out in the seismic section as strong reflectors. The fact that the intermediate reservoir layers are not present in the seismic sections may is due to the magnitude of the predominant frequency. There is a lower limit to the thickness that can be tracked, which corresponds to the half wavelength of the seismic waves. Based on the existing survey settings, the minimum thickness that can be detected is approximately 95m. The thickness of the intermediate layers of the reservoir is lower than this value and as a result they cannot be recognized through the seismic sections with the existing applied frequency.

The difference section that results from the subtraction of the post-injection stacked data from the initial stacked data, provides a time lapse imaging of the reservoir model. A time lag to the post-injection section is expected, since steam-bearing sandstone has a significantly lower seismic acoustic velocity than brine-bearing sandstone.
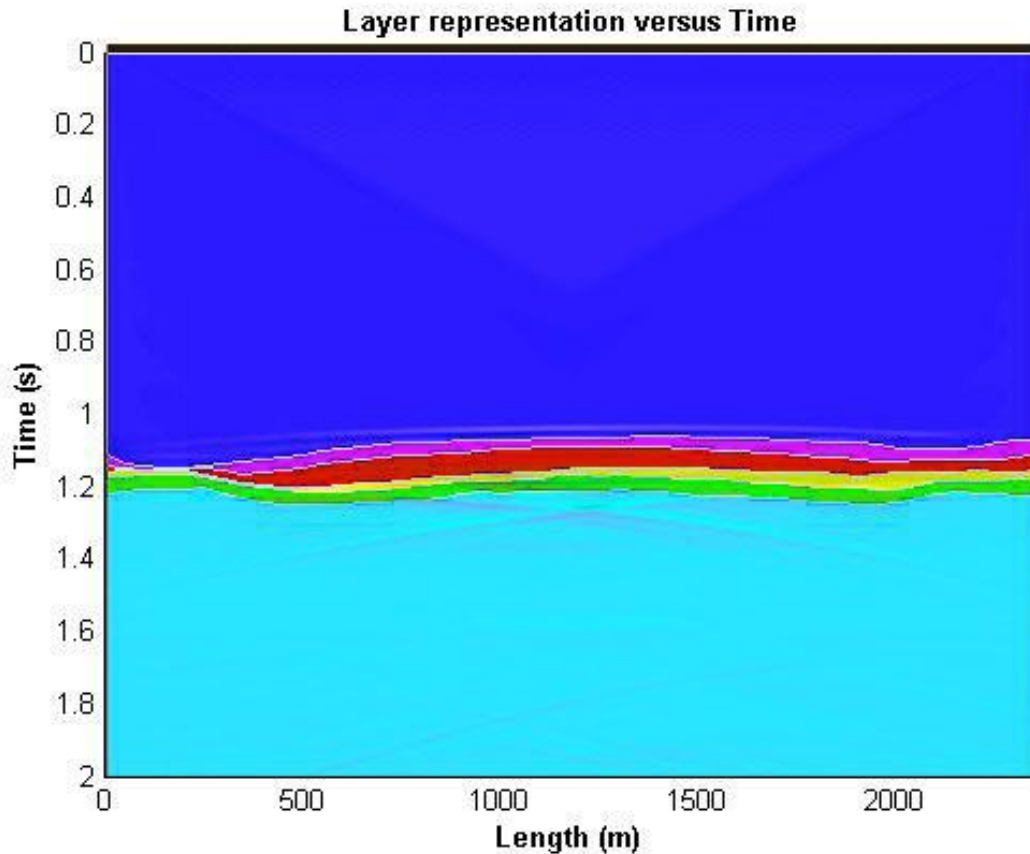
Figure 8.1: Full stacked section overlapped with RMS velocities.

Figure 8.1 illustrates a full stacked pre-injection section overlapped with the plot that represents the reservoir layers as a function of two-way travel time and that was created through the modeler. It can be clearly seen that the upper and the lower reservoir horizons coincide with these of the synthetic model.

The main conclusion of this thesis can be summarized in the following points:

➢ Surface seismic is an easy method for monitoring purposes. However, in this study, there is not achieved good resolution of the layers within the reservoir, which means that the signal is comparatively low in order to discriminate layers with such thickness. Despite that, the reservoir is clearly defined. The upper and the lower interface of the reservoir are depicted as strong reflectors, since these two interfaces show high contrast in acoustic impedance with their neighboring formations.

➢ As far as the processing procedure of the seismic data refers, there is mentioned no great difference between the stacked and the migrated seismic sections. Nevertheless, finite difference migration shows better results than Kirchhoff migration, since in finite difference section the upper and the last layer of the reservoir are depicted in a more discrete way.

➢ From the difference section there is expected to be shown any change in acoustic impedance in the reservoir that is caused by the steam injection project, in other words the steam face position in the reservoir layers. This not a fact in the final time-lapse sections.

➢ By comparing the two-way travel times that correspond to lower interface of the reservoir of the pre-injection case and the post-injection case, time delay is observed. Velocity pushdown for the lower interface provides an estimate of the steam distribution within the reservoir. Pushdown arises because steam-bearing sandstone has a significantly lower seismic velocity than brine-bearing sandstone. Another fact that determines the existence of steam within the reservoir layers is the amplitude increase that happens to the seismic waves in the case of the post-injection survey.

8.2. Recommendations

For future research on the examined injection site, the following recommendations are purposed:

➢ Predominant frequency higher than 20Hz for the described surveys.

➢ Examination of the synthetic data in pace with noise, for the creation of more realistic results.

➢ A borehole synthetic seismic survey in parallel with the surface seismic survey to be conducted in order to improve lateral resolution of the seismic sections.

➢ Layer stripping for the gradual implementation of the reservoir model leads to easier interpretation.

➢ Different scenaria of seismic monitoring surveys to be tested for more realistic results (different degrees of saturations, different reservoir layers being stimulated by steam, more seismic surveys along time).

➢ Better design of the absorbing boundaries in the seismic model.

References

Alterman, Z., and Karal. F. C., 1968, Propagation of elastic waves in layered media by finite-difference methods: Bull., Seismological Society of America, 58, 367-398

Alvarez, Johannes, and Sungyun Han. 2013. "Current Overview of Cyclic Steam Injection Process." 2(3): 116–27.

Barker, R. & Moore, J., 1998. The application of time-lapse electrical tomography in groundwater studies. *The Leading Edge*, 17(10), p.1454.

Batzle, M., Christiansen, R. & Han, D.-H., 1998. Reservoir recovery processes and geophysics. *The Leading Edge*, 17(10), p.1444.

Batzle, M., R. Christiansen, and D-H. Han. 1998. "Reservoir Recovery Processes and Geophysics." *The Leading Edge* 17(10): 1444.

Bianco E.2008."Seismic rock physics of steam injection" MSc Diploma Thesis, University of Alberta, Canada.

Boore, D.M. (1972), Finite difference methods for seismic wave propagation in heterogeneous materials, in Methods in Computational Physics, v. 11, Seismology: Surface waves and Earth oscillations, (Bolt, B.A., ed.), Academic Press, 1—37.

Dai N., Vafidis A., Kanasewich E., 1994"Composite Absorbing Boundaries for the Numerical Simulation of Seismic Waves". Bulletin of Seismological Society of America, Vol. 84, No.:185-191.

Dixit, Hemant Kumar, Akhil Puri, and Rajat Rathore. 2012. "Time-Lapse Seismic * -Concept , Technology & Interpretation Abstract :" (January): 66–72.

Donaldson et al.1985."Enhanced oil recovery I - fundamentals and analyses"

Drijkoningen G.G., Verschuur D.J. 2003."Seismic Data Processing".Delft University of Technology.

Fanchi, J.R., 2001. Feasibility of Monitoring CO2 Sequestration in a Mature Oil Field Using Time-Lapse Seismic Analysis. *SPE/EPA/DOE Exploration and Production Environment Conference, San Antonio, Texas, U.S.A., 26-28 February*.

Gottlieb D. and Turkel E.,"Dissipative Two-Four Methods for Time Dependent Problems," Mathematics of Computations, 30: 703-723, 1976.

Grathwohl, P., 2015. Th P3 01 Flow through Experiment on CO2-brine-rock Interaction in a Sandstone from the Altmark Gas Reservoir. , (June), pp.1–4.

Heaton, S.J. et al., 2000. Time Lapse Monitoring – Foster Creek SAGD Project. , pp.1–9.

Hutson, M., 2003. Acoustic Echo Cancellation Using Digital. , (November).

Johnston, D H, and Exxon Production. 1997. "A Tutorial on Time-Lapse Seismic Reservoir Monitoring."

Kalantzis F., Vafidis A., Kanasewich E.R. and Kostyukevich A.1996."Seismic monitoring and modeling of an enhanced oil recovery project at Cold Lake, Alberta, Canada".Canadian Journal of Exploration Geophysics. vol.32, No.2. 77-89.

Kanasewich E.R et al., 1985 "Least -squares of spatial seismic refraction data". Bulletin of the Seismilogical Society of America, Vol.75,No.3. 865-880.

Kanasewich E.R. 1999."Seismic Imaging of In Situ Bitumen Reservoirs and the Properties of Porous Media", Alberta, Oil Sands Technology and Research Authority

Kelly, K. R., R. Ward, W. S. Treitel, and R. M. Alford, 1976, Synthetic seismograms: A finite-difference approach: Geophysics, 41, 2–27.

Kiomourtzi, P, N Pasadakis, and a Zelilidis. 2007. "Geochemical Characterization of Satellite Hydrocarbon Formations in Prinos-Kavala Basin (North Greece)." *Bulletin of the Geological Society of Greece* XXXX(September): 839–50.

Kiomourtzi, P., N. Pasadakis, and a. Zelilidis. 2008. "Source Rock and Depositional Environment Study of Three Hydrocarbon Fields in Prinos - Kavala Basin (North Aegean)." *The Open Petroleum Engineering Journal* 1(1): 16–29.

Lumley, D., Adams, D. & Meadows, M., 2003. 4D seismic data processing issues and examples. *2003 SEG Annual Conference and E*, pp.2–5.

Michelakis M. 2010. "Three dimensional lithostratigraphical simulation of Prinos Oil reservoir" Diploma Thesis. Technical Unoversity of Crete, School of Mineral Resources.

Meyer, R., 2001. 4-D seismic and time-lapse reservoir geology. , 13.

Meunier, J. & Huguet, F., 1998. Céré-la-Ronde: A laboratory for time-lapse seismic monitoring in the Paris Basin. *The Leading Edge*, 17(10), p.1388.

Onajite, Enwenode. 2014. *Seismic Data Analysis Techniques in Hydrocarbon Exploration*.

Papaconstantinou, C M. 2004. "Prinos Basin -." XXXVI(April): 327–33.

Pasadakis, N., 2008. Source organic matter and depositional environment in Prinos oil basin (Greece. , (September 2015).

Sathaye, K. et al., 2014. Constraints on the magnitude and rate of CO_2 dissolution at Bravo Dome natural gas field. *Proceedings of the National Academy of Sciences of the United States of America*.

Schlumberger Oil Glossary: http://www.glossary.oilfield.slb.com/

Sheriff, D.E., and Geldhart, L.P., 1995, Exploration Seismology: Cambridge Univ. Press.

Smith R.G. and Maitland G.C.1998 "The Road Ahead to Real Time Oil & Gas Reservoir Management"

Sung, W., 2015. Th P3 07 Experimental Investigation for the Effect of CO_2 Sequestration on Oil Recovery under the Gravity Segregation in CO_2 EOR. , (June), pp.1–4.

Thompson, J S. 1960. "University of Alberta." *Canadian Medical Association journal* 82(14): 731.

Tsingas, C., 1989, Seismic reflection imaging over a thermally enhanced oil recovery site, PhD dissertation, University of Alberta, Edmonton.

Vafidis, A., Abramovici, F. and Kanesewich. E.R., 1992, Elastic wave propagation using fully vectorized high order finite difference algorithms: Geophysics, 57.218~232.

Virieux, J., 1986, P-SV wave propagation in heterogeneous media: Velocity stress finite difference method: Geophysics, 51, 889–901.

Watson, I.A., Lines, L. and Brittle K.F., 2002, Heavy-oil reservoir characterization using elastic wave properties, The Leading Edge, 21, 736-739.

Xie, Y. et al., 2010. Time-lapse seismic study of south China sea. *Society of Petroleum Engineers - International Oil and Gas Conference and Exhibition in China 2010, IOGCEC*, 4(June), pp.3254–3260.

Yilmaz, O. (2001). Seismic data processing. Society of Exploration Geophysicists.

Yuh, Sung et al. 2009. "Seismic Monitoring of Steam Flooding in a Depleted Mobile Heavy Oil Field : Model Studies of Steam Drive (SD) and Steam Assisted Gravity Drainage (SAGD)." *SEG Technical Program Expanded Abstracts*: 3889–93.

Zhang, X.W., 2015. Th P6 13 Time-lapse Seismic Monitoring for Reservoir Waterflooding Recovery at Nigeria Deep Sea. , (June), pp.1–4.

Appendix

Here, there are cited all the algorithms that compose the basic processing sequence and that were used for the fulfillment of this thesis. The processing of the seismic signals was performed on MATLAB™ interface.

%% SHOT GATHER

```
segy = SEGY_OpenFile('MODEL_Vx.sgy', 'r','b');%open the SEGY data file named MODEL

dt=0.001; % Sampling interval in seconds

groupinterval=10;% Hydrophone group interval in m

cmpinterval=groupinterval/2; % Common mid-point interval in m


segy = SEGY_FindShots(segy);

for shotcol=(1:59);

        [shotoffsets, t, shot] = SEGY_ReadShotGather(segy, shotcol);

        neartraceoffset=10; % Nearest offset in m

        SHOT=shot (1:2000,:); %choose the first 2000 samples of each trace

        xx=shotoffsets; % convert the offsets to m

        ttc=t(1:2000)*1e-6; % choose the first 2000 samples and convert the times to seconds

        shotlocation= segy.sx(shotcol); % find the corresponding shot location

end
```

%% CMP GATHER

```
segy = SEGY_FindCMPs(segy, 1);
neartraceoffset=10; % Nearest offset in m

refx=segy.sx(1)-neartraceoffset/2- cmpinterval; % Location of the CMP#1

CMPx=refx+segy.cmps; % CMP locations

cmpcol=200;

[h, t, cmpgather200] = SEGY_ReadCMPGather(segy, cmpcol, 1);

ttc= t(1:2000)*1e-6; % choose the first 2000 samples and convert the times to seconds

cmplocation=CMPx(cmpcol); % find the corresponding CMP location

CMPgather200= cmpgather200(1:2000,:); %choose the first 2000 samples %of each trace
```

%% Reads all the CMPs (1 up to 469)

```
for cmpcol=1:469
        [h, t, cmpgatherA] = SEGY_ReadCMPGather(segy, cmpcol, 1);
        ttc= t(1:2000)*1e-6; % choose the first 2000 samples and converts the times to seconds
        cmplocation=CMPx(cmpcol); % find the corresponding CMP location
        CMPgatherA= cmpgatherA(1:2000,:); %choose the first 2000 samples of each trace
        CMPgatherB{cmpcol}=CMPgatherA;
        hh{cmpcol}=h;
end
```

%% Geometrical spreading (cmp)

```
load 'Geometrical_Spreading'; %Geometrical_Spreading comes from the
%simulation algorithm

Geometrical_Spreading=Time_Velocity_Spreading{3}; %Time_Velocity %_Spreading is a cell array that
includes three matrices. Geometrical %Spreading data are incorporated in the third matrix of this cell
%array

GV=Geometrical_Spreading;
i=0;
m=0;
for cmp=1:10:469;
        i=i+1;
        for k=cmp:cmp+9;

                if k<=469
                        m=m+1;

                        for l=1:size(CMPgatherB{k},2)
                        TRS(:,l)=CMPgatherB{k}(:,l).* GV{i}(2:2001,:);
                        end
                        GS{m}=TRS;
                        clear TRS
                end
        end
end
SD=CMPx(100);
cmplocation=100;
[h, t, cmpgather100] = SEGY_ReadCMPGather(segy, cmplocation, 1);
a=GS{100};
Cmpgather100=cmpgather100(1:2000,:);
```

%% Full Stacking

```
load ('CMP_Time'); %CMP_Time matrix derives from the simulation %algorithm
load ('CMP_Velocity'); %CMP_Velocity derives from the simulation algorithm
Time_Velocity_Spreading{1}(1,:)=[];;
CMP_Time=Time_Velocity_Spreading{1};
Time_Velocity_Spreading{2}(1,:)=[];
CMP_Velocity=Time_Velocity_Spreading{2};
ii=0;
y=0;
for i=1:10:469
        ii=ii+1;
        Timescmpgather_S=CMP_Time(ii);
        Velscmpgather_S=CMP_Velocity(ii);
        for j=i:i+9
                if j<=469
                        y=y+1;
                        cmp_a=A{y};
                        hh_a=hh{y};
                        [CMPgathernmo]=nmo(cmp_a,dt,hh_a,Timescmpgather_S,
                        Velscmpgather_S,30);
                        CMPTrace=sum(CMPgathernmo,2);% Stack
                        Stacked(:,j)=CMPTrace;
                end
        end
end
```

%% Migration Finite Difference

```
depth_par=0.0001;
```

%Finite Difference migration uses V_rms_x_t_c matrix that derives from the simulation algorithm

```
[STCK_GS_SORTED_24ms_FD,tmig,xmig]=fd15mig(Stacked,V_rms_x_t_c,0.001,segy.cmps,depth_par);
```

%% Kirkchoff Migration

```
 [STCK_GS_SORTED_24ms_KIRK,~,xmig]=kirk(Stacked,V_rms_x_t_c,tv,segy.cmps);
```